POLITECNICO DI TORINO

Laurea Magistrale in Ingegneria Energetica e Nucleare

Evacuated tube solar collectors coupled with Membrane Distillation units

Relatore: prof. Eliodoro Chiavazzo

Correlatore: prof. Alberto Tiraferri

Candidata: Anna Mate

Marzo 2019

Water, water every where
And all the boards did shrink;
water, water every where,
Ne any drop to drink.

S. T. Coleridge, THE ANCYENT MARINERE

"He shall drink nought but brine, for I'll not show him
Where the quick freshes are."

CALIBAN, in W. Shakespeare THE TEMPEST, 3.2

Abstract

Water scarcity is a relevant issue of this age: it is estimated that more than four billion people on Earth are living in a situation of water stress. The population increase, changes in consumption patterns and groundwater exploitation are some of the most relevant drivers of this situation. Despite it seems far, there are already alarming situation, as in the case of Cape Town, where more than four million people face water shortage every day, and India, where 600 million people live in water-stressed areas and where actions on agriculture have been considered in order to alleviate the problem.

A solution to the problem is the use of desalination plants which, using a variety of processes, make it possible to obtain freshwater from saltwater withdrawn from seas, oceans or inland seas. Despite this, one of the greatest issues of the desalination is brine (water with a relevant salt concentration) disposal, due to the potential thermal and salt pollution. Membrane Distillation (MD), a process still in a research phase, can be a useful tool in the solution of this problem, due to its capacity to process water with high salt concentrations, also retrieving useful substances diluted in the water. Moreover, the coupling of desalination plants with renewable energy sources is a topic which is attracting growing attentions.

A model that couples solar heat collected through evacuated tube collectors with a Direct Contact Membrane Distillation (DCMD) process is developed using Simulink software; it includes also a storage tank and an auxiliary heater to face the periods during which solar irradiance is absent. The results for the city of Turin are deeply investigated, taking advantage of an economical analysis aimed at estimating water cost. After a standard case, with a production of 5186 litres of water in a year and a Solar Fraction (SF) of approximately 60%, a sensitivity analysis is performed, to understand the influence of some relevant parameters of the plant: the most important ones turns out to be the collectors connections, whose best configuration is the parallel one, and the mass flow in MD component, which increases water production at the expense of the Solar Fraction. All the improvements were implemented, with and advantage on both water production (6906 l/y) and SF (almost 80%). The case of Lampedusa island was considered as a comparison: its different location allows a greater water production in all the analysis performed.

At the end, the limits of the plant and further possible investigations are considered.

La mancanza d'acqua è un problema rilvante di quest'epoca: si stima che più di quattro miliardi di persone vivano in mancanza d'acqua. Alcune tra le cause più rilevanti di questo fenomeno sono l'aumento della popolazione, cambiamenti nelle abitudini di consumo e il grande sfruttamento di falde acquifere. Nonostante la questione possa sembrare lontana, ci sono già situazioni allarmanti, come nel caso di Cape Town, in cui più di quattro milioni di persone affrontano ogni giorno la penuria d'acqua, e in India, dove 600 milioni di persone vivono in zone con problemi di approvvigionamento di acqua e dove sono stati considerati interventi in ambito agricolo per alleviare il problema.

Una soluzione alla questione è l'uso di dissalatori che, usando svariati processi, consentono la produzione di di acqua potabile a partire da acqua salata estratta da mari, oceani o acqua salata. Nonostante ciò, uno dei grandi problemi della dissalazione è la gestione della salamoia (acqua con un'elevata concentrazione di sale) prodotta, a causa di un potenziale inquinamento termico, oltre a quello dovuto al sale. La distillazione a membrana (MD), un processo in fase di studio, può essere uno strumento utile per la soluzione del problema, grazie alla sua capacità di trattare acqua con grandi concentrazioni di sale consentendo anche il recupero di sostanze contenute all'interno dell'acqua. Inoltre, l'accoppiamento di impianti di dissalazione con fonti energetiche rinnovabili è un argomento the desta un'attezione crescente.

Si è sviluppato un modello che accoppi calore solare ottenuto tramite collettori solari sottovuoto con un processo di di distillazione a membrana a contatto diretto (DCMD) attraverso il software Simulink; esso include anche un accumulo termico e un bollitore ausiliario che gestiscono i periodi in cui la radiazione solare è assente. Si sono analizzati in maniera approfondita i risultati per la città di Torino, utilizzando anche un'analisi economica volta alla stima del costo dell'acqua prodotta. Dopo l'analisi di un caso standard, che garantisce una produzione di acqua di 5186 litri l'anno con una SF di circa il 60%, è stata condotta un'analisi di sensitività per capire l'influeza di alcuni parametri particolarmente rilevanti: i più importanti sono la tipologia di connessione dei collettori, la cui migliore configurazione è quella in parallelo, e la portata al componente di distillazione, che aumenta la produzione di acqua a spese della frazione solare. Tutti i miglioramenti individuati sono stati introdotti nel modello, garantendo un incremento nella produzione di acqua (6906 litri l'anno) e nella SF (quasi l'80%). A titolo di confronto è stato considerato il caso di Lampedusa: la dua differente posizione geografica consente una maggiore produzione d'acqua in tutte le analisi condotte.

Infine, i limiti del presente impianto e ulteriori possibili approfondimenti della questione sono delineati.

Contents

List of Figures

List of Tables

Chapter 1

Introduction

1.1 The water issue

Water is fundamental for the life on Earth. Among the large group of elements that ensure life on Earth, water is certainly the first one to come to mind. Its presence is relevant in more than one way: as an example, according to van Thienen et al. [84], water reduces lithosphere strength, that allows, in order, plate tectonics, inner cooling, the formation of a core, a "longstanding magnetic field", the presence of an atmosphere (since the magnetic field protects the planet from solar wind erosion), and at the end liquid water on the surface.

Considering the actual situation, since life has already spread towards the globe, water is one of the key elements for its survival. Apparently this is not an issue, since water covers around the 71% of our planet: nevertheless, the lack of water is globally arising as one of the issues of this century. It was estimated that more than 70 % of the global population experiences some form of water scarcity at least for one month a year, 66% (four billion) experiences severe water scaricity for at least one month a year; half a billion people live with severe water issues every day [64]. The following discussion has the aim to understand why.

1.1.1 Water scarcity

According to the World Economic Forum Global Risks Perception Survey 2017–2018, water crisis is one of the top ten global risks, as far as impact is concerned [44]. And even if water is not everywhere, it covers the 71% of Earth: but, on the total amount of water, only 2.5% of it is freshwater, and more than two-thirds of it is "blocked" in glaciers and ice caps. It remains less than 1% available freshwater: the most of it (more than 95%) is groundwater, and the remainig part is found for more than two thirds in ground ice and permafrost. The rivers, almost fundamental for water and human activity, account for only 0.49% of this very small fraction [77].

Available freshwater is not that abundant, and it is threatened by multiple factors that increase its demand and thus its depletion. Aqueduct Water Risk Atlas [54] shows the critical areas in which water access is yet compromised by a series of factors, ranging from human use, to climatic data and reputational issues, such as the media coverage of water-related matters.

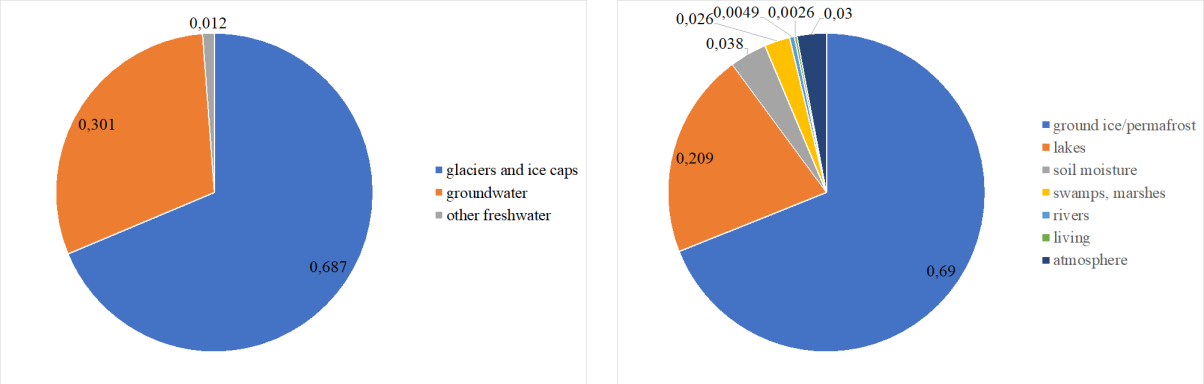

(a) Freshwater general distribution (b) *Other freshwater* distribution

Figure 1.1: Freshwater distribution

The resulting map shows a relevant high risk area; moreover, this area is believied to increase in the near future in every scenario (based on the IPCC 5th assessment report) considered in the analysis.

The two fundamental considerations that lead to a general worsening of water risk are fast depletion and slow reintegration.

The fast depletion is due to multiple causes [31] [64]:

- population growth. According to the United Nation 2017 Revision of World Population Prospects [27], the total population on Earth will increase from approximately 7.38 billion of individuals in 2015 to 9.77 billion in 2050 (and 11.18 billion in 2100). More people need more water to satisfy at least their basic needs.

- increasing living standards. A possible way of measuring this factor is the Gross National Income (GNI), which, starting from the Gross Domestic Product (GDP), integrates it considering the contribution of incomes produced in other countries, and it is generally preferred to GDP in the last years economic evaluations. This is the suggested choice to evaluate living standards according to the United Nations Development Programme in the computation of the Human Development Index (HDI) [73]. The analysis of the GNI per capita in the last thirty years confirms a global increase of it, and thus of the living standards [72].

- consuption patterns. The general increase of food consumption (estimated in kcal per capita per day) everywhere in the last fifty years [42] shows also the increase in the livestock consumption in terms of milk, eggs and diary products, which leads to an increase of land and water (for both the livestock and the pasture) that may become a concern [42].

- irrigated agriculture increase. In 2012, even though irrigated agriculture constituted the 20% of the cultivated land, it ensured the 40% of the food production, since it is often coupled with other tecniques to increase food production, such as the use of high-yield varieties of products and fertilizers and pesticides. In particular, the last fifty years were

characterized by a large usage of irrigation in Asia, leading to a significant reduction of undernourishment in the area [41]. In general, FAO states that 40% of developing countries uses irrigation for more than 20% of their irrigated soil [39], and this value is expected to increase [43].

Slow reintegration may appear as a complicate question. Due to water cycle, water on planet Earth is considered to be constant, so it may not be straightforward to understand why its reintegration may be an issue. So, it is necessary to analyse the sources from which freshwater is extracted.

Rivers, often used since they are the easiest way to withdraw water, are affected by this phenomenon. There are months in which almost all water is extracted for human use; the most critical areas which are expected to experience water shortage by 2050 are the Ganges Delta, the Arabian Interior and some rivers in West Africa [62].

As Figure 1.1a shows, the main exploitable water source is groundwater, i.e. water stored underground: over two billion people rely upon this source [22]. However, groundwater takes a very long time to achieve equilibrium [22] and its use experiences a large increase since 1990, due to the fact that it was the main way to compensate the water demand increase during these years [93]: this may lead to groundwater depletion [93]. It is indeed estimated that, in the year 2000, nonrenewable groundwater provided 20% of the global irrigation [92]. The term nonrenewable indicates "additional water gained by groundwater abstraction in surplus of groundwater recharge" [92]. Two areas in which this practise regards a relevant amount of nonrenewable groundwater are Pakistan and California [92]. A recent study ([46]) shows that modern (i.e. younger than fifty years old in terms of recharge) groundwater amounts to less than 6% of the total groundwater: the majority of it has a longer recharge time, so its natural reintegration is more difficult.

As a proof of the effective depletion, it was estimated through NASA satellite GRACE (Gravity Recovery And Climate Experiment) that 13 over 37 major groundwater reservoires in the world are highly, extremely or overstressed, meaning that (to various extent) the inlet water that recharges the aquifer is not able to compensate water extraction [11] [75]. Moreover, reliable estimations of groundwater amounts are not available at the present time, leading to an uncertainty of the remainig water that varies e.g. from 10 to 21000 years for one of the overstressed major aquifer in the world, the Northwest Sahara Aquifer System [11] [76].

Moreover, it was stated that hydrological droughts are influenced by groundwater responsiveness as mush as by climate, leading to a urgent need of mapping and proctect groundwater systems [91].

To deeply understand the causes of this massive use of freshwater, it is important to analyse the amount of water that every person needs in average. It is common thought that the water a person needs is destined to drinking and washing (themselves, clothes or dishes). But also the water consumption of every product used should be considered to obtain a reliable and complete water footprint (i.e. the quantity of water used directly or indirectly to obtain a product, including production processes, transport etc. [45]).

Considering only the tap water, daily consumption may appear limited, even tough a relevant dependence from the country considered is clear: while in Italy Istat estimated domestic water consumption at 175 liters per day per capita [82], the per capita estimation in the US amounts

to 80-100 gallons, or 300-380 liters per day [78]. Considering the water footprint, the average value is approximately 4000 liters per capita per day, considering that developed contries usually contribute with a value of around 5000 liters per capita per day, even though countries like the United States contribute with almost the double of the average value, 8000 liters per capita per day [45].

While it may be of some comfort to know that approximately 75% of this value on a global basis consists of green water (the part of precipitation which reamins in the soil [50]), while the remainder is distributed between blue (freshwater in rivers, lakes and aquifers[50]) and grey water (which indicates the amount of freshwater polluted excluding the black water[50]), 92% of the water yearly used regards agriculture, while industrial products and direct water consumption account for approximately the same value on the remaining fraction [45]. On average, 22% of water consumption regards traded goods: this partly justifies the huge water consuption of the US, since it is a country which exports lots of water intensive products [45]. For a visual representation of these data, see Figure 1.2.

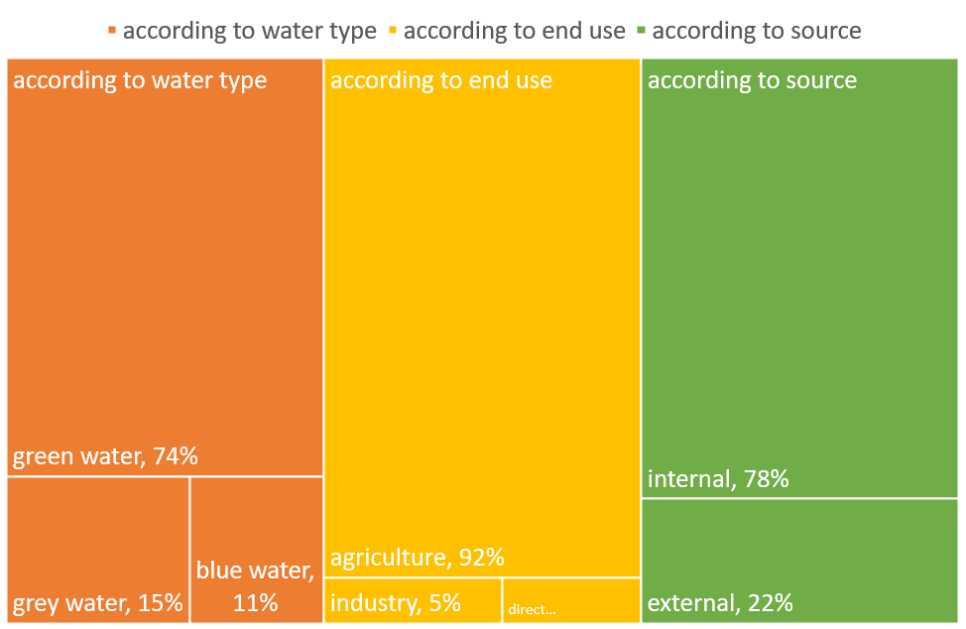

Figure 1.2: Water subdivision according to different paramenters (data from [45])

As it is possible to see in Figure 1.2, agriculture is the most critical water end user. As stated before, irrigated agriculture constituted the 20% of the cultivated land, and yet its water consumption is huge: FAO estimates that 1 000 - 3 000 m^3 of water are needed to harvest 1 000 kg of cereals [39], which represents 61% of harvested irrigated crops area [41]. On this terms, rice is a particular critical cereal to be planted. In fact, it is the most irrigated cereal (covering a half of the area irrigated for cereals growth), it requires, in addition, a constant layer of water on the ground [41] and it has one of the highest water needs [40]: FAO has identified a reduction of rice-cultivated land as a way to control agriculture increasing need of water [38]. This choice will be particularly challenging in some areas of the world, as Asia, where rice had a paramount

importance in decreasing hunger and malnutrition [25].

1.1.2 An example: Cape Town

Apparently, everything that was written before is a signal of a crisis far into the future, but it is not like that. A demostration is the situation of Cape Town, one of the biggest cities in South Africa, accounting for more than 4 millions inhabitants [48]. This city is indeed experiencing a drought of such proportions that it could be "the first time a modern city could have the taps run dry", according to CNN journalist David McKenzie [63].

The city is experiencing severe water restrictions from December 2015, asking citizens to use 100 liters of water a day at the end of May 2017 (with dam storages effective levels at 9.7%) [15], down to 50 liter per day in the end of January 2018, when the dams were at 16.3% of effective level [14]. The matter is so important that the day in which no more water will be available for the citizens has its own name: Day Zero, and that the first two trending topics on the city website are *Dam levels* and *Draft Water Strategy* [13]. Thanks to all the efforts made and a more favorable weather condition in the last period, 105 liters per person per day are allowed since 1 March 2019 [16].

The main causes of such a situation are [66] [23]:

- a growing population, which increases from 2.5 millions in 2006 to 4 millions in 2016 [48];
- a rapid changing in climate patterns with a desertification trend, as stated by the IPCC [19];
- ENSO, i.e. El Niño Southern Oscillation, which generates dryer than usual conditions [70].

This crisis was announced almost 30 years ago: a 1990 Water Research Study claimed a water crisis in 17 years and, despite a general worsening situation (the first water restrictions date back to 2005 [15]), no significant efforts were made during these years to differentiate the water source of the city [63]; so, the use of desalination plants and groundwater is planned but actually impossible since the plants are under construction [63] [16].

The most relevant information is that this water crisis will be a long-term problem for Cape Town rather that a short term one.

Figure 1.3: A poster from the Cape Town City to guide citizen during the Level 6 - 50 liter per person per day period of the drought crisis [16].

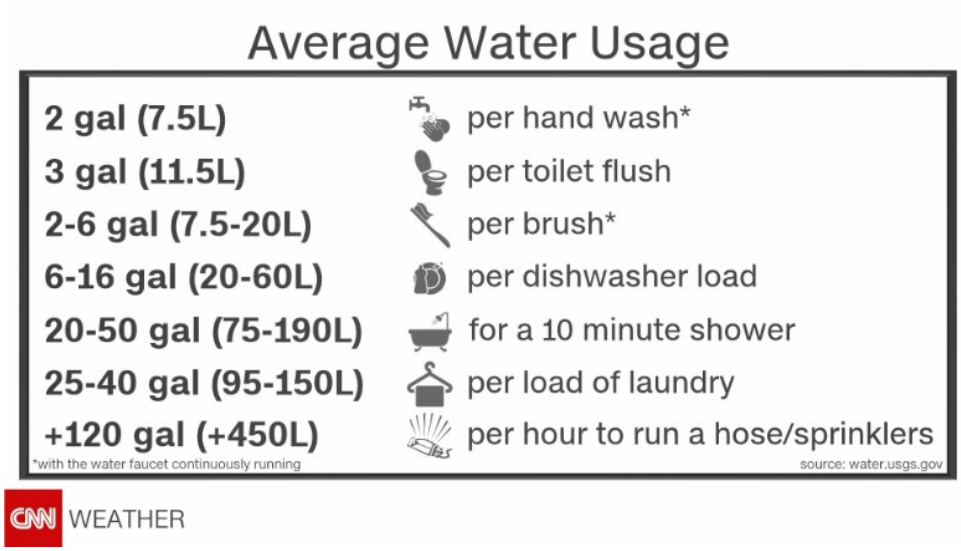

Figure 1.4: Average water use for daily actions ([23], data from [78]).

1.1.3 An example: India

The lastest estimate on Indian population claims that it amounts to almost 1 300 million inhabitants [29]. Almost half of them, 600 million, have to deal with water scarcity and due to it about 200 000 people die every year, 21 major cities are likely to run out of groundwater within netx year, and the estimated economic loss is estimated as the 6% of Indian GDP in 2030 [2]. Since the 80% of water demand is connected to agriculture [2], the reduction of its use is the key point of scientists and think-tanks promoted by the local government to provide tools and solutions to face the crisis. This choice is particularly consistent with the collected data: Indian farmers indeed use from 3 to 5 times the water used by their colleagues in the US, China or Israel to harvest the same amount of crop [2]. Moreover, the wheat/rice production, which was crucial to alleviate the malnutrition problem, has depleted freshwater resources due to bluewater extraction and a weakening monsoon, and a nutrient problem persists, since these two crops lack in components, like iron, which are fundamental for a correct diet [25].

Figure 1.5: Infographic showing actual water situation in India [2]

A study of the last year ([25]) proposes to change the cultivated crops to solve both problems at once. In fact, 20-30% of these water intensive crops (rice in particular) are planted in the northern areas of the country, where an extreme water stress is persistent and that are, in general, drought-prone areas: this choice exacerbates the water problem and threatens the area with a lack of food [2]. More in detail, rice water issue is connected to its own water requirement, while wheat is problematic since it grows during the rabi (non monsoon) season, so it is forcibly more dependent on blue water resources [25]. Despite this, the NITI - National Institution for Transforming India states that a high proportion of rain-fed agriculture in an area is not a good

sign, focusing on the implementation of micro-irrigation systems [2]. Besides the think-tank, a series of projects with NGOs and FAO were carried on during the last years, such as APFMGS - Andhra Pradesh Farmer-Managed Groundwater Systems, which arose consciousness about groundwater resources in a drought prone area of India [37]: estimates states that 10 millions m^3 of water were saved between 2005 and 2007 in the area [2]. There is a general hope that these countermeasures may be a good starting point to face the expected increase in water demand by 2050, which is expected to be close to 60% of the actual consumption.

1.2 Desalination technologies

One of the developed solutions to face the water crisis, in particular in places not far from seas, oceans or salt lakes, is desalination. That seems a logic choice since, as stated in subsection 1.1.1, the mayority of water on Earth is salted.

Since water and salt do not separate spontaneously, some kind of effort, i.e. energy, is neede to make this happen. According to it, it is possible to subdivide desalination processes into three main categories: the ones which use mechanical energy, the ones which use electrical energy, and the ones which use thermal energy (by far the most large group). For the technologies listed in bold in Figure1.6, a brief explanation of its key characteristics is provided. Some types of desalination processes, such as freezing and humidification/dehumidification, are present as concepts or only on experimental scale, and will be neglected; despite this, a brief description of the technologies listed in italics will be provided since, despite their scarce competitiveness, are fed by renewable sources.

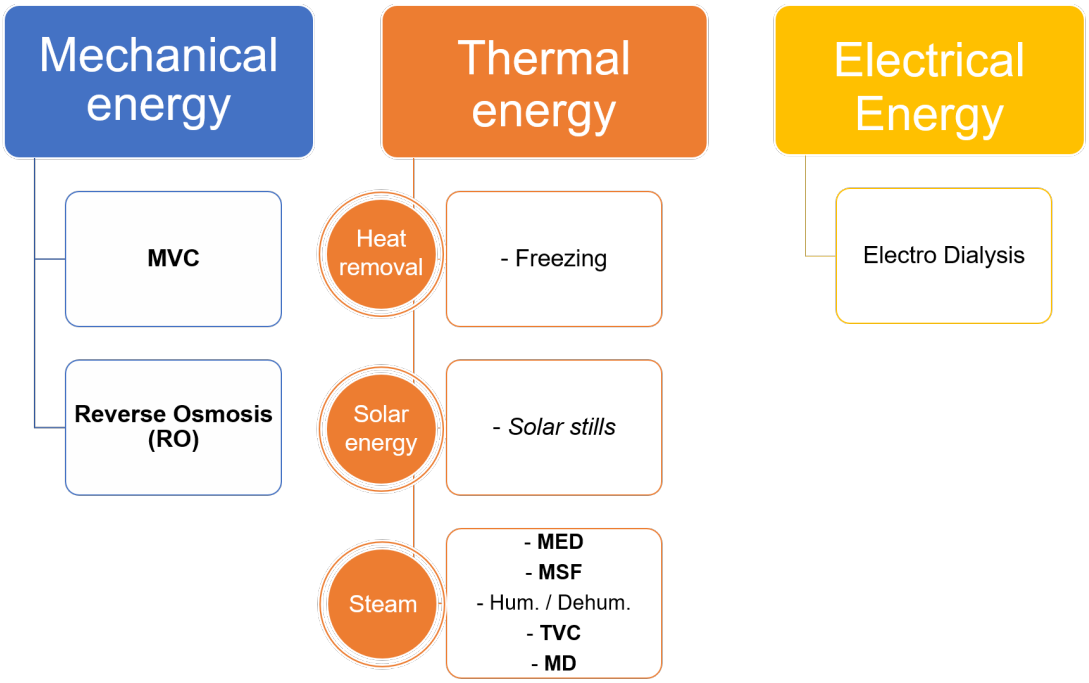

Figure 1.6: Desalination systems according to required energy [18]

Mechanical energy - MVC

MVC, or Mechanical Vapour Compression, is a system fed only by the electrical power needed for the mechanical compressor. The compressed vapour of pure water flows inside a series of tubes, while brine is distributed through a series of nozzles on their outside surface. A part of the saltwater injected through nozzles reaches the bottom of the component, but the other part evaporates, and so the salt present in saltwater is separated. The freshwater vapour flux thus obtained, further purified by a demister, is often used to pre-heat the saltwater, and the condensed product is finally collected [33] [49].

Despite it seemed a competitive technology at the beginning, the RO process is now generally preferred.

Reverse Osmosis

Reverse Osmosis is, at the present time, the leading technology for desalination. It is based, as the noun suggests, on the osmosis principle. Given a suitable semipermable membrane (which is a key component of the plant) which separates two solutions with the same solvent and a different solute concentration, the solvent spontaneously flows to the side where the concentration is higher. At the end of the process, the result is that the membrane separates two different quantities of a solution with the same solute concentration. The notion of osmotic pressure is fundamental for the osmosis: it is the pressure value (function of the temperature and the concentration of the solution) which, if applied to the more concentrated side of the solution,

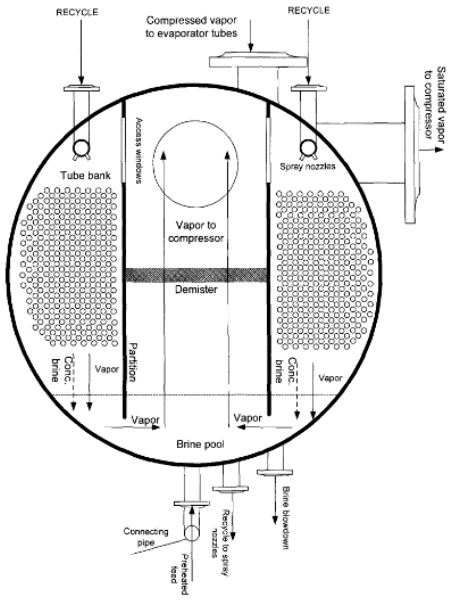

Figure 1.7: Single effect MVC - cross section of the evaporator. [49]

prevents osmosis to happen. It can be written as [21]:

$$\Pi = RT \sum_i \nu_i c_i \tag{1.1}$$

Osmotic pressure of seawater has a value of approximatley 2.5 MPa [21], while the operating pressure of a RO plant is generally below 7 MPa [34]: it is intuitive that, if the osmotic pressure can stop the process, a pressure greater than the osmotic pressure can reverse it, creating a flow (in the case under analysis) of pure freshwater (solvent) to the freshwater side (less-concentrated side), leaving a water with a higher salt concentration.

Membrane choice plays a fundamental part on the performance of such a plant, otherwise relatively simple. The most used polymers are cellulose acetate blends and aromatic polyamides, usually arranged in the convenient spiral wound [34]. In this configuation, where multiple membranes are linked to a permeate tube, and then wounded around it, 40 m^2 of active area per permeate tube can be obtained [34].

RO experienced a particular increase on the western market, where large installations were built in the last 20 years [34]; it accounts for approximately 50% of the total market [33].

Thermal energy: MED

MED, or Multiple-Effect Distillation, is a clever way to obtain a high heat recovery while producing freshwater, and can be used also in combinatio with MVC or TVC. It is made by a series of stages, called effects: evaporation of saltwater takes place in each of them, obtaining freshwater. In the first effect, saltwater is sprayed over tubes in which a compressed vapour, at a temperature usually lower than 70 °C, flows. The freshwater pressurized vapour thus produced

flows inside the tube of the following effect, allowing more freshwater to be extracted, and so on: an industrial plant can reach up to 12 effects [33].

This process is almost 500 years old and it was recently improved starting from the end of World War II and, even though it has not a big freshwater production compared to other systems, it has a marekt share particularly in the Gulf region [34].

Thermal energy: MSF

The Multi Stage Flash is by far the most used thermal-driven desalination technology: a single unit can provide freshwater for 300 000 people [33]. A typical plant consists of a series of flashing chambers, where flash evaporation occurs. For a better understanding, the discussion follows the saltwater flux. Seawater flows inside the plant from the last stage to the first, recovering heat from the process and thus increasing its temperature; the desired brine top temperature is guaranteed by a heat exchanger, usually fed by steam. Now, hot saltwater entering the first chamber experiences a pressure lower than its vapour pressure at that temperature: a flash evaporation occurs and the evaporation heat is transferred to the saltwater in the tube for its pre-heating; distillate and brine are separately collected and discharged; during winter, a part of the brine recirculates with new saltwater inside the system [33] [3].

Due to the enormous economic advantage of this kind of plant when built on a large scale (50 000-75 000 m^3/day), MSF plants are comeptitive, and widely diffused in the Gulf area [34].

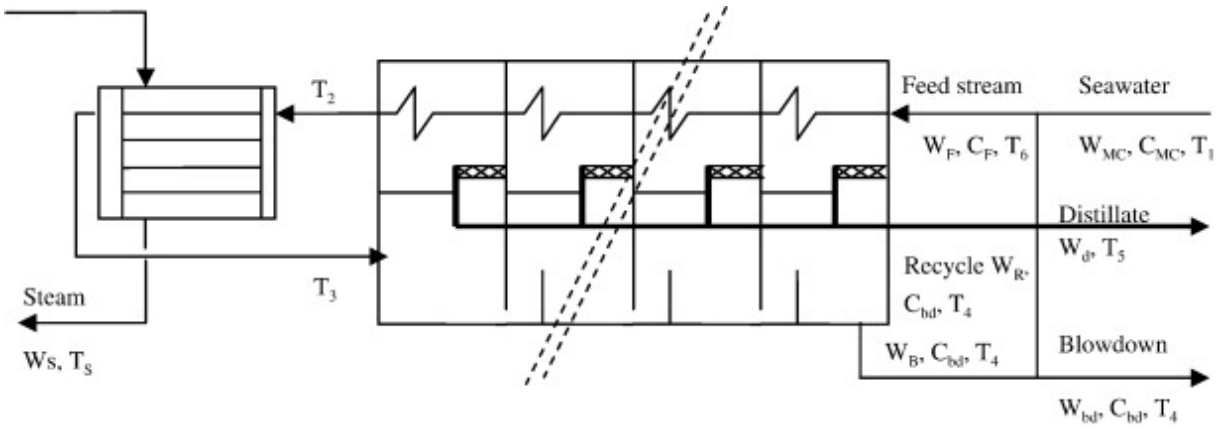

Figure 1.8: MSF conceptual scheme [3]

Thermal energy: TVC

Thermal Vapour Compression has the same concept of MVC, but in this plant compression is performed by a steam ejector, requiring no mechanical/electrical energy. This plant is often used coupled with MED, to increase its performance.

Thermal energy: MD

The Membrane Distillation process is the one on which this work is focused. It is a novel technology, based on the use of a microporous hydorphobic membrane, which allows water to cross it only as a vapour phase: since the membrane is hydrophobic, no liquid saltwater can flow to the freshwater side. So, hot saltwater below its boiling point circulates on the feed side, and its vapour can flow on the other cooler side, where a freshwater flux is present [18] [58]. Further details about this tecnology are provided in section 2.7.

There are four main types of MD technology [58]:

- Direct Contact MD (DCMD), where both membrane sides are in direct contact with a liquid, saltwater on feed side and freshwater on permeate side;
- Air Gap MD (AGMD), where an air gap is present between the permeate side of the membrane and the coolant fluid: permeate flux condenses on the coolant cold wall, reducing losses through the membrane and decreasing both energy consumption and permeate flux;
- Sweeping Gas MD (SGMD), where there is a gas flow with the role of stripping pure water vapour, taking it to an external condenser; this system allows a higher vapour flux;
- Vacuum MD (VMD), where vacuum is applied on the permeate side increasing the driving force of the process, allowing a general increase in permeate flux.

1.2.1 Renewable coupling

Since only 1% of the operative desalination plants is fed by renewable sources [47], it is worth exploring the possible strategies to implement this solution, since it can be particularly useful in remote areas or small islands, where access to conventional energy carriers might be challenging.

A very simple, but inefficient solution is the solar still. Its concept is easy: it is realized with an insulated basin full of saltwater exposed to the sunlight. The basin is covered with some transparent material that allows sunlight to reach the basin and, if well engineered, to aviod the dispersion of the reflected rays. The energy trapped heats up the water and the vapour, which condenses on the cover, is driven to permeate channels on the basin sides thanks to the inclined shape of the cover. This very simple concept is hindered by its cost [17].

Considering the renewable thermal power that can be obtained from the Sun, all thermal-driven processes can be fed by solar heat produced by solar collectors, concentrating or not-concentrating according to the required temperature: in general, the brine top temperature is barely over 100 °C, which is compatible with such technologies. Also the electrical-fed processes can take advantage of renewable sources, through PV (photovoltaic) systems, thermo-electric power plants coupled with high temperature collectors or wind power, or a combination of the abovementioned sources [47] [17]. The most used combinations so far are PV/RO and wind/RO, since the former technologies are consolidated, and RO is the leader desalination technology at the time being [86].

An example of the combination between solar thermal resources and MD systems (as the one on which this work is focused) is present on the Grand Canary Island within the framework of the MEMDIS EU project, as stated in [69]. The concept, even if pre-commercial, shows a

relevant series of advantages, such as the low temperature and ambient pressure operation, the high quality of the produced water and the minor impact of the seawater salinity [69].

1.2.2 The brine issue

It is estimated that desalination plants around the world can produce approximately 95.37 million m^3 every day; RO accounts for 69% of this volume (65.5 million m^3/day). These plants are generally located in some high income countries with dry climates and on small islands: almost half of the production is located in the Middle East and North Africa region [56]. A problem of these plants is the production, as a waste usually discharged into the sea, of a water with a relevant salt presence: the brine, that represents both an environmental and economical issue.

Salinity of the brine may be very high: considering a SWRO (seawater reverse osmosis) plant, its typical Practical Salinity Unit (PSU: 1 PSU=1000 mg/l) ranges between 65 and 85, which means it can contain twice the original concentration; other tecnologies, as MSF, diluite the exiting brine, obtaining a final concentration usually 15% higher than the entering one. Moreover, a difference in salinity implies a difference in density and, being it higher, brine is prone to fall to the seafloor, slowly dispersing. Thermal pollution may also be an issue, since the brine temperature is usually higher than the seawater one [60].

According to oceanografic conditions, care must be taken not to compromise aquatic environment; in fact, only a few marine species are able to face a relevant increase of salinity for a long period of time. Conversely, a thermal perturbation of this enviroment may promote or hinder the life of the local sea species; its effect has to be carefully studied. Anyway, most of the countries interested in seawater desalination have developed guidelines to control marine habitat conditions [60].

The last available data on brine production states that its amount is 141.5 million m^3/day, 49% more than the freshwater thus produced and almost 50% more than estimated [56]. A closer look to the composition of this value adds useful information: the Middle East and North Africa region, which produces around 48 million m^3/day, produces also 99.4 million m^3/day, the double of the freshwater produced and more than 70% of the global brine production. This is explained by the fact that Gulf region, due to thier huge oil production, historically uses thermal desalination and low recovery ratios (the fraction of feed water that is converted into freshwater); in particular, the worst technology as far as brine production is concerned is the SW-MSF (which globally produces 16.7 million m^3/day of freshwater and 60.1 million m^3/day of brine) [56]. Other countries produce as much brine as freshwater or, in the case of other high income regions, less than their freshwater production.

The most diffused way to dispose of the brine are, besides the sea/ocean injection, the injection on siutable wells or brine evaporation ponds [56].

Some solutions to handle the brine issue were proposed, such as diluite brine with power plant colling water or other alternative sources, to make it suitable for sea immission, systems to enhance brine mixing with seawater, metal recovery from brine. One of the most interesting proposals is the reuse of brine for aquaculture, turning a problem into an economic resource. It is in general a good choice to increase the recovery ration of the desalination plants, in order to produce less brine; that may not reduce the cost of its disposal due to its increased salinity.

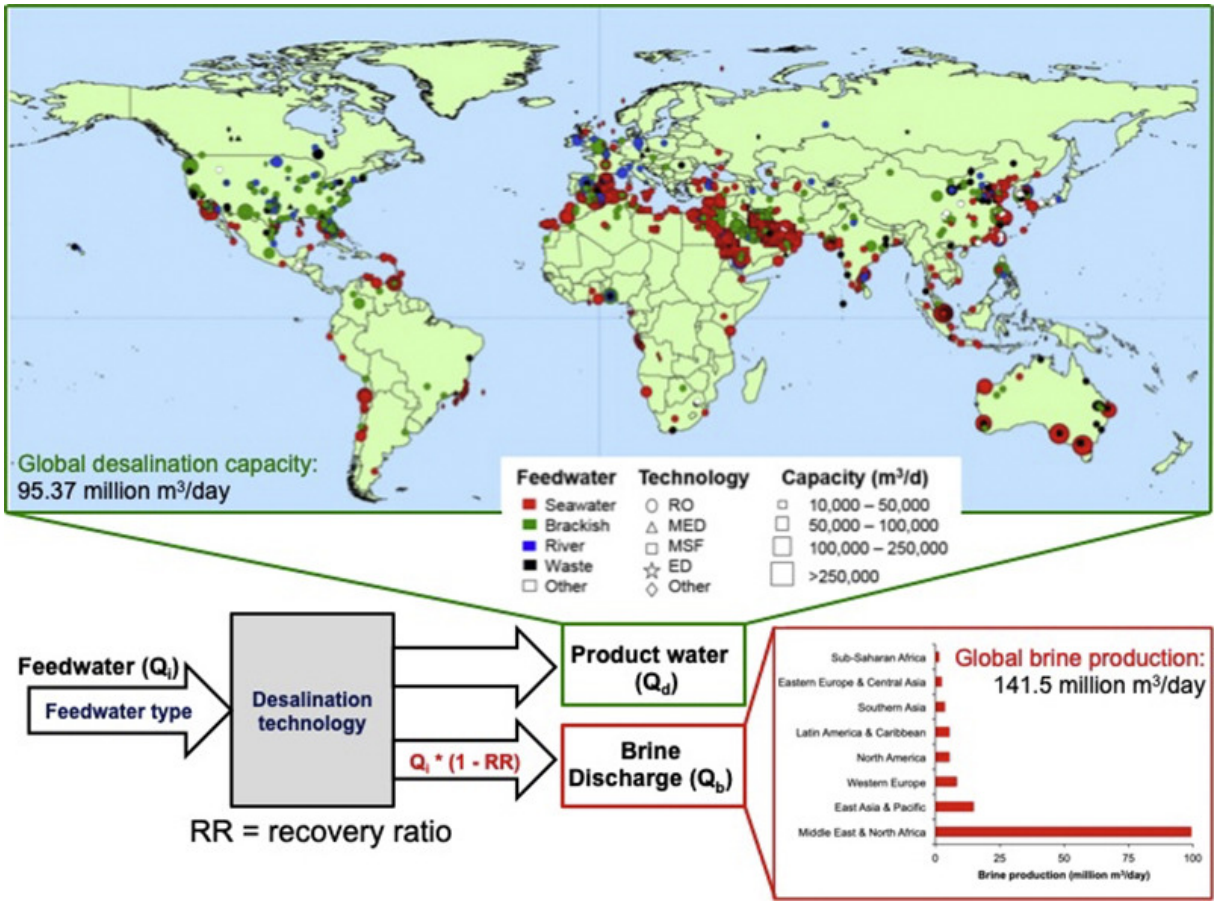

Figure 1.9: A scheme that successfully sums up some of the most relevant topics of this last section: desalination plant locations and technologies, and the brine issue, with a ficus on the biggest brine producers. [56]

1.2.3 MD: why it is a promising solution

After this analysis, a question remains unsolved: why may it be convenient to choose MD?

MD process, even if still at a R&D stage, has some interesting characteristics that, once the technology is further developed, may let it become a competitive technology in the desalination landscape.

Some of its advantages are:

- its salt rejection is very close to 100% [32], so it is preferentially employed when retentate concentrations are required due to its membrane characteristics [21];
- it can be integrated in a series of production cycles [21];
- it works at ambient pressure and low temperature: this implies

  - low material cost (membrane excluded) due to the low thermal performances requested;
  - easy coupling with alternative heat sources (RE, industrial waste heat, ...);
  - low maintenace cost.

- it has no instability issues related to rapid changes of temperature [58];

Moreover, some relevant applications are foreseen [32]:

- MD can be used for the treatment of concentrated brines (even though its permeate flux has a decline), in particular in combination with affirmed technologies such as RO and NF (Nano Filtration): more water is obtained and the high concentrated outlet feed flow can be used in a crystallization process to recover solutes;
- it can be integrated with solar, geothermal and nuclear energy (waste heat);
- it can be used for the treatment of wastewater to retrieve valuable compunds and to produce cleaner water, that may be discharged in the environment;
- it can be used for the production of high quality water for pharmaceutical and industrial use.

The abovementioned characteristics make MD technolgy worth investigating, even though it is a R&D process with uncertain costs and specific energy consumption [32].

Chapter 2

Model

The model has the aim to compute the total amount of freshwater that can be produced during a year. Since this system has a dynamic behaviour due to the variation of the irradiance (that determines the amount of heat that can be collected) and the inertia of the storage component, the software employed to realize the model is Simulink, a simulation tool with a good compatibility with Matlab, since they are both owned by Mathworks. Simulink includes every operation that can be performed in it inside a rectangle called *block* that accepts values through *Input ports* and returns the computed values through *Output ports*. The computed values, or more correctly *signals*, can be used as inputs in other blocks through graphical arrows. A set of operations can be contained in a particular block called *Subsystem*: in the developed model, it was used to group equations referred to each component of the plant. A useful block for the purpose of this analysis is the block *Matlab function*, that allows to write code directly into Simulink (this is particularly useful when the use of a *for* cycle is requested).

The composition of the system under study is the following:

- In the *Sun subsystem*, the irradiation per unit area of collector is computed, starting from the solar data and assumed azimuth and slope of the collector;
- the conversion from irradiation to a mass flow with a high temperature happens through the presence of a certain number of solar collectors, that are modeled in the *Collector subsystem*;
- a *Control logic subsystem*, coupled with the logic included in collectors and storage components, guarantees the best use of the obtained solar heat avoiding dangerous conditions for the components involved;
- after the flow in pipes, modeled in *Pipe subsystem*, the fluid enters the *Storage subsystem*, where heat is stored to be used inside the MD module;
- *Auxiliaries subsystem* ensures that the minimum temperature of the MD fluid is equal to a fixed threshold;
- *MD subsystem* mimics a MD unit behaviour, converting hot saltwater into cooler freshwater.

The model is shown in Figures 2.1 and 2.2.

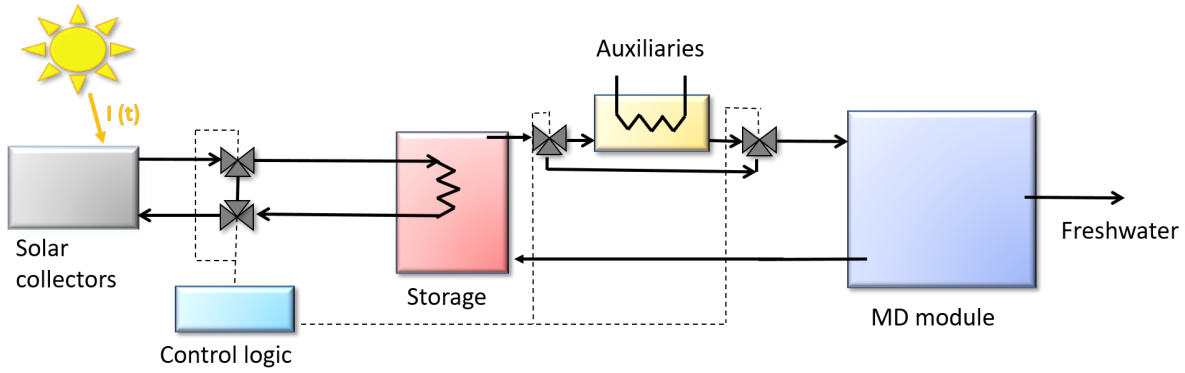

Figure 2.1: Model sketch; the most relevant components are shown

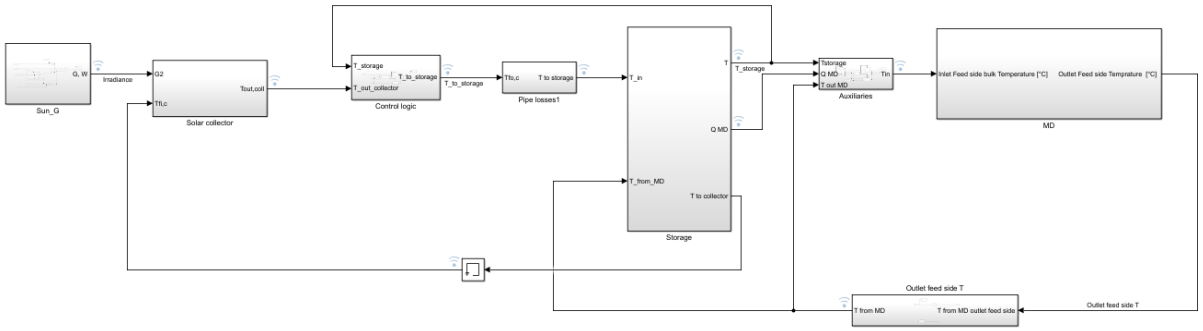

Figure 2.2: Simulink model; every subsystem represents a component of the real plant

In mode detail, the system developed in the following discussion works on hourly basis, i.e. one step of the system corresponds to an hour of system functioning: in fact, the solar input data (see Section section 2.1) are provided for every hour, and a more detailed analysis (every minute or every second) will only increment the computational time without providing relevant additional information. The system simulates five consecutive years of work: to ensure that the inital guess value of the starting temperature of the storage tank does not affect the final results, only tha data from the last year are used to perform the analysis (it was verified that five years is a reasonable amount of time to ensure the stability of the system). As far as the solving method to deal with the dynamic part of the system is concerned, Simulink automatically selects the one that suites best the model under study: in this case the used solver is *ode3*, the Bogacki-Shampine method.

2.1 Sun subsystem

The aim of the Sun subsystem is to compute the hourly radiation on the collector surface.

Input data are retrieved from the Photovoltaic Geographical Information System (PVGIS)© [71]. This tool, available thanks to the contribution of the European Commission, collects reliable data related to the solar resource through an analysis on satellite data [52]. For the purpose of this work, with the aim to obtain a robust analysis, data come from the construction of a Typical Meteorological Year (TMY), performed by the tool itself [74].

A TMY is a fictitious year which is able to forecast climatic data for a year in a specific location thanks to analysis performed on such data for a relevant number of years (at least ten). The tool provided by PVGIS© elaborates 10 consecutive years of hourly data to obtain a TMY which is made up picking, for every month, the most representing one among the considered in the analysis. The data thus retrived useful for this work are the dry bulb temperature, the Global Horizontal Irradiance GHI (i.e. the global irradiance on a horizontal plane), the Diffuse Horizontal Irradiance DHI (i.e. the radiation received by a horizontal plane due to scattering) and the Beam Normal Irradiance BNI (i.e. the irradiance on a surface normal to its direction, without scattering).

Being the last three elements irradiances (in W/m^2) and not radiations (in J/m^2, or far more often in kWh/m^2), the hourly radiation on the collector will be obtained through two steps: at first, the irradiance on the collector surface is computed, and then the radiation is retrived under the assumption that the irradiance remains constant during the hour in which it was measured (as performed in [52]).

The equation which calculates the irradiance on a tilted surface G is [95]:

$$G = BNI \cos\theta + DHI F_{c-s} + \rho GHI F_{c-g} \tag{2.1}$$

where:

- θ is the angle of incidence of BNI on the surface (in the present case, the collector), its cosine allows the computation of the fraction of BNI able to reach the surface ;
- F_{c-s} is the collector-sky view factor:

$$F_{c-s} = \frac{1 + \cos\beta}{2} \tag{2.2}$$

- ρ is the albedo, i.e. the fraction of the global irradiance which is reflected back by the ground and reaches the collector;
- F_{c-g} is the collector-ground view factor:

$$F_{c-g} = \frac{1 - \cos\beta}{2} \tag{2.3}$$

- β is the slope, i.e. the angle between the surface and the horizontal plane.

$\cos\theta$ is usually calculated through the following relation[30]:

$$\cos\theta = \sin\delta\,\sin\phi\,\cos\beta\,-\,\sin\delta\,\cos\phi\,\sin\beta\,\cos\gamma + \cos\delta\,\cos\phi\,\cos\beta\,\cos\omega\,+\cos\delta\,\sin\phi\,\sin\beta\,\cos\gamma\,\cos\omega + \cos\delta\,\sin\beta\,\sin\omega \quad (2.4)$$

where only the positive values have to be considered, since the negative ones indicate that the Sun is behind the surface. In this equation:

- δ is the declination, i.e. the position of the Sun at noon with respect to equator plane, and it varies between -23.45°(N) and 23.45°;
- ϕ is the latitude (positive towards North);
- γ is the surface azimuth angle, i.e. the angle between the South direction and the projection of the normal of the surface on the horizontal plane (positive towards West);
- ω is the hour angle, considering that Earth rotates on its axis 15°per hour (negative in the morning).

Declination is usually found through the approximate Cooper formula [30]:

$$\delta = 23.45\,\sin\left(360\frac{284+n}{365}\right) \quad (2.5)$$

where n is the day of the year (e.g. January 1st is 1, February 1st is 32, and so on).

The output of this subsystem is the irradiance on the collector for every hour, that will be the input of the next subsystem.

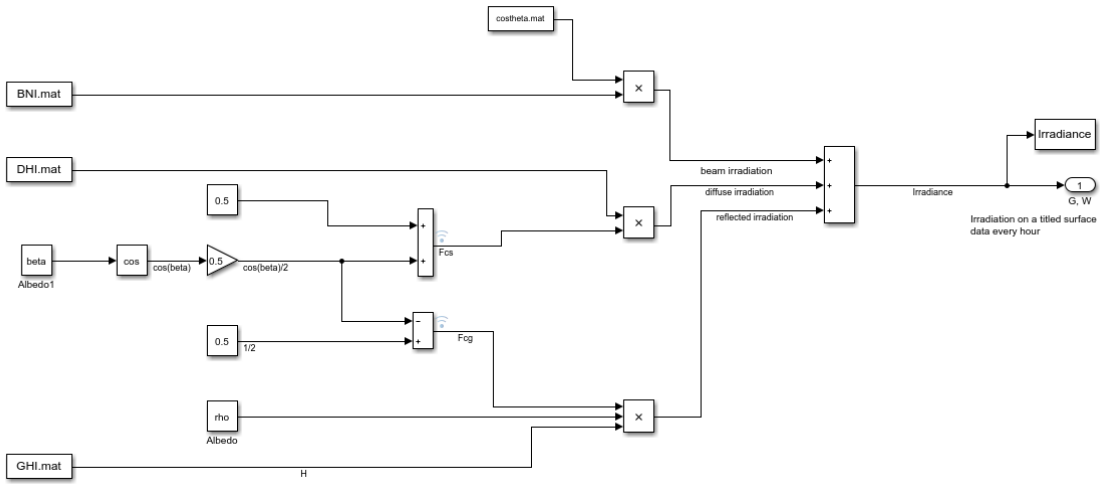

Figure 2.3: Simulink model of the Sun Subsystem

2.2 Collector subsystem

The collector subsystem is the component whose aim is to transform the irradiance coming from the Sun in a fluid flow at high temperature.

A solar collector is a peculiar kind of heat exchanger, which receives heat through solar radiation and delivers it to a stream of water or, less often, air or other Heat Transfer Fluids (HTF) that are meant to feed Domestic Hot Water (DHW) plants, low-temperature space heating or air conditioning or low-temperature industrial application of any kind. From the suggested applications it is easy to guess that the temperature of the fluid exiting the component is low, usually between 70 and 160 °C, depending on atmosferic conditions and performance of the collector itself. Collectors are usually placed on roofs or walls in houses and buildings, or on the ground in case of major installations, always with the foresight to avoid any effect of shading.

Solar collectors may be classified in two main categories according to their shape: Flat-plate collectors (FPC) and Evacuated tube collectors (ETC). They are both non concentrating devices, i.e. they are not able to focus the radiation they receive to increase it and obtain higher temperatures as output, and they are fixed, i.e. they lack the equipment to track the Sun rays in a way that they are always normal to collector surface. These characteristics are the main responsible of the abovementioned low output temperature.

Despite these similarities, these two categories differ due to other features. The FPC is usually made of some transparent cover, that reduces losses and protects the absorber plate and the undelying tubes in which water to be heated flows. Everything is surrounded by suitable insulation. This system allows temperature to rise until 100-120 °C [61]. The main issue of this configuration is the top dispersion due to convection between the glazing surface and the absorber one: since a solar collector receives heat through radiation, it is impossible to use standard insulation material on the top of it, because they do not fulfill the transparency requirement. So, to reduce such a dispersion, in ETC each tube with its absorber plate is contained in a cylindrical glass cover with vacuum inside: due to this peculiarity these collectors are also known as Vacuum tube collectors (VTC). This solution allows an exiting temperature of 140-160 °C [61]. This solution has a disadvantage: due to the cylindrical shape of the cover, VTC have a bad optical efficiency (i.e. the fraction of solar radiation able to reach the absorber plate through the cover). Part of the solar radiation is not collected because there are no absorber plates in the gaps between the cylindrical covers, and this behaviour is more relevant when the incident rays are normal to the absorber surface.

One of the key parameters of a solar collector is its efficiency η, defined as [30]:

$$\eta = \frac{\int \dot{Q}_{u,coll}\, dt}{A_{coll} \int G dt} \tag{2.6}$$

where:

- $\dot{Q}_{u,coll}$ is the useful power retrieved from the collector, in W;
- A_{coll} is the collector area, in m^2.

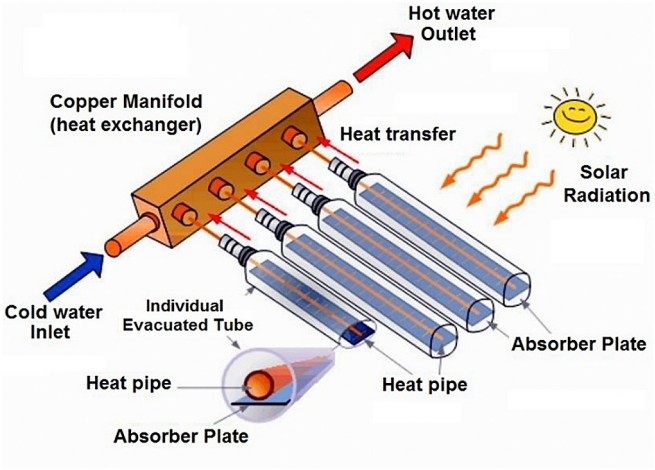

Figure 2.4: VTC schematics [55]

$\dot{Q}_{u,coll}$ can be calculated through [30]:

$$\dot{Q}_{u,coll} = A_{coll}[G - U_L(T_{pm} - T_{amb})] \tag{2.7}$$

where:

- U_L is overall loss coefficent, in W/(m^2 K);
- T_{pm} is the mean (absorber) plate temperature, in K or °C;
- T_{amb} is the ambient temperature, in K or °C.

Since T_{pm} is not easy to retrieve, solar collector manifacturers usually provide the efficiency in this form, which is the basis of the standard EU collector efficiency formulation:

$$\eta = \eta_0 - c_1 x - c_2 G_k x^2 \tag{2.8}$$

where:

- η_0 usually represents the optical losses due to the glass cover;
- x is:

$$x = \frac{T_{m,coll} - T_{amb}}{G_k} \tag{2.9}$$

$$T_{m,coll} = \frac{T_{in,coll} + T_{out,coll}}{2} \tag{2.10}$$

- G_k is a constat value, equal to 800 W/m^2.

For the particular case of this work, $T_{m,coll}$ has been calculated for each step starting from the inlet and outlet temperature of the collector in the previous step though the block *Memory*.

So, the final set of equations solved in the Collector subsystem is:

$$\dot{Q}_{u,coll} = \eta \, A_{coll} \, I_T \tag{2.11}$$

$$T_{out,coll} = T_{in,coll} + \frac{\dot{Q}_{u,coll}}{\dot{m}_{coll} c} \tag{2.12}$$

where:

- I_T is the irradiation on the collector during an hour in J/h, computed as:

$$I_T = G \times 3600 \tag{2.13}$$

- $\dot{m}_{coll}$ is the collector mass flow rate, in kg/s;
- c is the specific heat of the HTF, in J/(kg K).

The chosen collector is the model VTK 1140/2, manifactured by Vaillant [88]. The most significant parameters for the model are listed in Table 2.1. In Figure 2.5 a comparison between VTK 1140/2 and VFK 155 V [89] (also manifactured by Vaillant, see Table 2.2) efficiencies is performed. It shows what stated before: at lower temperatures (i.e. at lower x) the FPC has a better performace due to its redued optical losses. With the increase of temperature also the convective losses increase, thus undelying the advantages of a VTC in such conditions.

	VTK 1140/2
η_0,%	64.2
c_1, W/(m^2/K)	0.885
c_2, W/(m^2/K^2)	0.001
absorbing surface, m^2	2.0
volume flow, l/h	48

Table 2.1: Data of collector VTK 1140/2 [88]

	VFK 155 V
η_0,%	85.0
c_1, W/(m^2/K)	3.77
c_2, W/(m^2/K^2)	0.015

Table 2.2: Data of collector VFK 155 V [89]

The HTF which flows in the collector considered is a mixture of 20% propylene glycol in water, a common practice to obtain an antifeeze solution[24]. The properties of water, glycol and the mixture are listed in Table 2.3.

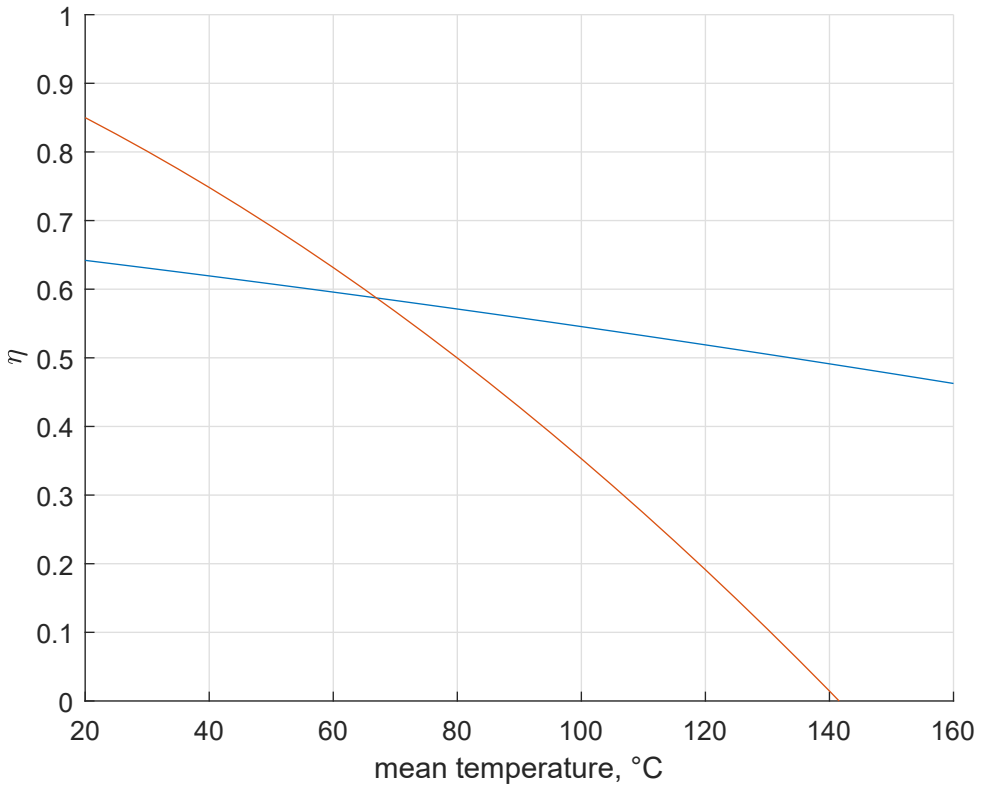

Figure 2.5: Comparison between VTK 1140/2 and VFK 155 V collector efficiencies

	Water [85]	Glycol [85]	HTF
specific heat, J/kgK	4186	2480	3843
density, kg/m^3	1000	1036	1007
dynamic viscosity, Pa s	10.7×10^{-4}	5.79×10^{-4}	9.72×10^{-4}
thermal conductivity, W/(mK)	0.599	0.201	0.519

Table 2.3: Properties of the fluids in the system under analysis

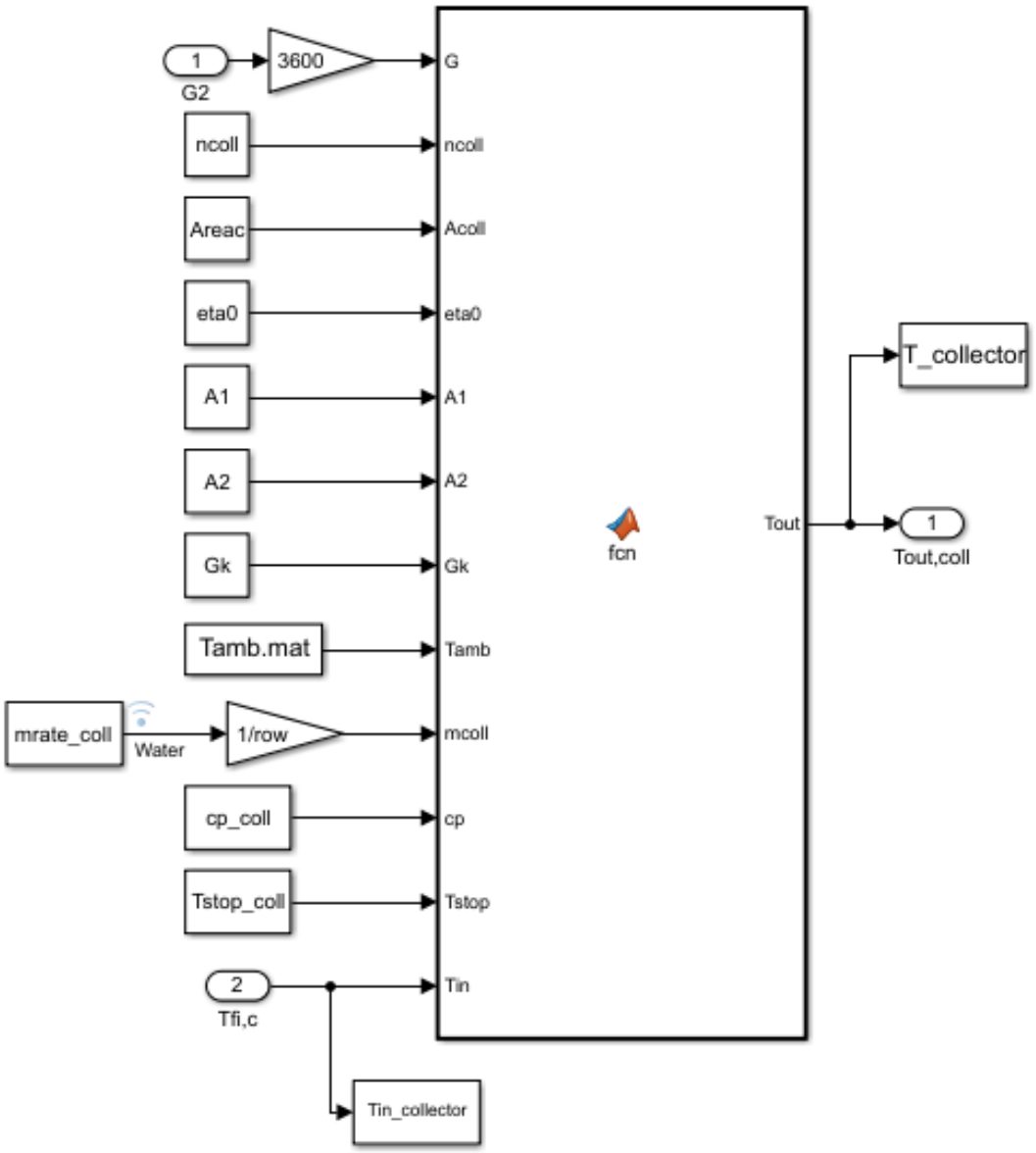

Figure 2.6: Simulink model of the Collector Subsystem

2.3 Pipe losses subsystem

This subsystem mimics the heat dispersions due to the motion of the HTF from the collector to the storage tank.

It is supposed that the collector is on top of a four-floors building and the storage is placed at the ground floor. The dimension of the pipe is the one of the connection diameter indicated in the data sheet of the collector (see [88]), and it is hypotetically insulated through a certain thickness of glass wool. All data are listed in Table 2.4.

length of the pipe, m	12
pipe diameter, m [88]	15×10^{-3}
insulation thickness, m	1×10^{-4}
thermal conductivity of glass wool, W/(mK) [85]	0.039

Table 2.4: Data used to define the pipe losses model

Since the thermal conductivity of the insulation material is known, the next step is the computation of the convection heat transfer coefficient. To do so, the following equations are used [53]:

$$Nu = \frac{hd}{k} \tag{2.14}$$

where:

- h is the convection heat transfer coefficient, in W/m^2 K;
- d is the tube diameter, in m;
- k is the heat conductivity, in W/m K.

Nu is the Nusselt number, which represents the ratio between conduction and convection in a fluid. Considering an internal flow and forced convection, as it is inside the tube, it is equal to:

- if the flow is laminar:

$$Nu = 3.66 \tag{2.15}$$

- if the flow is turbulent or in transition region (in the last case Nu will be overestimated):

$$Nu = 0.023 Re^{0.8} Pr^n \tag{2.16}$$

In the previous equation:

- Re is Reynolds number, which represents the ratio between inertia and viscous forces:

$$Re = \frac{\rho v d}{\mu} = \frac{4\dot{m}_{coll}}{\pi d \mu} \tag{2.17}$$

- Pr is Prandtl number, which represents the ratio between momentum and thermal diffusivity:

$$Pr = \frac{c\mu}{k} \tag{2.18}$$

- n is equal to 0.3 if the fluid is cooling (as in the present case) or 0.4 if it is heating;
- ρ is the density, in kg/^{3};
- v is the fluid mean velocity, in m/s;
- μ is the dynamic viscosity, in Pa s.

It is supposed that the insulation surface has the same temperature of the enviromnent, that is a conservative assumption. In this way, the heat dispersed in a infinitesimal portion i, that can be reasonably assumed as at the constant temperature T_{in}, is equal to:

$$\dot{Q}_{disp,i} = K A_{in} (T_{in,i} - T_{amb}) \tag{2.19}$$

$$K = \left[\frac{1}{h} + r_i \frac{log(\frac{r_e}{r_i})}{k_{ins}} \right]^{-1} \tag{2.20}$$

where:

- $\dot{Q}_{disp,i}$ is the dispersed heat in the infinitesiaml portion i of the tube, in W;
- K is the global heat transfer coefficient W/m^2 K;
- A_{in} is the internal area of the pipe, in m^2;
- r_i is the internal radius of the pipe (without the thermal insulation), in m;
- r_e is the external radius of the pipe (with the thermal insulation), in m;
- k_{ins} is the thermal conductivity of the thermal insulation, in W/m K.

Considering the HTF that flows inside the pipe in the abovementioned infinitesimal portion, the dispersed heat is also equal to:

$$\dot{Q}_{disp,i} = \dot{m}_{coll} c_{HTF} (T_{in,i} - T_{out,i}) \tag{2.21}$$

And the outlet temperature of an infinitesimal portion is the inlet temperature of the subsequent one. The outlet temperature of each pipe portion and, for the last portion, of the pipe that will flow into the storage is equal to:

$$T_{out,i} = T_{in,i} - \frac{1}{\dot{m}_{coll} c_{HTF}} [K A_{in} (T_{in,i} - T_{amb})] \tag{2.22}$$

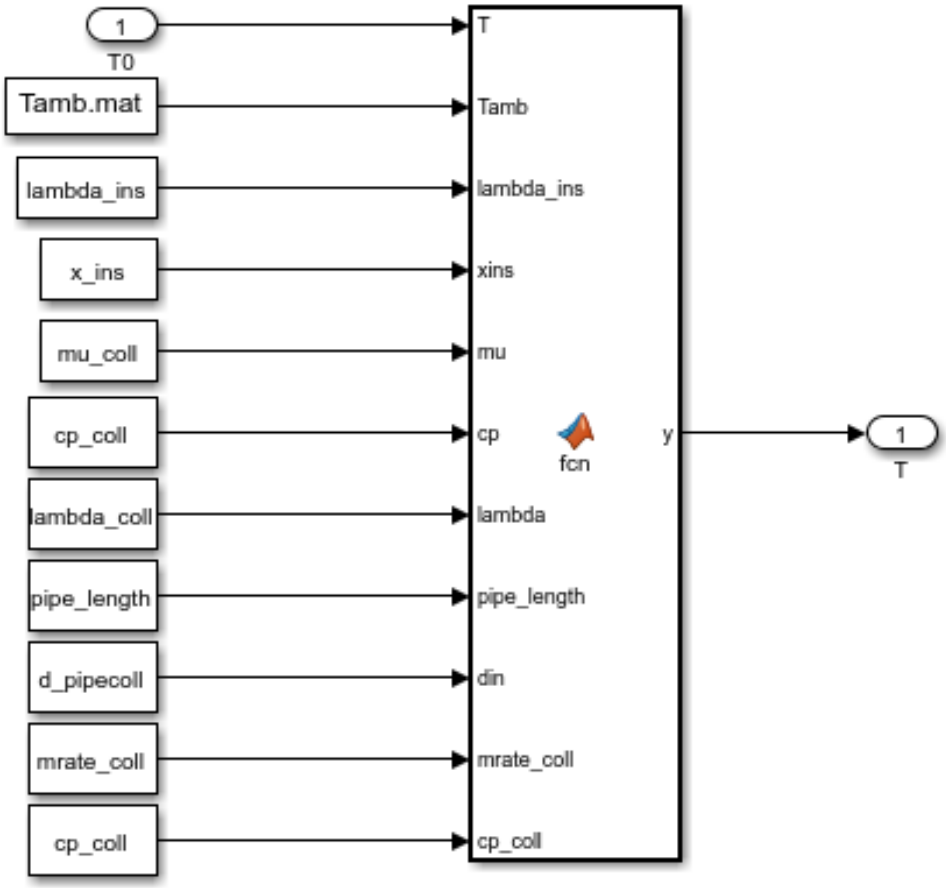

Figure 2.7: Simulink model of the Pipe losses Subsystem

2.4 Control subsystem

The control subsystem represents the work of a control unit that regulates the flows inside the collector and MD circuit. It is usually made with a series of thermostats and a control unit that compares these signals, activating or deactivating the solar pump and thus allowing the HTF from the collector to flow towards the storage, and from the storage to the MD unit.

This unit performs a number of controls to fulfill a series of requirements that is possible to divide into two main categories:

- controls to protect the components of the circuit from extreme conditions (e.g. too high temperature);
- controls to ensure that the termodynamic condition are suitable for the purpose of the

component (e.g. the storage is cooled instead of heated by collector HTF).

The total control process is performed in various steps:

- The first step, that is performed in the Collector subsystem, check that the outlet temperature of each collector is not higher than the maximum temperature set for the collector and the fluid safety; if so, the maximum temperature set is considered to be the outlet temperature of this component.
- The second step, that is performed in this subsystem, checks if the HTF in the collector is heated or not, i.e. if it is convenient to let it flow or not. Usually, the control logic compares the outlet temperature of the collector with the storage temperature or, if the storage is stratified, one of the bottom layers. If the difference between these two temperatures is at least positive (usually, bigger than a certain fixed value, among 2 or 5 degrees) HFT is allowed to flow, it is not otherwise. The relation used is:

$$T_{in,st} = \begin{cases} T_{out,pipe} & T_{coll,pipe} \geq T_{st} + 2 \\ T_{st} & otherwise \end{cases} \tag{2.23}$$

  The last case mimics the absence of a flow in the storage from the collector.
- The third step, which is performed in the storage subsystem, checks the temperature inside the storage. Due to construction reasons, the water inside this component has to be kept below a certain threshold defined as T_{stop} (for further explanations, see subsection 2.5.1). So, if the water inside the storage has already reached this threshold, the solar pump is deactivated and HTF does not flow.
- The fourth step, also perfomed in the storage subsystem, compares the storage temperature with the outlet feed temperature. If the latter has a higher value than the former, the MD contribution in the storage is neglected. Inded, since the saltwater flowing in the storage will be cooled down instead of heated up, that flow goes in the Auxiliary subsystem to obtain the desired temperatue increase.

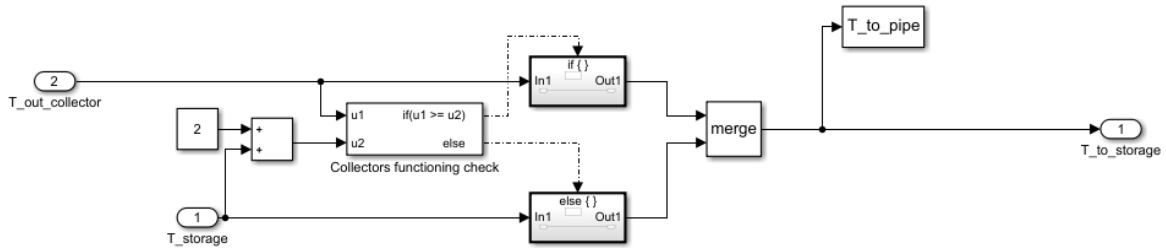

Figure 2.8: Simulink model of the Control logic Subsystem

2.5 Storage subsystem

2.5.1 Storage tank

The storage subsystem is the component where the heat is stored to be later used for fresh water production. It usually consists of a tank full of a substance characterized by a series of features: in fact the relation that expresses the amount of heat stored in the storage is:

$$Q = mc(T - T_0) \tag{2.24}$$

where:

- Q is the energy stored, in J;
- $m = \rho V$ is the mass of the storage, in kg.

In general, the goal is to maximise the energy stored keeping the volume as low as possible. If the useful temperature is set at a specific value or in a predetermined range, usually connected to the application of the stored heat, the storage medium is chosen in a way that it meets the following criteria:

- The medium has not to experience changes of state during the charge or discharge (unless it is specifically requested: this is the case of the *latent heat storage*), in particular between the liquid and vapuor state. In this case, the variation of density ρ of the substance is such that it may become a critical issue for the structural stability of the tank which contains the selected medium.
- Related to the previous point, the temperature range in which the medium is expected to operate has to match the temperature range in which it is in the desired physical state.
- The medium has to have the highest specific heat possible; this is particularly useful to reduce the envelope of the system.

Besides these fundamental thermodynamic requirements, the choice of the storage medium is related to:

- a good thermal conductivity, to make easier the heat transfer process;
- high safety requirements, such as low toxicity and corrosivity, that determines a lower cost as far as the tank material and the related equipments are concerned and in general reduces damages in case of an incident;
- a long life, that reduces the needs in terms of medium susbstitution;
- a reduced cost, to make it affordable.

Considering all these requirements, it seems obvious to consider the water as the medium of choice for this use. It has indeed a huge specific heat, one of the highest in nature ($c_{water} = 4186\ J/kgK$), even though its density is still relevant. The derisory cost of it, its safety and

the vastity of its use (drinking, cooking, cleaning, and in fields like agriculture and industry in general) that makes availabe a enormous variety of components for its storage and transport are additional good reasons to use it.

The case presented in this work has some peculiarities that makes the choice of the storage medium not obvious. The main purpose of this system is indeed to produce fresh water. This need may arise in two different situations.

- In the first case (as the present one), the system is used for research purposes. If it is not possible to obtain saltwater directly from its source (a saltwater lake, a sea or an ocean), it has to be obtained and then stored somewhere, then there is the need to thermally feed it with the heat produced through the collector before it enters the MD unit and crosses its membrane.
- In the second case, the sistem is used for production purposes. Even if the saltwater may be continuously obtained from its source without the need of a dedicated storage, to use water for storage purposes (i.e. not using it for the needs it is intended) may lead to some concerns.

Due to these considerations, it was supposed to use saltwater itself as a storage medium. This avoids the need of a further heat exchanger (HE) that allows heat to flow from the storage medium to saltwater itself, leading to additional thermal losses. Some thermodynamic properties at the reference temperature are listed in table 2.5 [18]. For a detailed list of saltwater properties and the way to compute them, see A.

reference saltwater salinity, ppm	35 000
density, kg/m^3	1024
specific heat, kJ/(kgK)	3.998

Table 2.5: Saltwater thermodynamic properties at the reference temperature of 20 °C [18]

2.5.2 Mixed storage

The storage is cosidered to be not stratified, i.e. in a mixed configuration. This implies making tha assumption that the temperature of the mass of fluid inside the tank depends only on time, and not on any spatial coordinate: $T = T(t)$. A first principle analysis is carried on to underline the various contribution to the sistem and their importance, providing useful values for the sensitivity analysis (see section 3.5). The contribution to the system are:

- The positive contribution of the heat flow coming from the collector. Since the HTF in the collector is water with an addition of propylene glycol and the fluid inside the storage tank is saltwater, the heat trasfer is mediated by a heat exchanger. The one considered in this work is a plate heat exchanger. Through the data provided in [10], its main parameters where found (see section B.1).

In order to understand the fraction of heat able to cross the HE, a $\epsilon - NTU$ analysis was performed, under the assumption that the HE is in counter-current flow. The details can be found in section B.1.

According to the discussion abovementioned, the heat flow from the collector into the storage is equal to:

$$Q_{from\,coll} = \varepsilon \dot{m}_{coll} c_{coll} (T_{from\,coll} - T_{stor}) \tag{2.25}$$

The temperature of the flow that comes back into the collector is computed as:

$$Q_{from\,coll} = \dot{m}_{coll} c_{coll} (T_{from\,coll} - T_{to\,coll}) T_{to\,coll} = T_{from\,coll} - \frac{Q_{from\,coll}}{\dot{m}_{coll} c_{coll}} \tag{2.26}$$

- The negative contribution of the losses towards the environment. Despite the insulation of the storage tank, being it a sensible storage, it dissipated part of its energy. According to the information retrieved by the storage tank data sheet, the losses wil be simply computed, since given in kWh/24h (convertible in J/s or J/h):

$$Q_{loss,stor} = Q_{loss} \tag{2.27}$$

- The negative contribution of the heat flow going to the MD unit. A flow of saltwater at the storage tank temperature flows towards the auxiliaries and the MD unit feed side, from this side it comes back to the storage tank at a lower temperature. It is easily computed as:

$$Q_{to\,MD} = m_{to\,MD} c_{sw} (T_{stor} - T_{out,feed}) \tag{2.28}$$

The overall equation is:

$$\begin{aligned} m_{stor} c_{sw} \frac{dT_{stor}}{dt} &= Q_{from\,coll} - Q_{loss,stor} - Q_{to\,MD} \\ &= \varepsilon \dot{m}_{coll} c_{coll} (T_{from\,coll} - T_{stor}) - Q_{loss,stor} - m_{to\,MD} c_{sw} (T_{stor} - T_{out,feed}) \end{aligned} \tag{2.29}$$

To solve it, an integration of the component $\frac{dT_{stor}}{dt}$ is performed through the apposite Simulink component.

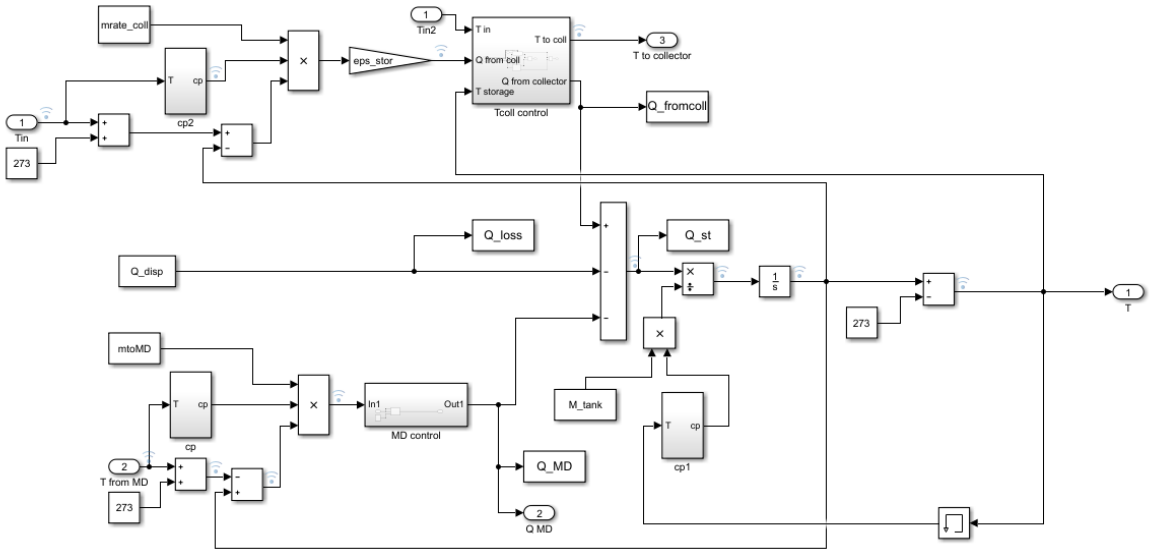

Figure 2.9: Simulink model of the Storage Subsystem

2.6 Auxiliaries subsystem

The auxiliaries subsystem is the component which guarantees that the minimum temperature in the MD unit is equal to $T_{MD,min}$=50 °C, to ensure that a minimum water production always occurs. So, this system operates only when the storage tank temperature is below this threshold, heating only the water that is flowing in the MD unit. Its contribution is computed as:

$$Q_{aux} = \begin{cases} m_{to\,MD} c_{sw} (T_{MD,min} - T_{stor}) & if\, T_{stor} < T_{MD,min} \\ 0 & otherwise \end{cases} \tag{2.30}$$

The computation of the total heat produced by this unit is of utmost importance for the estimation of the solar fraction SF (see the following chapter).

The component chosen for this application is aguaFLOW exclusive VPM 20/25 /2 W manifactured by Vaillant [87], which is able to guarantee 25 l/min of water at the desired temperature.

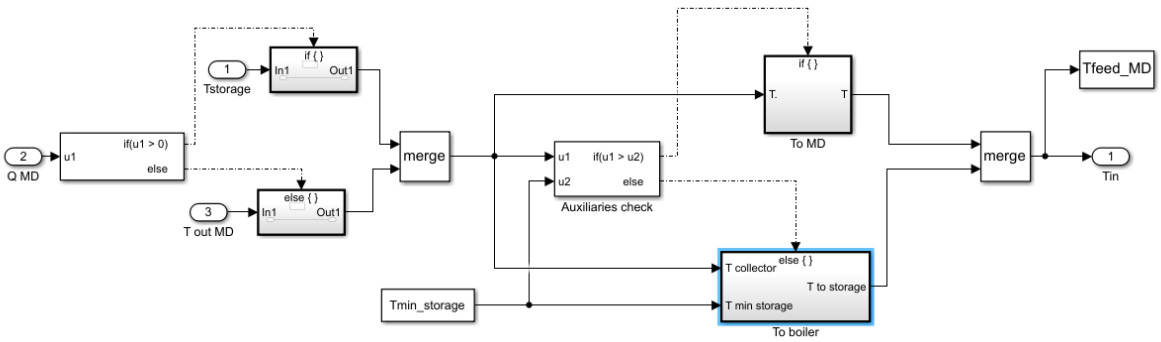

Figure 2.10: Simulink model of the Auxiliaries Subsystem

2.7 Membrane Distillation subsystem

The MD unit is the fundamental component of this plant, since it is the one that ensures the conversion of hot saltwater into freshwater. This happens due to the peculiarities of the membrane from which the process takes its name. This polymeric membrane has two main relevant features:

- it is microporous, i.e. its pores are significantly bigger than the dimension of a water molecule (0.1-0.4 µm [58]);
- it is hydrophobic.

This implies that, since the membrane is hydrophobic, the liquid saltwater cannot flow from one side of the membrane (the feed side) to the other (the permeate side), but, being the pore size relevant, vapour water can flow through it. So, pure water molecules flow from one side to the other generating a small flow of freshwater, while a part of water and all the salt in it remain confined on feed side. The amount of freshwater produced depends on the quantity of water vapour present on both sides, and so on the vapuor tension p_v [58] [4]:

$$N_w = C\Delta p_v \tag{2.31}$$

where:

- N_w is the mass transferred per unit area of the membrane, in kg/(s m^2);
- C is the membrane distillation coefficient in kg/(s m^2 Pa);
- Δp_v is the difference of vapour pressure, in Pa.

Since the membrane has large pores, it lets water form a meniscus in each pore on each side of the membrane; care must be taken to avoid that these menisci make contact, hopelessy destroying the process, ensuring that the LEP (Liquid Entry Pressure) reamins higher than the hydrostatic pressure [58]. The membranes with such characteristics used in this process are PTFE, PVDF and PP [58].

Using a MD process provides a series of advantages:

1. no additional pressure gradient is strictly needed, since the system operates taking advantage of the vapour pressure;
2. no high temperatures are needed, as opposed to other desalination processes, since a difference in vapuor tension is present also at low temperatures (such as 30-40°C);
3. directly connected to point 2., low quality heat can be used, such as the one coming from other processes, solar heat, etc.;
4. directly connected to point 2., less expensive materials can be used, due also to less severe corrosion issues [4];
5. it can process also brine water (water with a very high salt content) such as the one coming from the RO process [4];
6. the system has also been used to purify water from heavy metals [4] [97] and radioactive waste [4] [96].

It also has a series of disadvantages, of which the most relevant are:

1. it has a low permeate flux (i.e. the flux that flows to the permeate side) compared to other desalination technologies;
2. the permeate flux depends heavily on the feed temperature;
3. high thermal losses due to conduction. [4]

Now, it is considered with more attention every contribution to equation 2.31.

The membrane distillation coefficient C is the key characteristic of the membrane, i.e. it depends heavily on the material of the membrane and on its structure, while it has a low dependence on temperature. In general, the membrane coefficient depends on two other coefficient, each describing a mechanism of the water vapour mass transfer, that are:

- the Knudsen diffusion, that is supposed to be relevant when the pore size is small, so the most relevant collisions are the ones between the water vapour molecules and the pores walls in the membrane [4] [28]. It is usually considered to be the dominant phenomenon [58] [36]. One of the ways to define the Knudsen coefficient C_{Kn} is [58] [57]:

$$C_{Kn} = \frac{2\pi}{3}\frac{1}{RT}\left(\frac{8RT}{\pi M_w}\right)^{1/2}\frac{r^3}{\tau\delta} \tag{2.32}$$

  where:

  - R is the ideal gas constant, equal to 8.314 J/(mol K);
  - T is the temperature, usually considered as the mean between the temperatures at the membrane surfaces, in K;
  - M_w is the molar mass of water, equal to 0.018 kg/mol;

- r is the pore radius, in m;
- τ is the pore tortuosity, dimensionless;
- δ is the membrane thickness, in m.

In particular, the term $\left(\frac{8RT}{\pi M_w}\right)^{\frac{1}{2}}$ represents the average velocity of the pores [58].

- the molecular diffusion into air, more relevant in continuum region, described through the diffusion coeffiicient C_D, one of the forms in which it may be expressed is [58] [57]:

$$C_D = \frac{\pi}{RT}\frac{PD}{P_{air}}\frac{r^2}{\tau\delta} \tag{2.33}$$

where:

- P_{air} is the air pressure in the membrane pore, to be computed, in Pa;
- D is the diffusion coefficient, in m^2/s;
- P is the partial pressure of air and water vapour, in Pa.

The general equation that links these coefficents is[58]:

$$\frac{1}{C} = \frac{1}{C_{Kn}} + \frac{1}{C_D} \tag{2.34}$$

Anyway, in the following the membrane distillation coefficient will be assumed as constant (in particular, independent from temperature). To do so, it is needed to choose a membrane. The data considered in this work along with their sources are listed in Table 2.6 (data from source [35] are referred to the Aquastill membrane referred to as PVDF1).

thickness, µm ([35], table 8)	77
ε, % ([35], table 8)	83
average pore diameter, µm ([35], table 5)	0.2

Table 2.6: MD membrane properties

From these data, consulting other sources or though suitable correlations, it is possible to retrieve C, that, given the material and the pore size, is equal to $14.5 \times 10^{-7} kg/(m^2 Pas)$ ([4], table 4).

The difference of vapour pressure Δp_v explains the strong connection between the permeate flux and the temperature. The vapour pressure varies with temperature as represented in Figure 2.11. It is worth noticing that the higher the temperature, the higher the increase in vapour pressure: the advantage of working at higher temperature is even more relevant.

The temperatures abovementioned are the ones of the membrane surfaces, that are unknown: a model is needed to retrieve them and, to do so, heat transfer in the MD unit has to be studied.

Three main mechanisms of heat transfer occur [81]:

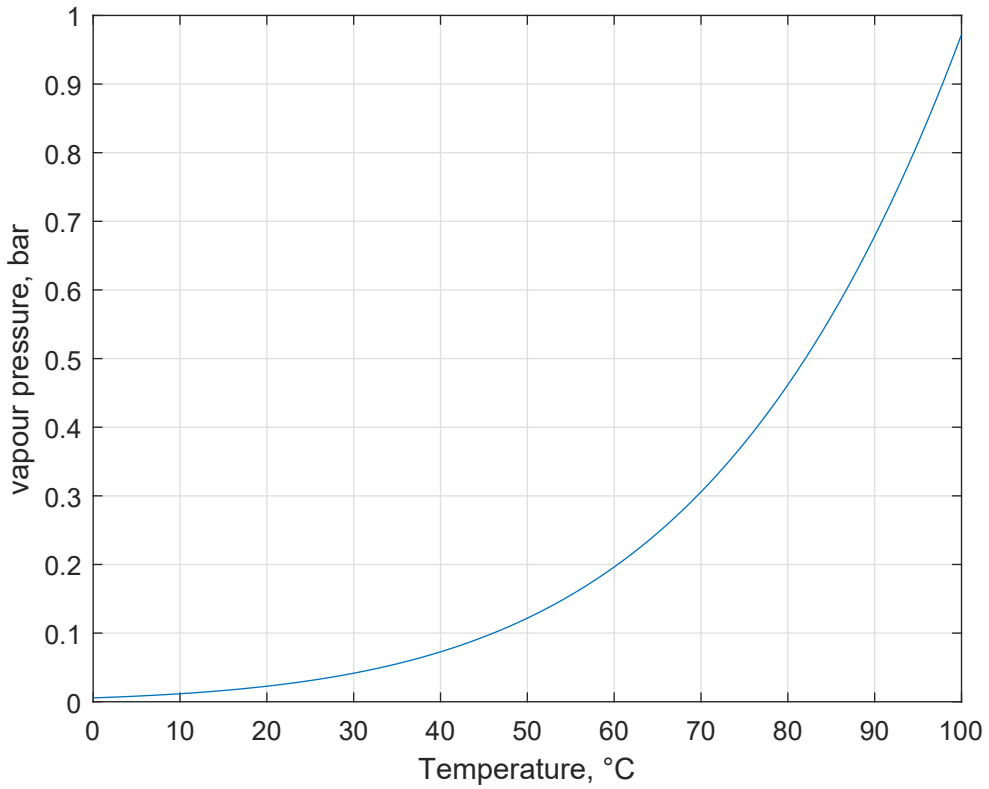

Figure 2.11: Vapour pressure for saltwater (see Appendix A for further information)

- convection heat transfer between the feed bulk and the membrane surface on feed side:

$$q = h_f(T_f - T_1) \tag{2.35}$$

where:

  - q_f is the heat per unit area, in W/m^2;
  - h_f is the convective heat transfer coefficient referred to the feed side, in W/(m^2 K);
  - T_f is the feed bulk temperature of the fluid, in °C or K;
  - T_1 is the temperature of the membrane surface on the feed side, in °C or K.

- heat transfer in the membrane due to conduction and latent heat of vapour molecules:

$$q = N_w \Delta H_v + \frac{k_m}{\delta_m}(T_2 - T_1) \tag{2.36}$$

where:

  - ΔH_v is the latent heat of water, in J/kg;
  - δ_m is the membrane thickness, in m;

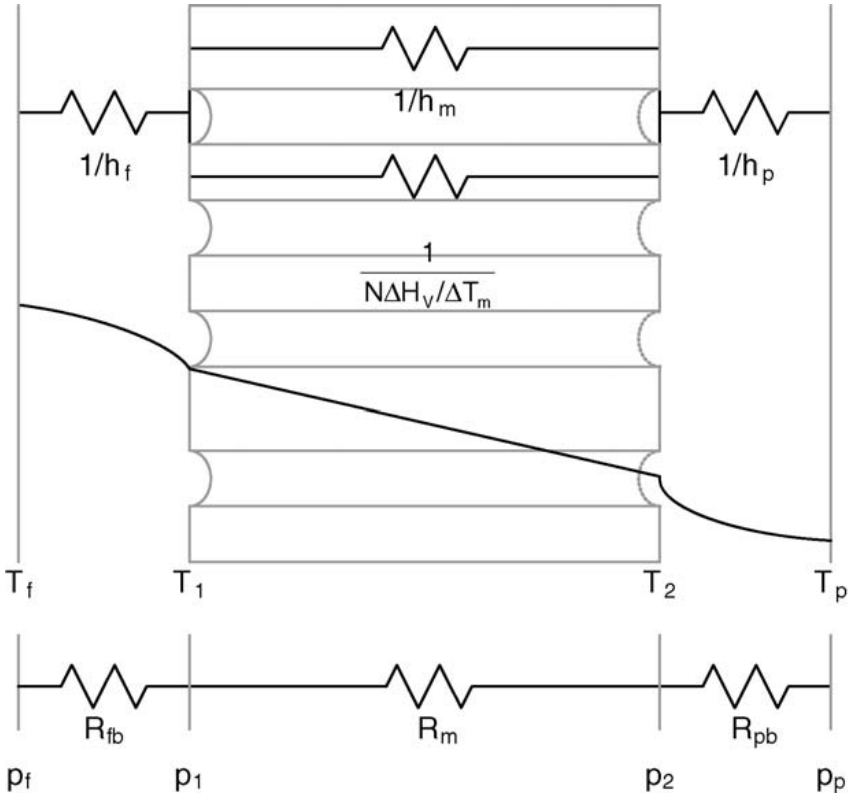

Figure 2.12: A model of thermal resistances, temperatures and transoprt resistances in a MD module [81]

– T_2 is the temperature of the membrane surface on the permeate side, in °C or K.

The membrane thermal conductivity k_m is estimated as 0.27 W/(mK) [4].

- convection heat transfer between the membrane suface on permeate side and the permeate bulk:

$$q = h_p(T_2 - T_p) \tag{2.37}$$

where T_p is the permate bulk temperature of the fluid, in °C or K.

Writing k_m/δ_m as h_m, the following equations are obtained to find T_1 and T_2:

$$T_1 = \frac{h_m(T_p + (h_f/h_p)T_f) + h_f T_f - N\Delta H_v}{h_m + h_f(1 + h_m/h_p)} \tag{2.38}$$

$$T_2 = \frac{h_m(T_f + (h_p/h_f)T_p) + h_p T_p + N\Delta H_v}{h_m + h_p(1 + h_m/h_f)} \tag{2.39}$$

So, $N = f(T_1, T_2)$, $T_1 = f(N)$ and $T_2 = f(N)$: to take into account this interdependence an iterative procedure has been performed, to ensure the correct value of all variables.

Since the temperature of the feed bulk is known since it comes from the storage tank and the auxiliaries, the temperature of the permeate bulk is fixed at 20 °C (to mimic the behaviour of the chiller unit, that guarantees such temperature), the membrane heat transfer is defined as well as the water latent heat, and the permeate flux was previously defined, the two heat transfer coefficients h_f and h_m have to be evaluated. To estimate Nu (see section 2.3 for futher details) are used:

- as far as laminar flow is concerned ($Re < 2100$), the Graetz-Leveque correlation:

$$Nu = 1.86\left(Re\, Pr \frac{d_h}{L}\right)^{0.33} \tag{2.40}$$

- as far as turbulent flow is concerned, the Dittus-Boelter correlation (see Equation 2.16).

At this point, the only missing element is the outlet feed side temperature $T_{f,out}$. To compute it, a first principle analysis has been carried on on the feed side:

$$\dot{m}_{to\,MD} c_{sw}(T_f - T_{out,f}) - (N_w A_m)\Delta H_v - h_m A_m(T_1 - T_2) - Q_{loss} = 0 \tag{2.41}$$

where:

- A_m is the membrane area, in m^2, equal to 0.05 m^2[6];
- Q_{loss} are the system losses, evaluated from experimental data as[8]:

$$Q_{loss} = -780.0180 + 33.1084\, T \tag{2.42}$$

with T in °C, validity range between 50°C and 80°C.

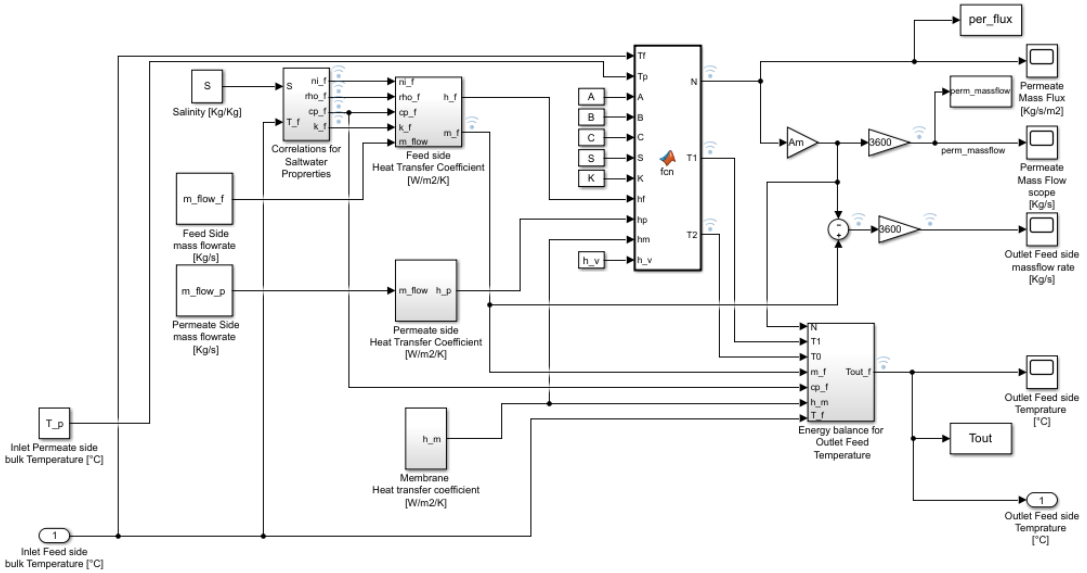

Figure 2.13: Simulink model of the MD Subsystem

Chapter 3

Results

3.1 Standard case

3.1.1 Input data

The model thus composed was used to perform an analysis on the water that can be produced in the city of Turin, Italy. The city is placed at a latitude ϕ=45°. The list of input data is in Table 3.1.

Solar data	
φ	45°
β	φ
Υ	0°
Collector data	
number of collectors	6
number of rows	1
Storage data	
storage volume, l	150
MD unit data	
feed side flow rate, l/h	100

Table 3.1: Input data for the standard model in Turin

The abovementioned data are educated guesses on the best configuration, which will be analysed in detail in the following paragraphs. The reasoning behind Table 3.1 are:

- the slope equal to the latitude and the azimuth equal to 0 (head towards South) are often close to the best to obtain the highest SF[65];
- such number of collectors should provide approximately 6 kW of thermal power[90];
- only one row should provide higher temperatures;

- a reduced storage volume should help to keep a high temperature to be sent to the storage;
- the feed side flow rate is an intermediate value in the range guaranteed by the control system.

3.1.2 Output data

The following paragraphs will analyze the output of each subsystem to better understand the system behaviour and the key parameters for sensitivity analysis.

Sun subsystem

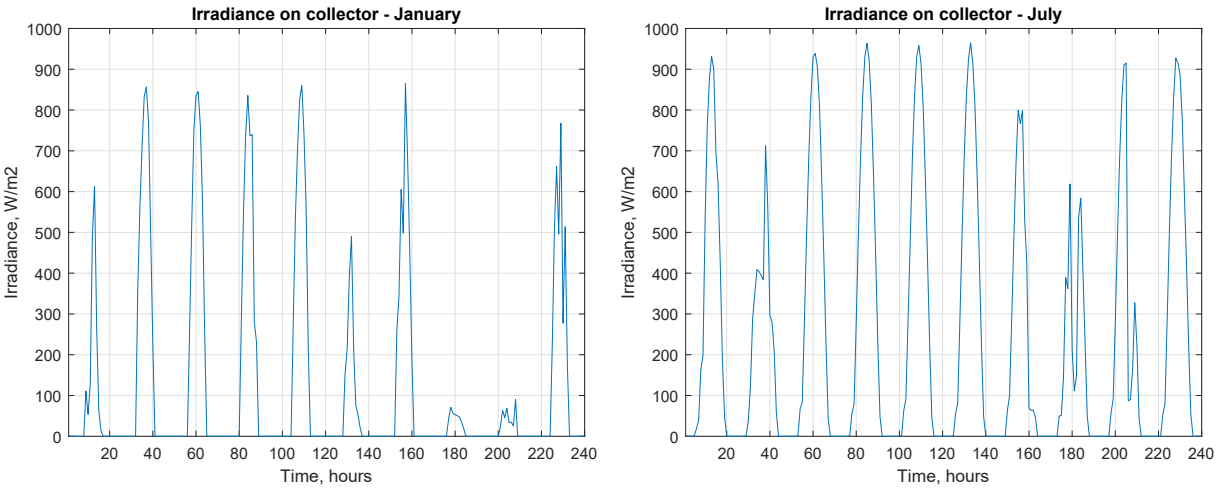

(a) First ten days of January

(b) First ten days of July

Figure 3.1: Irradiance per unit area of collector

In Figure 3.1, the irradiance (in W/m^2) per unit area of collector is represented. The maximum values are, as expected, close to 800-1000 W/m^2, and are higher in July (or, in general, in summer months). Besides, the weather influence is evident: despite a general maximum irradiance value of approximately 850 W/m^2 on the first month of the year, on the 8^{th} and 9^{th} of January this value is almost null (below 100 W/m^2) and so the solar contribution during these days is roughly negligible.

Considering the whole year, Figure 3.2 shows the irradiance per unit area of collector for the 15^{th} day of each month.

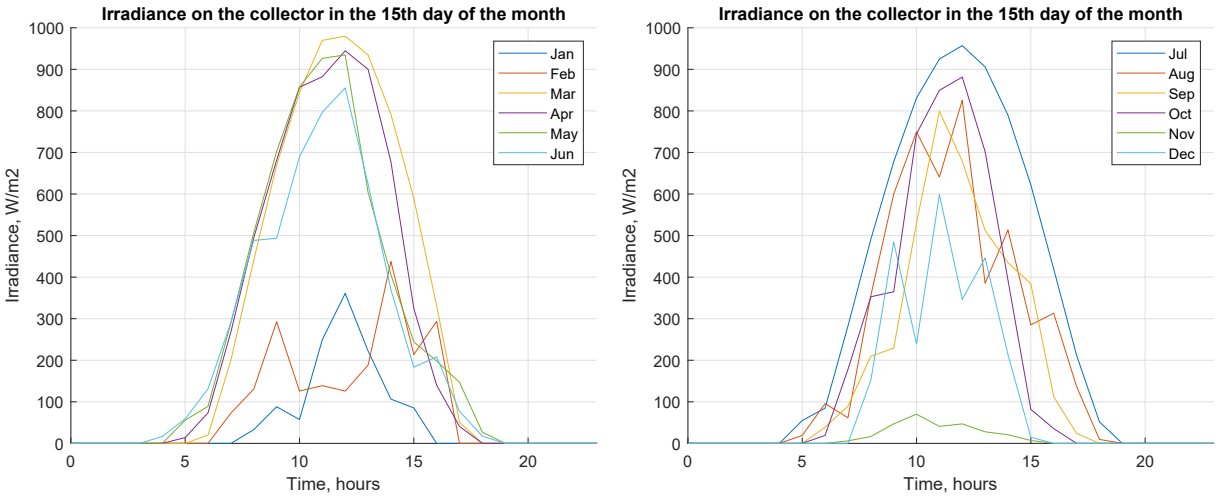

Figure 3.2: Irradiance per unit area of collector on the 15$^{\text{th}}$ day of each month

Collector subsystem

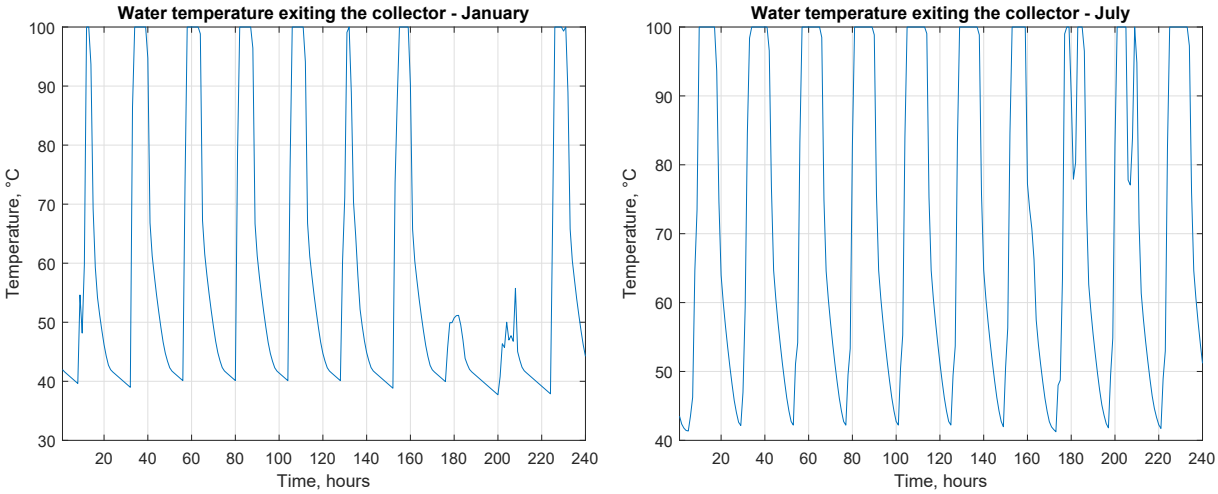

(a) First ten days of January

(b) First ten days of July

Figure 3.3: Collector outlet temperature

The outlet collector temperature is plotted in Figure 3.3. The temperature reaches easily the temperature of 100 °C when a significant irradiance is present. During night, it reaches a value close to 40 °C (slightly higher in summer), due to the absence of solar heat. When the irradiance is very low due to bad weather, the temperature increase is reduced, and it barely reaches 50 °C (minimum temperature set for MD feed side).

Storage subsystem

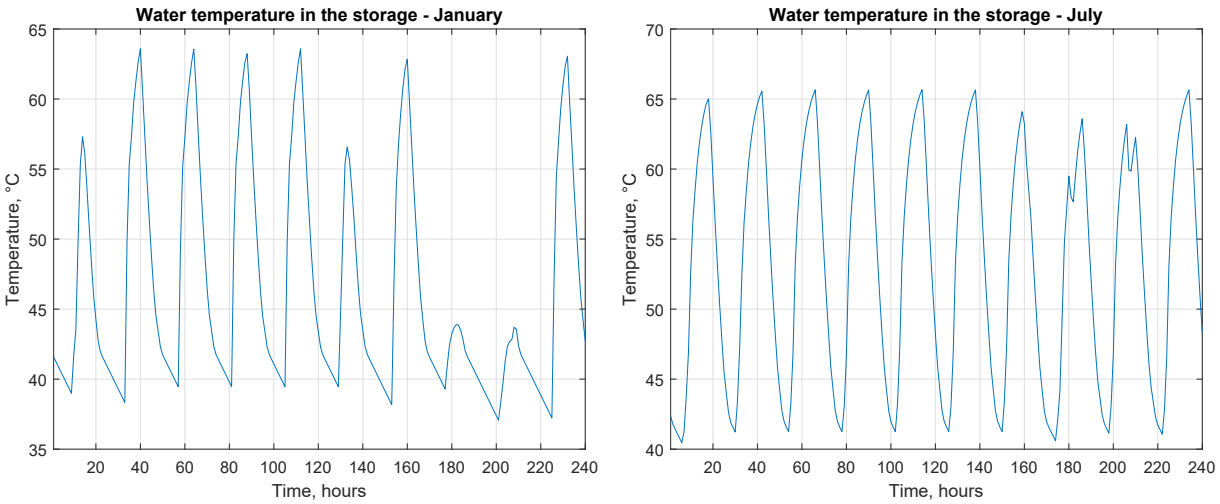

(a) First ten days of January

(b) First ten days of July

Figure 3.4: Storage temperature

After very low losses in the pipes, the heat retrieved by the Sun reaches the storage tank. As it can be seen, the characteristic pattern of higher temperatures during sunny hours and lower during night/shaded ones is mantained, but the temperatures are significantly lower. To obtain a deeper understanding of this behaviour, Figure 3.5 shows each contribution to Equation 2.29.

The storage heat $Q\,storage = Q\,from\,collector - Q\,loss - Q\,MD$ is often negative because the heat contribution of the collector is not able to compensate the heat request of the MD unit: auxiliaries contribution is crucial in this configuration.

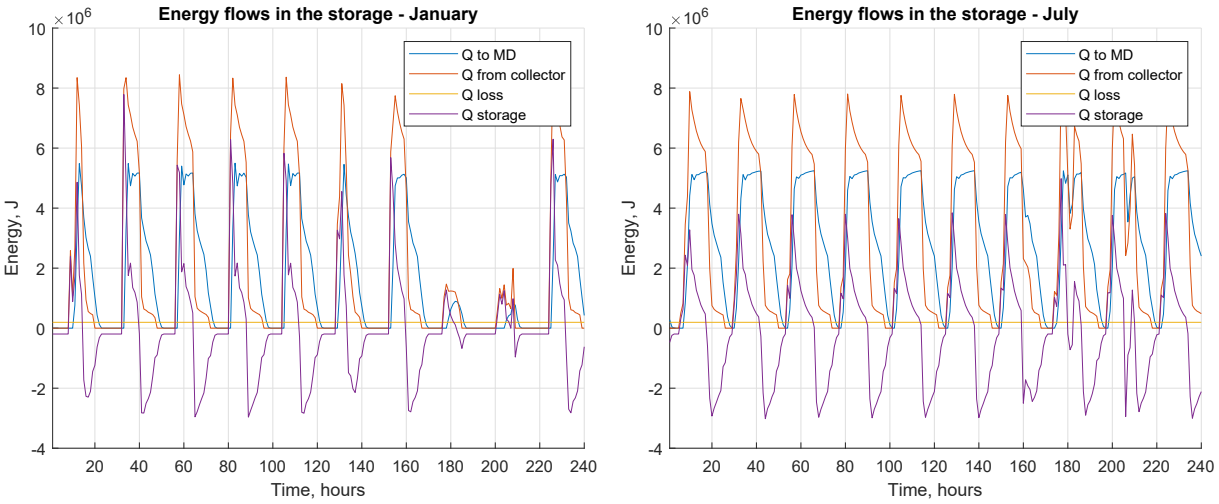

(a) First ten days of January

(b) First ten days of July

Figure 3.5: Storage energy flows in an hour

Auxiliaries subsystem

To ensure the required minimum temperature at the MD unit feed side, the auxiliary system intervenes every time the heat provided by the collector is not sufficient. As shown in Figure 3.6, the auxiliaries work mostly at night, wher no collector heat contribution is available. Moreover, they work for less time during summer, when the solar radiation is available for a longer period of time: this is evident since the width of the Sun energy peaks increases in July, while the auxilaries energy one decreases. The higher values of solar energy during winter, that are counterintuitive, may be explained considering that this collector configuration does not allow the use of all the heat available, since the system stops working when it reaches too high temperature for construction reasons. Hence in winter, when the storage tank temperature (and so the inlet collector temperature) is lower (see Figure 3.4), more energy may be used to increase the temperature of the HTF inside the collector without issues. If that energy is available (likely at noon, and the shape of the solar energy plot has a steep increase specifically at that time) the collector uses it, otherwise it is forced by the control logic to waste it.

In general, it is evident that the auxiliaries contribution in this configuration is relevant.

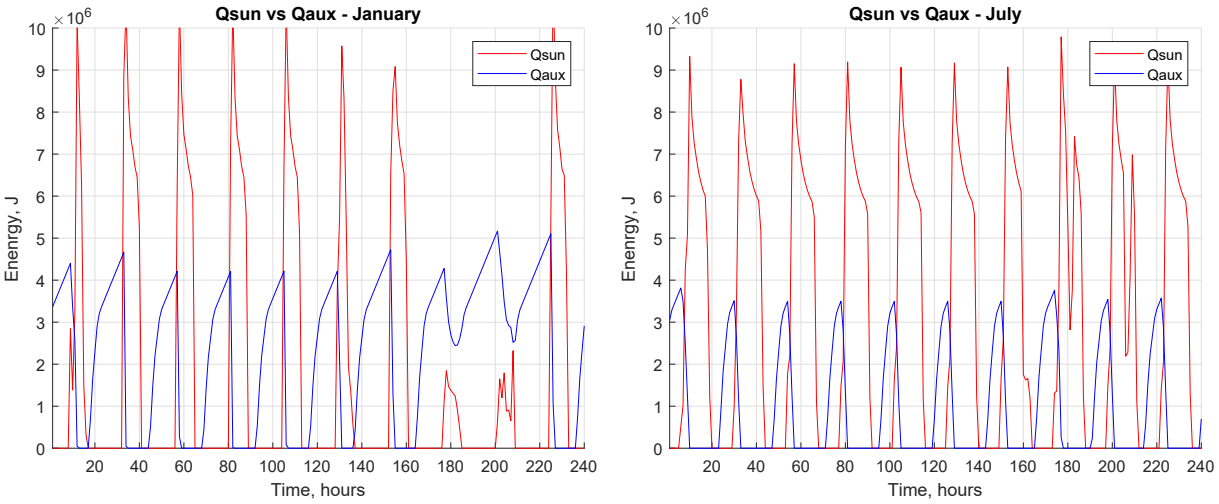

(a) First ten days of January

(b) First ten days of July

Figure 3.6: Solar and auxiliaries contribution

MD subsystem

As it is evident in Figure 3.7, the temperature of the saltwater entering the MD unit has a temperature higher than the 50 °C threshold when the Sun contribution is most relevant, with a maximum increase of 13 °C in winter and 15 °C in summer. The pattern highlighted before is evident also in this figure: the width of the temperature peaks is bigger in summer due to more irradiance hours. The collector contribution during the 8^{th} and 9^{th} of January (when the irradiance is very low) is negligible: in this period (and during night hours) the collector and storage act as pre-heaters.

As expected, water production is influenced by the different feed side inlet temperature (Figure 3.8. Auxiliaries, through the imposed threshold, guarantee a minimum water production of 0.51 kg/h.

As shown in Figure 3.9, the global water production has an almost constant behaviour over the year, due to the low temperature contribution of the solar component: in fact, the maximim temperature in the feed side is 65.5 °C, 15.5 °over the minimum value of 50 °C; moreover the temperatures are not high enough to guarantee a significant increase of the vapour pressure (see Figure 2.11).

Table 3.2 sums up the most relevant output of the standard model.

A solar fraction higher than 50% is a good starting point, as it usually indicates a good solar contribution in the system. The water production is in good agreement with a typical MD system: the water production can span between 7 and 70 l/(m^2h), with the membrane area considered, 0.35- 3.5 l/h [35].

Figure 3.10 shows the mean temperatures of the most representative streams of the plant. The most relevant temperature drop is located in the storage tank, whose mean temperature over the year is slightly below 50 °C.

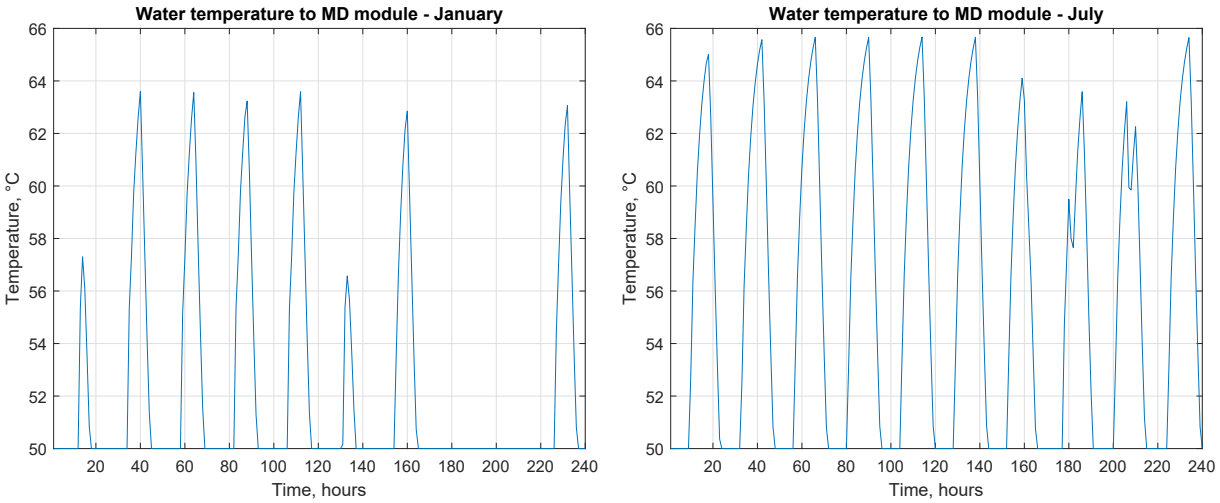

(a) First ten days of January

(b) First ten days of July

Figure 3.7: MD feed side inlet temperature

SF, %	60.13
Yearly water production, l	5186
Daily average water production, l	14.1
Hourly average water production, l	0.592
Global energy consumption, kWh/m^3	1915

Table 3.2: Main output for the standard model

The same behaviour is observed considering reduced intervals of time. The most relevant difference is between the temperatures of the collector block, approximately ten degrees higher in July than in January.

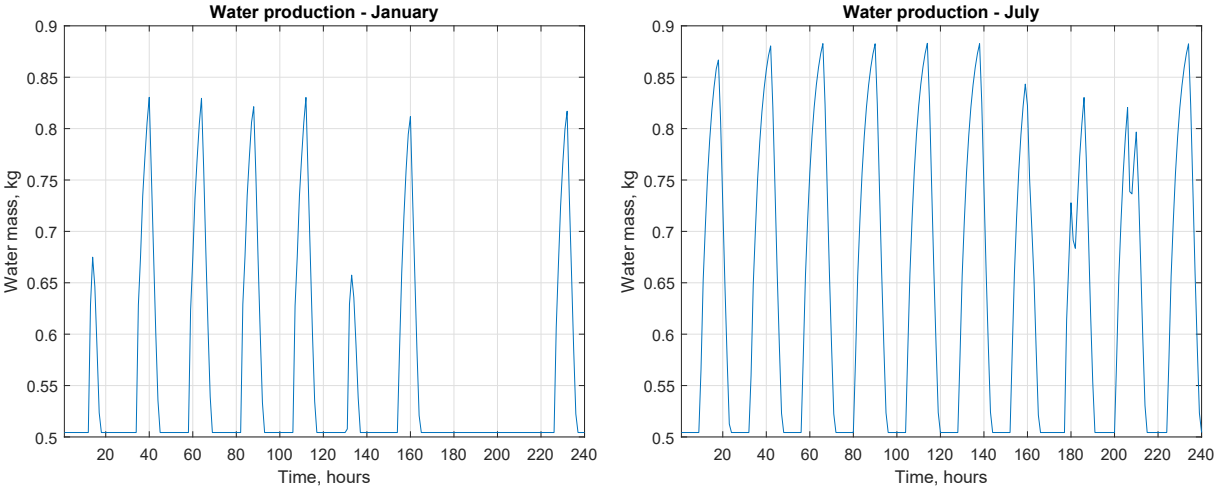

(a) First ten days of January (b) First ten days of July

Figure 3.8: Hourly water production

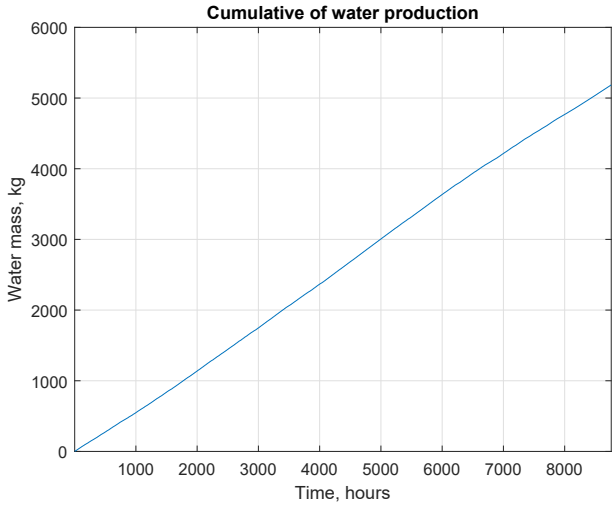

Figure 3.9: Yearly water production

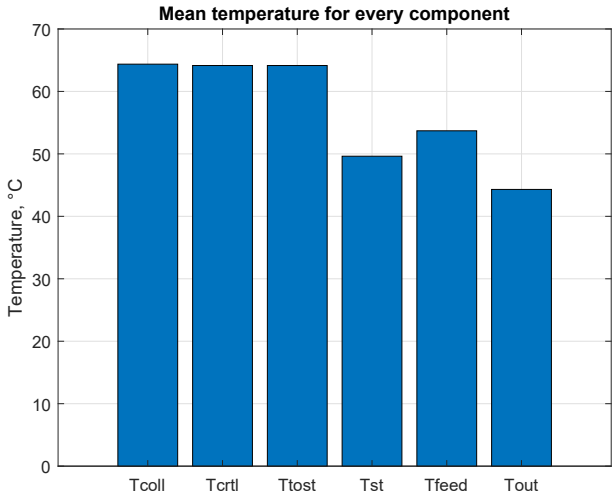

Figure 3.10: Relavant yearly mean temperatures

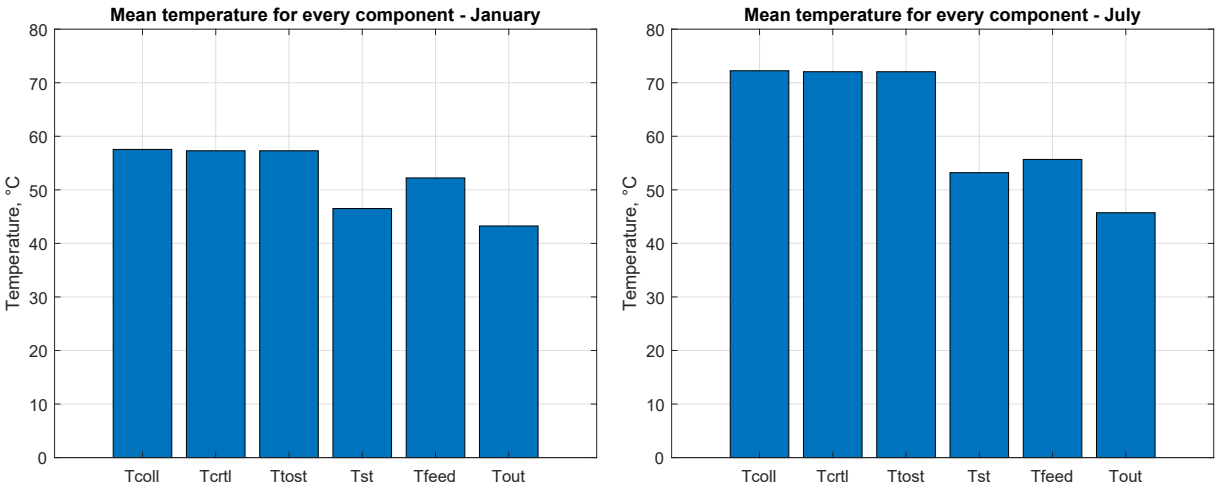

(a) First ten days of January

(b) First ten days of July

Figure 3.11: Relavant mean temperatures over ten days

3.1.3 Economical analysis

To provide, when needed, a further instrument to understand deeper the sensitivity analysis, a basic economic analysis is performed. Its aim will be to define the cost of water, i.e. the ideal cost at which the water has to be sold to obtain a PayBack Time (PBT) equal to the life of the plant (in other words, to reach the breakeven). To do so, the notion of Net Present Value (NPV) is introduced:

$$NPV = \sum real\, cash\, flow = \sum discount\, rate \times cash\, flow \tag{3.1}$$

where:

- $discount\, rate$ is a factor that converts the value of the computed cash flow into the value at a specific year, usually the first. It takes into account the fact that the lack of availability of revenues all at once (they are considered to be gained only once a year,) leads to a different value of money earned depending on the year in which they are collected. It is computed as:

$$discount\, rate = (1 + WACC)^{-(n-n_0)} \tag{3.2}$$

  where:

  - n is the year in which the cash flow is computed;
  - n_0 is the starting year;
  - $WACC$ is the Weighted Average Cost of Capital, computed as:

$$WACC = \%_e c_e + \%_d c_d \tag{3.3}$$

    where $\%_e$ is the percentage of equity (i.e. the percentage of liabilities financed by equity capital), $\%_d$ is the percentage of debt (i.e. the percentage of liabilities financed by debt), c_e is the cost of equity and c_d is the cost of debt.

- $cash\, flow$, the money flux entering or exiting the company, computed as:

$$cash\, flow = \begin{cases} cost + income & if\, cost + income < 0 \\ cost + income - t(cost + income & \\ \quad -depreciation) & if\, cost + income > 0 \end{cases} \tag{3.4}$$

  where:

  - $cost$ is computed as:
    - CAPEX (capital expendidure) on year 0, i.e. the amount of capital needed to start the activity;
    - OPEX (operating expedidure) on the following years, i.e. the maintenance cost, estimated as a fraction of CAPEX, and the cost of the fuel needed by the auxiliaries, estimated as:

$$fuel\, cost = c_{fuel} V_{fuel} = c_{fuel} \left(\frac{Q_{aux}}{\eta_{aux} H_{fuel}} \right) \tag{3.5}$$

where c_{fuel} is the fuel cost in €/Nm^3, η_{aux} is the efficiency of the auxiliaries and H_{fuel} is the Lower Heating Value (LHV) of the assumed fuel, natural gas.

- *income* is the amount of water produced times its price;
- t is the tax rate (that is paid only when the company earns during the considered year);
- *depreciation* is a method of cost allocation provided by Italian law to let companies distribute taxes payment related to investment cost over a certain amount of years, usually equal to the life of the plant: so, if the plant has a revenue during a certain year, its owner can pay less taxes decreasing the revenue of a fixed quantity that takes into account the investment cost [20].

All the values assumed to perform this analysis are listed in Table 3.3.

CAPEX	
collector cost, € [83]	1192.01
storage cost, € [83]	1131.16
auxiliaries cost, € [83]	899.16
heat exchanger cost, € [10]	155.00
MD cost, € (private communication)	30 000.00
OPEX - maintenance cost	
CAPEX percentage, % [12]	2
OPEX - fuel consumption	
η_{aux}	0.8
LHV_{fuel}, MJ/Nm_3 [85]	0.8
c_{fuel}, €/Nm_3 [7]	0.7782
depreciation	
number of years in which depreciation is applied [20]	30
discount rate	
$\%_{\text{e}}$,% [80]	50
$\%_{\text{d}}$,% [80]	50
c_{e},% [67]	3
c_{d},% [67]	5
expected life of the plant, years [59] [12]	30
tax percentage, % [26]	24

Table 3.3: Economic data

Figure 3.12 shows the CAPEX composition. It is evident that the main cost is represented by the MD module: this is due to the fact that the technology is still relatively new, and that

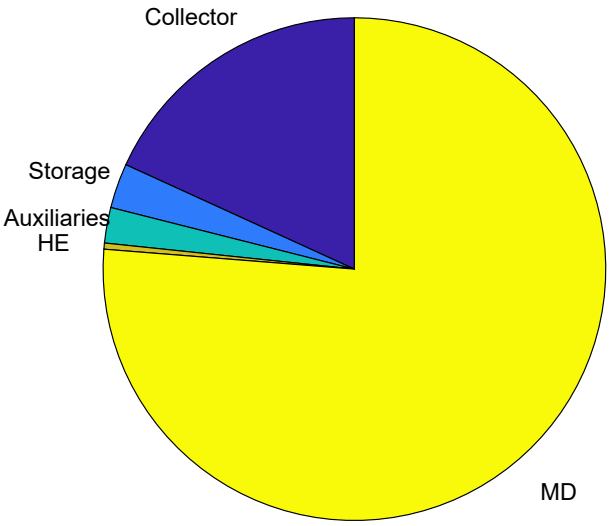

Figure 3.12: CAPEX composition

the unit is a lab one, thus equipped with a series of measuring instruments. The second entry in order of importance are the collector, since there are a relevant number.

Figure 3.13 shows the NPV evolution as long as the plant is working. To obtain breakeven during the lifetime of the plant, a minimum price of 0.7133 €/l of produced water has to be set. This is very huge, since the price of water in Turin is actually equal to 0.4181 €/m^3[1], i.e. more than 1000 times higher. This is a very unrealistic number, mostly linked to the fact that the MD unit is a laboratory system, and laboratory equipment usually cost 100 times more than a production plant. For this reason, the same analysis has been conducted considering the cost of the MD unit reduced of a factor of 10 and of 100; obtaining a water cost of 0.2678 and 0.2232 €/l respectively.

The results may still seem unsatisfactory. To understand why, some characteristics of this plant must be considered. In this work, the term "plant" is inappropriate, since the analysis is carried on a small laboratory MD unit. The main goal is to assess the performance of such a system and to understand the VTC-MD coupling behaviour, at first retrieving data from the model, afterwards from real measurements, to understand the feasibility of such coupling on a larger scale in the future. This analysis gives back a general trend of the economic performace of such a configuration, and will be of some relevance during the sensitivity analysis on the number of collectors.

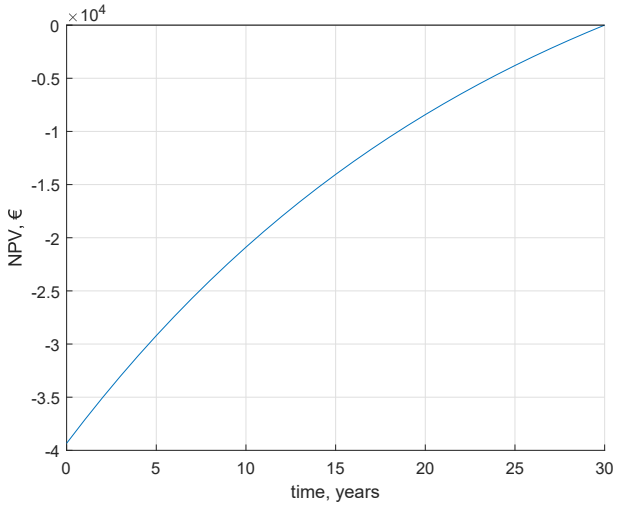

Figure 3.13: NPV over the years

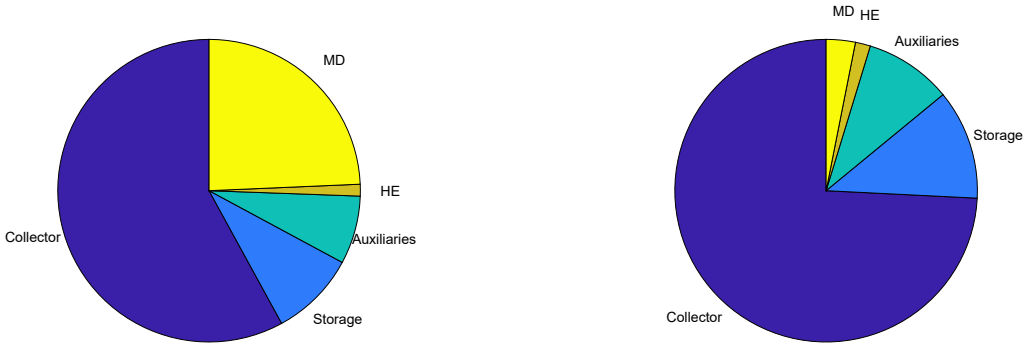

(a) MD unit cost reduced by a factor of 10 (b) MD unit cost reduced by a factor of 10

Figure 3.14: CAPEX variation with MD cost variation

3.1.4 Parameters for sensitivity analysis

Due to the assessments made before, the following parameters are identified to perform a sensitivity analysis:

- slope and azimuth;
- number of collectors / collector area;
- series/parallel connections;
- tank dimension;
- flow rate to MD feed side.

Each one will analysed separately to obtain a deeper understanding of the variation induced. The main parameters on which the choice of the best configuration is based are the SF and the yearly water production.

3.2 Slope and azimuth - sensitivity analysis

The best position of a collector is an important parameter, since it allows to use at best the solar energy available. The incident angle has indeed a strong influence on the fraction of the irradiance that the solar collector is able to capture (see Eq. 2.1).

The intervals considered for the sensitivity analysis is a ten degrees spaced vector ranging from $\phi - 20°$ to $\phi + 30°$ for the slope β, and from $-45°$ to $45°$ divided in five subintervals for the azimuth γ. All the other parameteres were left unchanged.

3.2.1 Output data

The Figure 3.15 show the SF and the yearly water production for every β and γ.

The best azimuth angle is -22.5°for every slope, that means a slight orientation towards West. This may be due to the fact that, since the temperature increase in the collector is very steep in the late morning, a small amount of heat (i.e. a small increase of temperature) in early morning has a negligible influence on the system, since it remains under the threshold temperature and the auxiliaries have to work. Instead, the afternoon heat is converted in a flux higher than 50°C: the auxiliaries do not need to work in this period, so SF increases, and, since the temperature is higher than the minimum value, the water production is positively influenced.

As far as slope is concerned, both SF and water production increase when β decreases. This is probably due to the fact that the system exploits at best summer radiation when the slope is lower (since during summer the altitude of the Sun is higher): this is the moment in which the maximum temeprature in the collector lasts longer, the temperature in the collector increases and so the water productivity increases too.

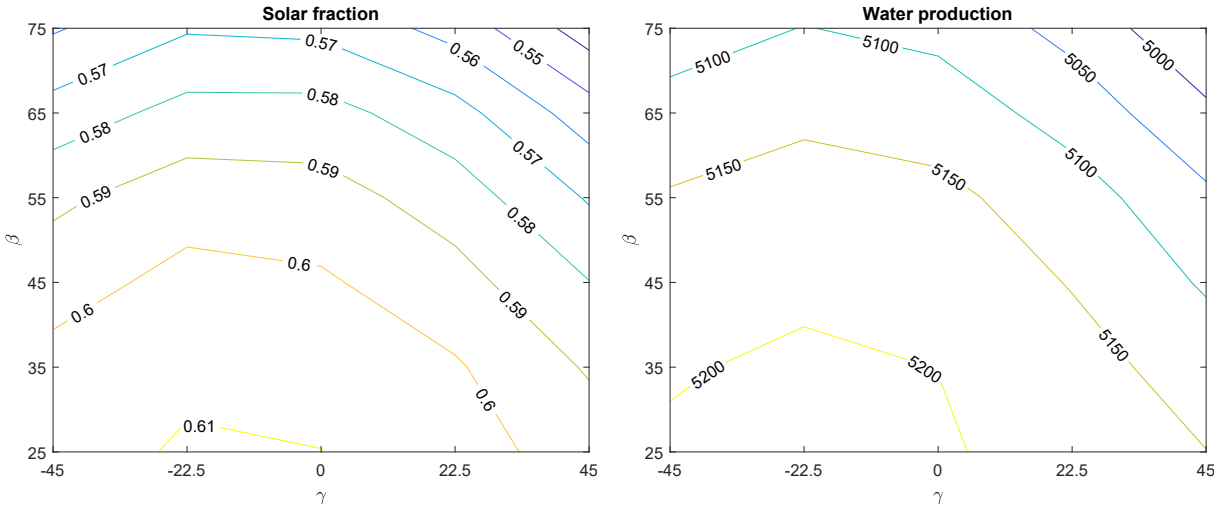

(a) SF variation

(b) Water produced variation

Figure 3.15: SF and water produced vs β and γ

3.2.2 Comparison between the best configuration of slope and azimuth and the standard one

As shown in Figure 3.16, the irradiance has an increase (in some specific moments very relevant) in summer months (as in Figure 3.16b) and a reduced decrease in winter months (as in Figure 3.16a). So, the global contribution of the collector is higher in this configuration, leading to a bigger SF and water production. This trend is reflected in the collector temperature (Figure 3.17), storage temperature (Figure 3.18) and water production (Figure 3.19).

The percentual increase of SF is 1.6%, while the increase of water production is 0.5%.

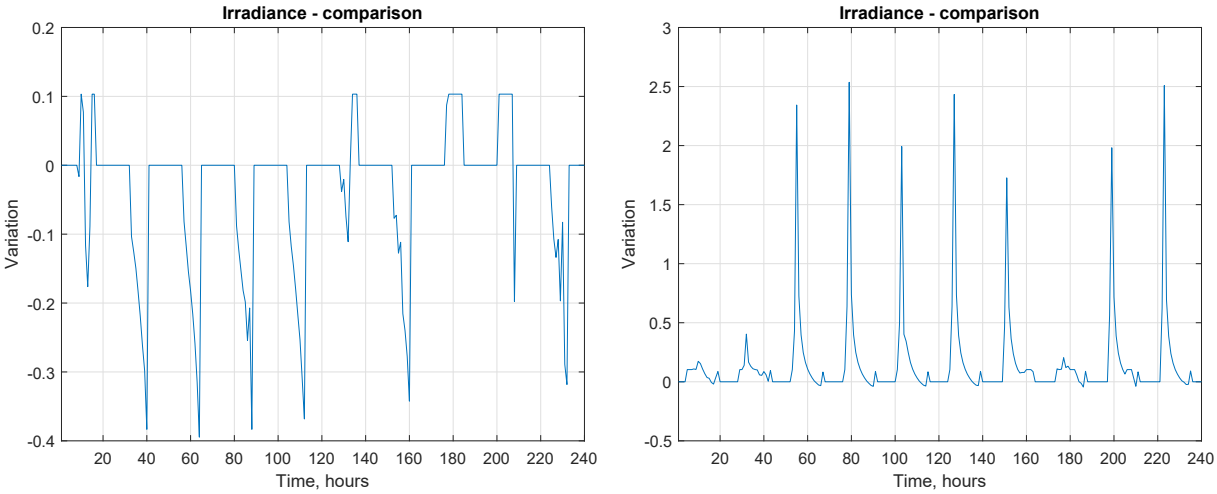

(a) First ten days of January (b) First ten days of July

Figure 3.16: Irradiance variation with β and γ over ten days

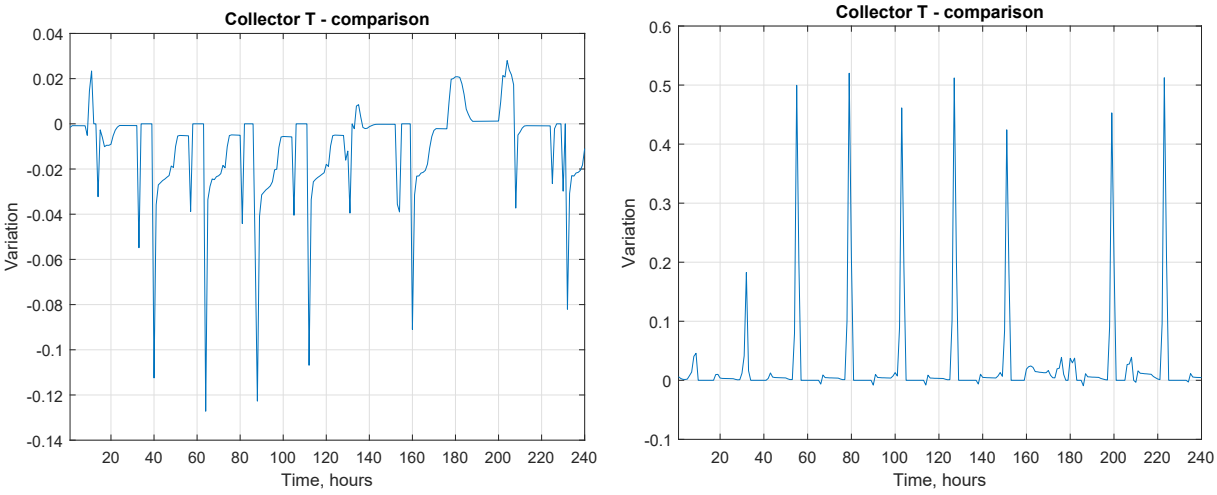

(a) First ten days of January (b) First ten days of July

Figure 3.17: Collector temperature variation with β and γ over ten days

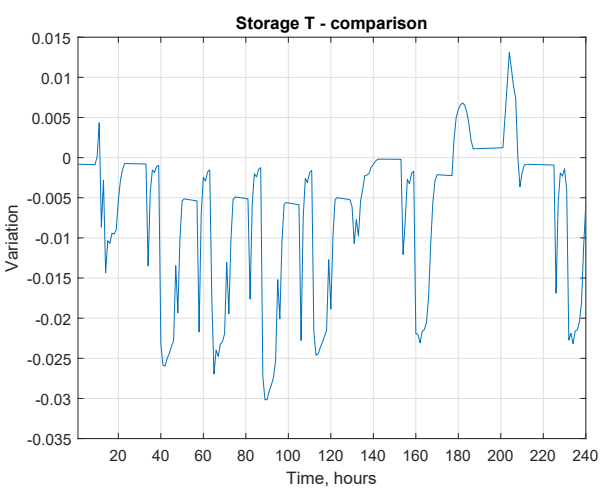

(a) First ten days of January

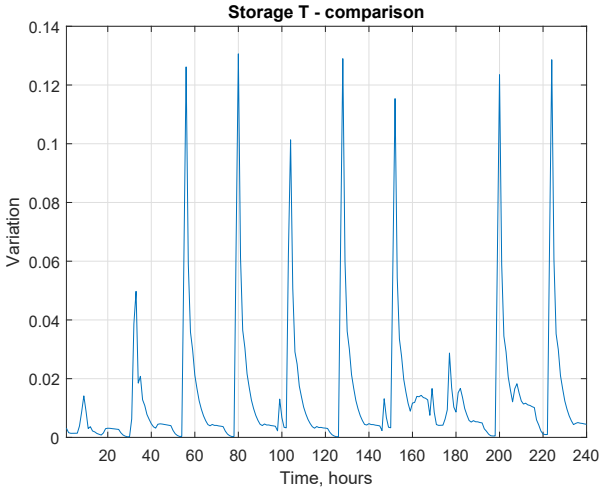

(b) First ten days of July

Figure 3.18: Storage temperature variation with β and γ over ten days

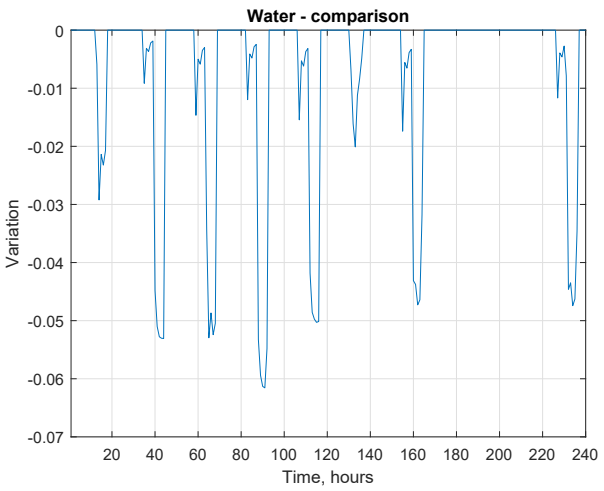

(a) First ten days of January

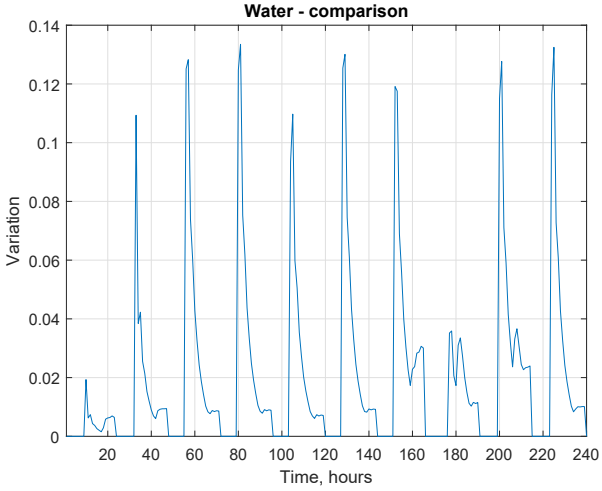

(b) First ten days of July

Figure 3.19: Storage temperature variation with β and γ over ten days

3.3 Number of collectors

The number of collectors influences the amount of heat that can be collected by the solar plant, since it is porportional to the collector area, proportional to the number of collectors (see Eq. 2.12).

The intervals considered for the sensitivity analysis is a two spaced vector ranging from four to thirty collectors; since each one has a 2 m^2 area, the area ranges from 8 to 60 m^2. All the other parameteres were left unchanged.

3.3.1 Output data

The Figure 3.20 lists the variation of SF and water productivity with the number of collectors.

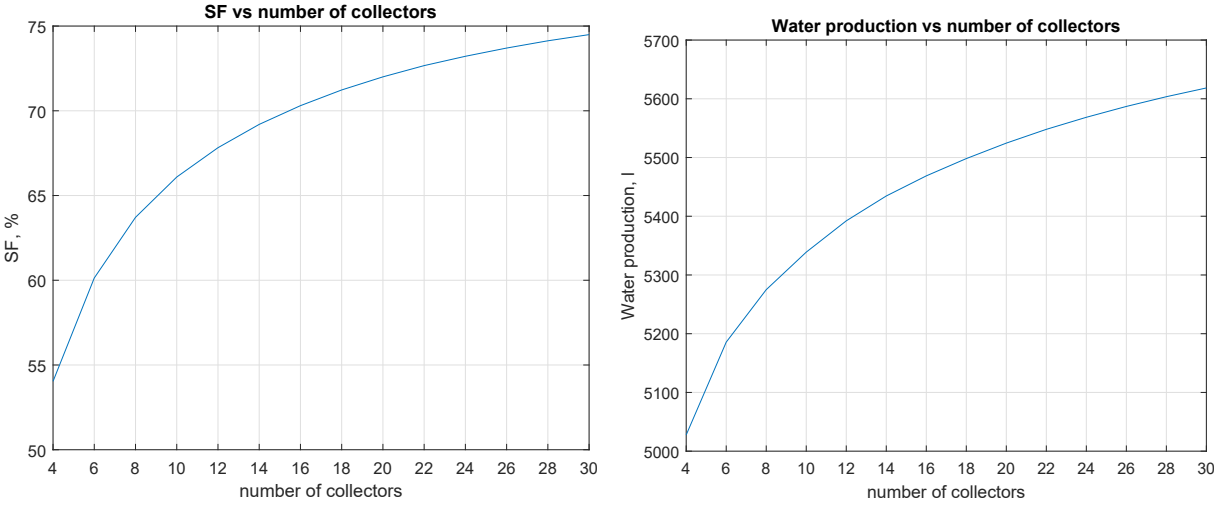

(a) SF variation

(b) Water produced variation

Figure 3.20: SF and water produced vs number of collectors

As expected, both SF and water production increase when the number of collectors increase, since the capacity of the system to capture solar radation increases when the absorber area increases. So, as a first assumption, the largest number of collectors, 30, is used as best configuration.

3.3.2 Comparison between the best configuration of number of collectors and the standard one

As shown in Figures 3.21, 3.22 and 3.23, the general increment in performance of the system is more relevant in winter, when the wider collector area allows the system to increase more the temperature of the collector HTF: this is more evident analysing Figure 3.24. A huge number of collectors allows to capture more energy in early morning and late evening, when the radiation is lower. A evident demonstation of what stated is the behaviour of the collector temperature on 8^{th} and 9^{th} January. While in the standard configuration the temperature increase is approximately

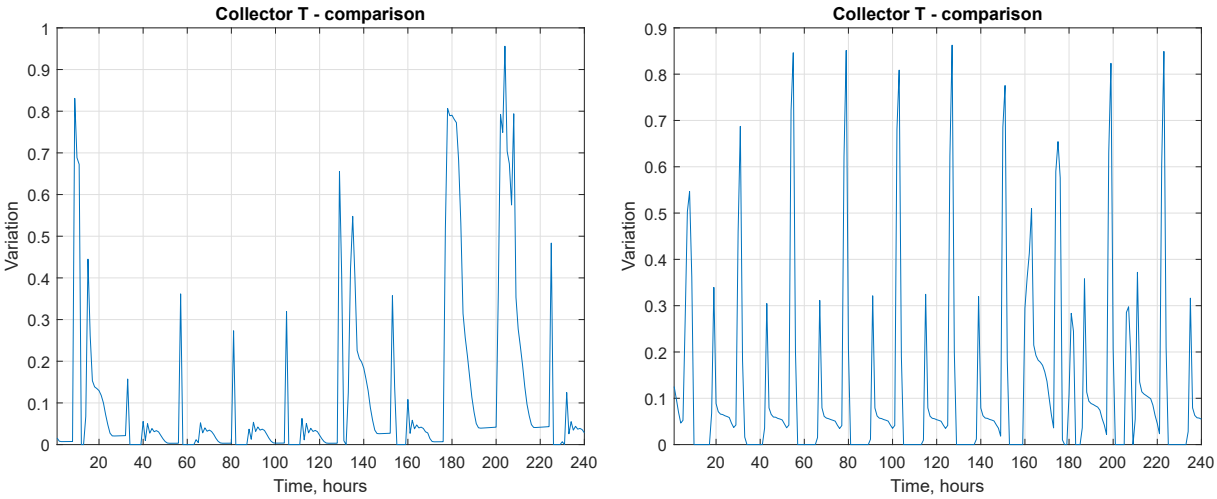

(a) First ten days of January

(b) First ten days of July

Figure 3.21: Collector temperature variation with number of collectors over ten days

ten degrees, the installation of a moltitude of collectors leads to temperature higher than 90 °C when Sun shines.

This choice has a relevant impact over the cost of the plant, so the total cost of water is a parameter to be taken into account when performing such analysis.

To do so, the cost analysis has been performed in such cases; results are shown in Figure 3.25.

It is self-evident that the cost of water increases almost linearly, due to the increase of the cost of the collector: in case of thirty collectors, their cost is more than half of CAPEX. To understand better the matter, a Pareto curve is drawn (Figure 3.26). The Pareto curve plots the total water production over the lifetime of the plant vs. the total cost (CAPEX and OPEX for every year) of it. To find the optimum, i.e. the configuration that considers the maximum value of the produced water and the minimum cost, the following function was used:

$$\max(water - cost) \tag{3.6}$$

According to this analysis, the best configuration is the standard one, with six collectors.

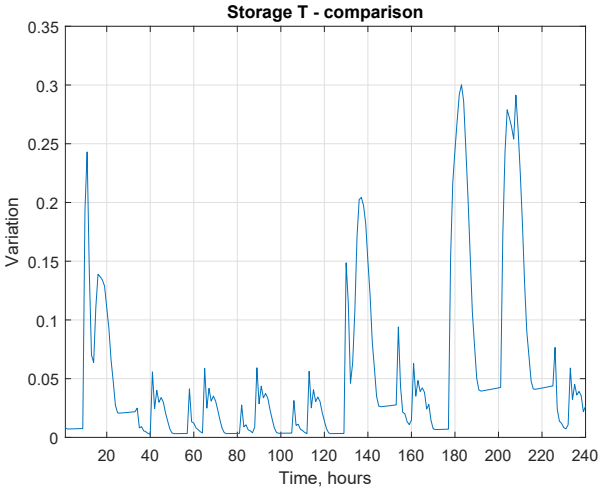

(a) First ten days of January

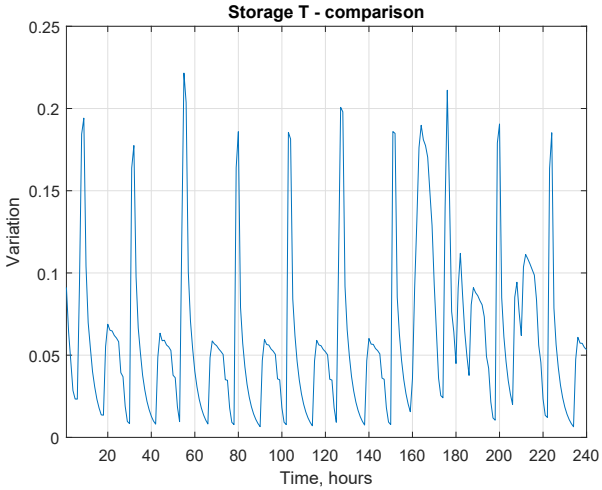

(b) First ten days of July

Figure 3.22: Storage temperature variation with number of collectors over ten days

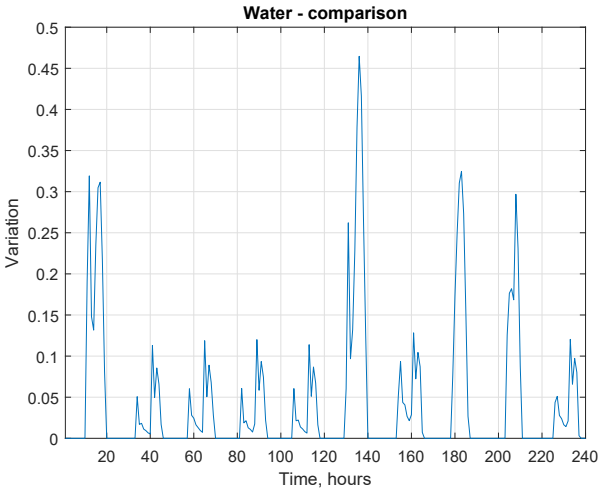

(a) First ten days of January

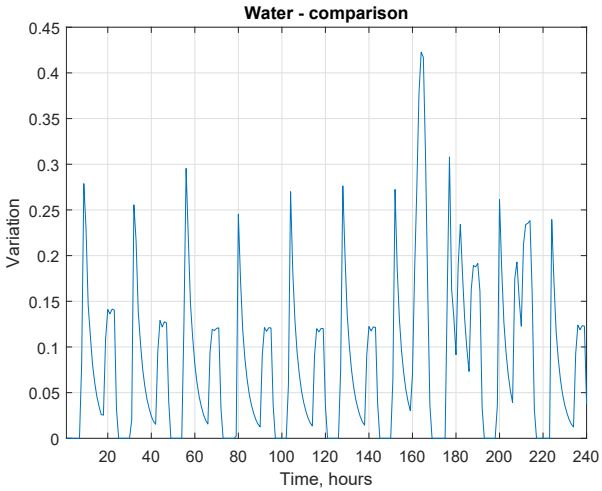

(b) First ten days of July

Figure 3.23: Water production variation with number of collectors over ten days

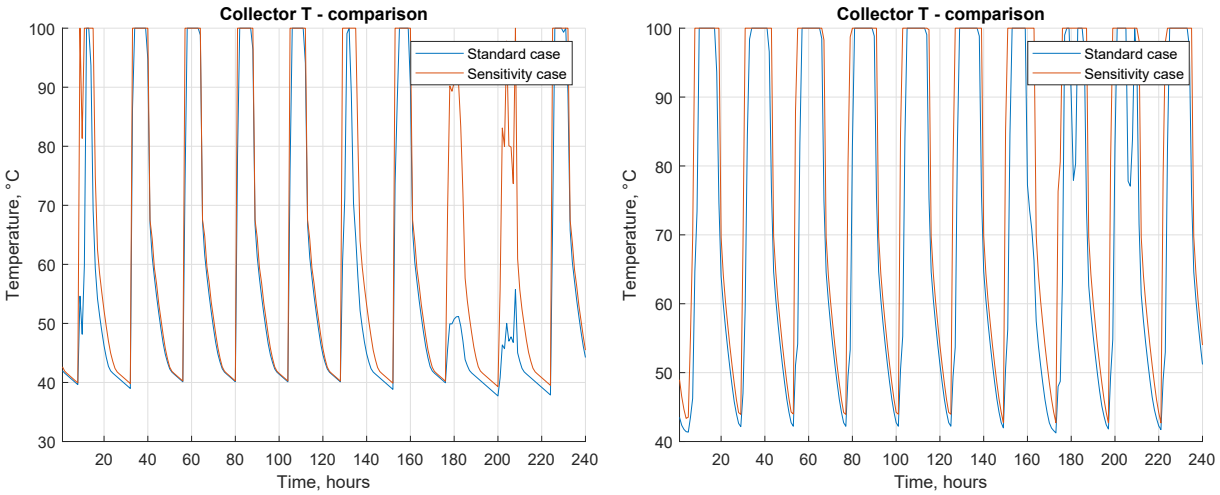

(a) First ten days of January

(b) First ten days of July

Figure 3.24: Collector temperature comparison with number of collectors over ten days

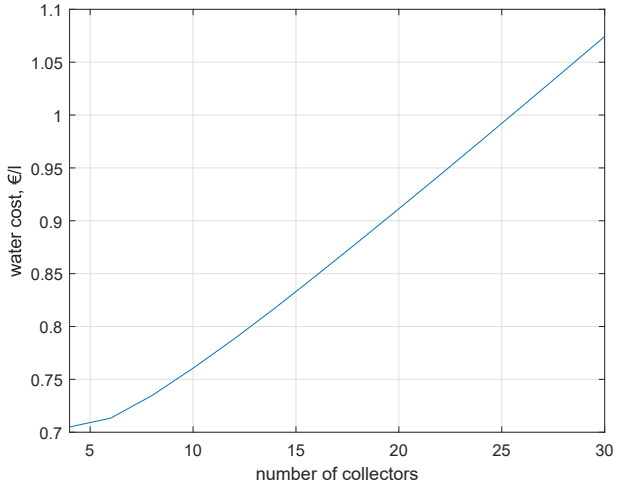

Figure 3.25: Cost of water wrt the number of collectors

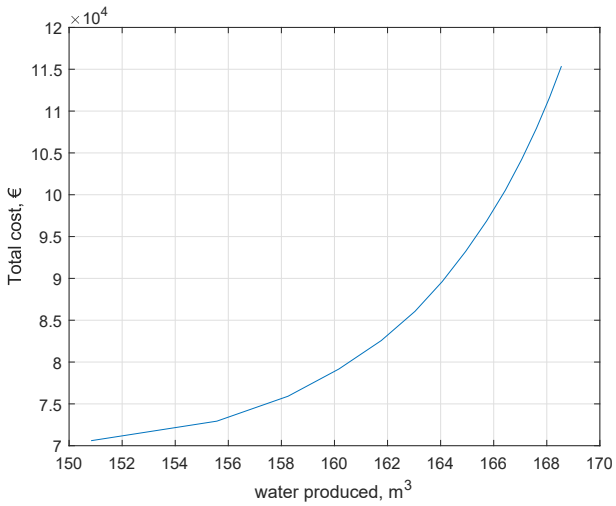

Figure 3.26: Water produced wrt total cost of the plant

3.4 Series/parallel connections

The series/parallel connections influence both the outlet temeprature of the collector and the mass flow rate of the collector to the storage. In fact, under the hypothesis that the collector rows are perfectly equal, the nominal mass flow rate in each collector is the same, but the mass flow rate entering the storage is equal to the mass flow rate of a collector times the number of rows. The smaller number of the collector in a row, on the other hand, should increase the outlet temperature, but, since the system stops when the temperature is too high, a configuration with multiple rows may help not to wate solar energy.

The intervals considered for the sensitivity analysis spans from the series configuration (one row) to the parallel configuration (six rows) considering also the two intermediate solutions of two and three rows. All the other parameteres were left unchanged.

3.4.1 Output data

Figure 3.27 shows the variation of SF and water productivity with the number of rows. As expected from what stated before, the number of rows increase produces a relevant increment of both SF and water production, making the parallel connection configuration the best one, with a SF equal to 80.68%, and a water production that reaches 6903 l/y.

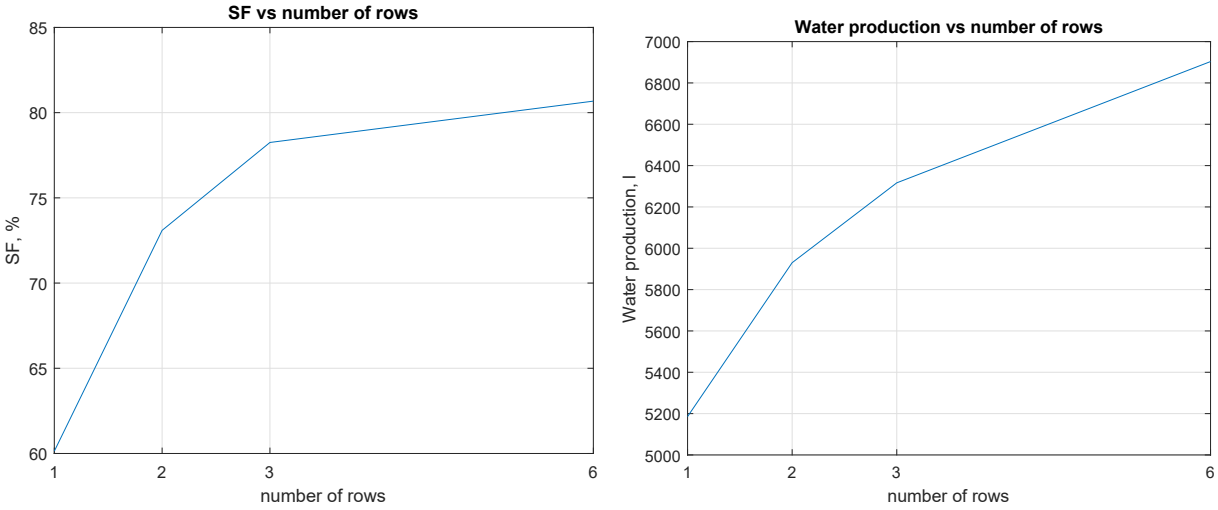

(a) SF variation

(b) Water produced variation

Figure 3.27: SF and water produced vs number of rows

3.4.2 Comparison between the best configuration of series/parallel connections and the standard one

Figures 3.28, 3.29 and 3.30 clarify the behaviour of the system. Collector temperature experiences wider variations during a day with higher temperatures during day (due to the reduced number of collectors per row) and lower temperatures during night time (due to the higher mass

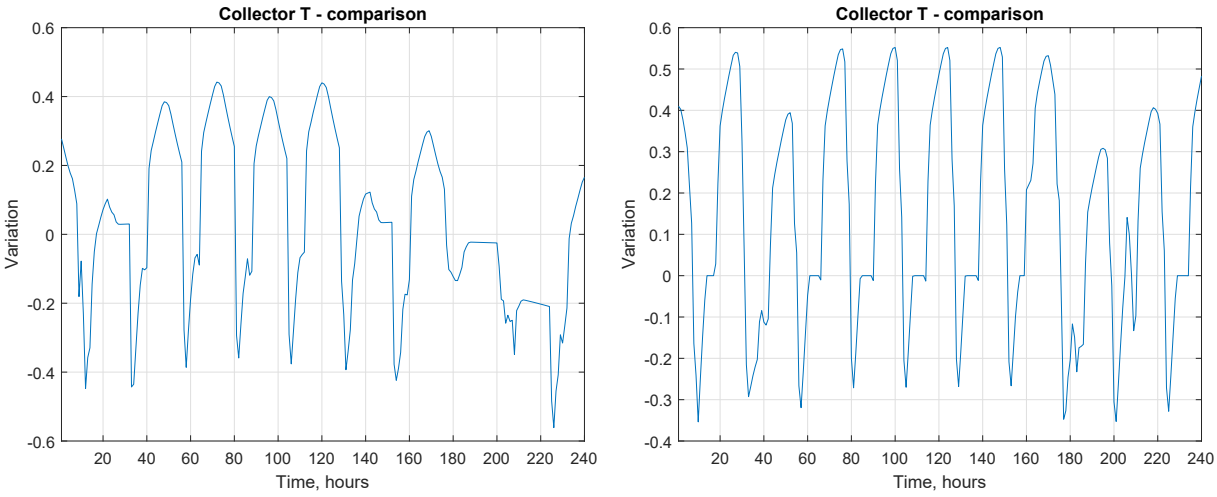

(a) First ten days of January

(b) First ten days of July

Figure 3.28: Collector temperature variation with number of rows over ten days

of water flowing into the storage, and so the higher inertia of the system) (see Figure 3.31). Storage temperature has indeed an increase, almost at any moment of the day in summer, quite often in winter, reaching temperatures higher than 80 °C (see Figure 3.32). As a result, water production increase turns out to be relevant, with peaks higher than 80% of increment even during some winter hours.

The percentual increase of SF is 34.2%, while the increase of water production is 33.1%.

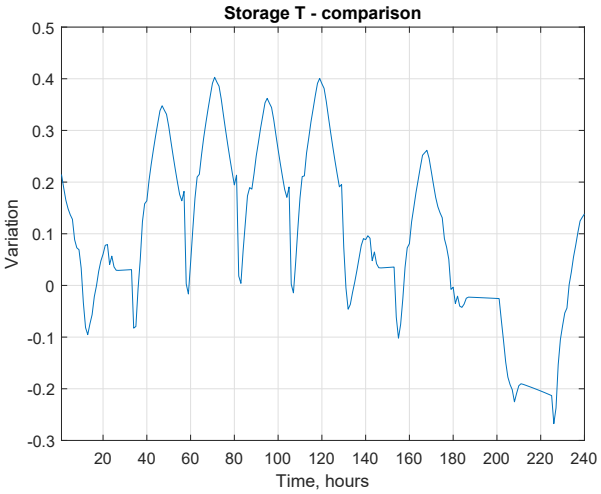

(a) First ten days of January

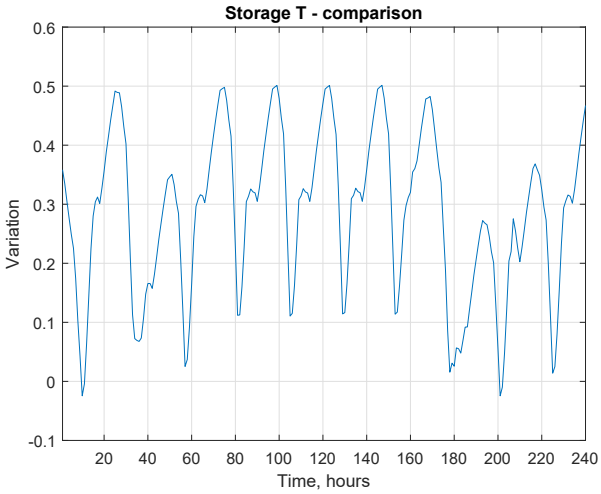

(b) First ten days of July

Figure 3.29: Storage temperature variation with number of rows over ten days

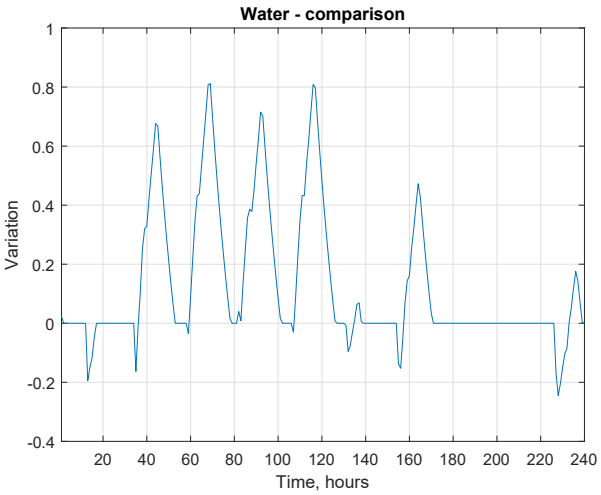

(a) First ten days of January

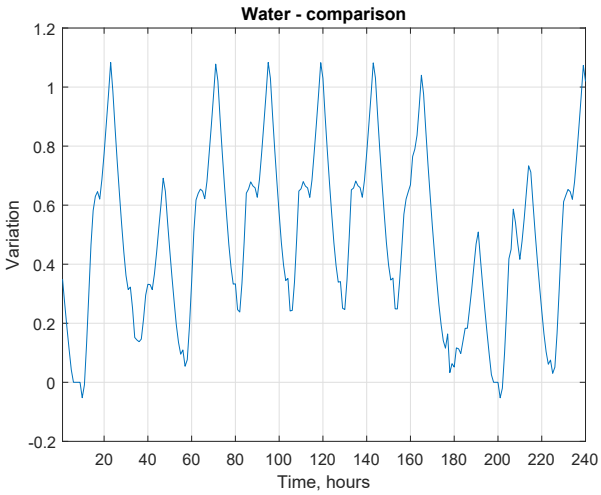

(b) First ten days of July

Figure 3.30: Water production variation with number of rows over ten days

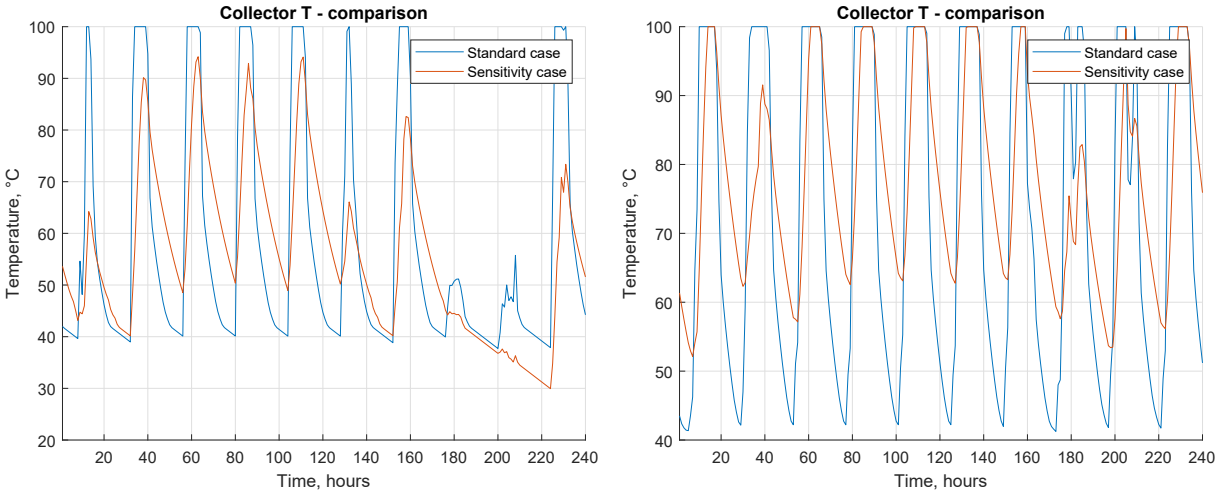

(a) First ten days of January (b) First ten days of July

Figure 3.31: Collector temperature comparison with number of rows over ten days

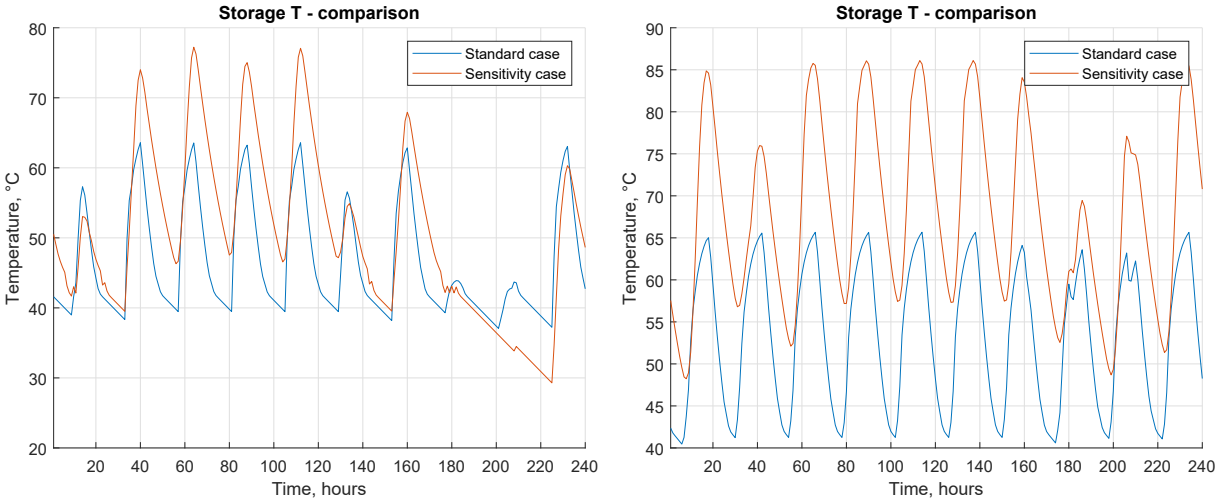

(a) First ten days of January (b) First ten days of July

Figure 3.32: Collector temperature comparison with number of rows over ten days

3.5 Tank storage size

The volume of the tank is a parameter of paramount importance in the dimensioning of a renewable energy fed system. It determines the amount of energy that can be stored for later use and, due to the relevance of the temperature for the MD mechanism, the temperature of the storage tank (see Eq. 2.29).

The analysis interval regards two series of Vaillant products: the auroSTEP warm water storages, whose volumes are 150, 250 and 350 l, and the allSTOR storages, whose volumes are 303, 491, 778, 962, 1505 and 1917 l. Each collector is charaterized by its losses, defined through kWh lost during a day. A summary of the main characteristics of the considered storage tanks is listed in Table 3.4. All the other parameteres were left unchanged.

ID n.	Collector name	Volume, l	Losses, kWh/24h
1	auroSTEP VIH 150/3 Mi	150	1.3
2	auroSTEP VIH 250/3 i	248	2.1
3	allSTOR VPS 300/3	303	1.7
4	auroSTEP VIH 350/3 i P	389	2.1
5	allSTOR VPS 500/3	491	2.0
6	allSTOR VPS 800/3	778	2.4
7	allSTOR VPS 1000/3	962	2.5
8	allSTOR VPS 1500/3	1505	2.9
9	allSTOR VPS 2000/3	1917	3.3

Table 3.4: Storage tank data

The increase of the storage tank size is expected to decrease the temperature of the saltwater mass inside the storage, but the fluctuations of the temperature troughout the day should be reduced.

3.5.1 Output data

As shown in Figure 3.33, the SF increases with the increase of tank storage size, while the water production decreases. This is due to the fact that the storage temperature decreases: the water production decreases since the times in which the MD inlet temperature exceeds 50°C are reduced, while the SF increases, because the temperature tends to have less variations during the day and the storage along with the collector system acts as a pre-heater.

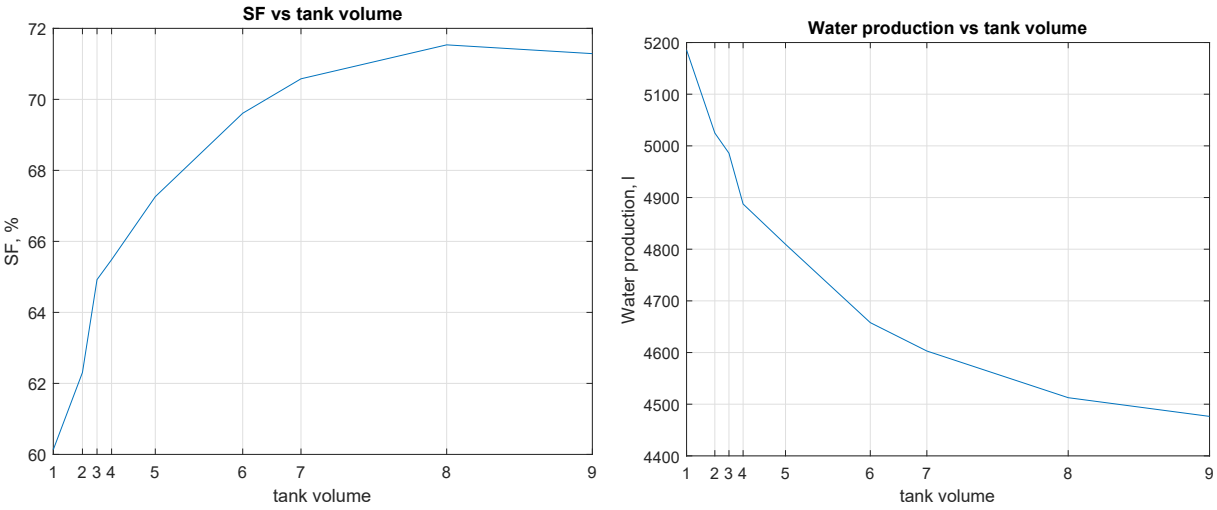

(a) SF variation

(b) Water produced variation

Figure 3.33: SF and water produced vs storage tank size

3.5.2 Comparison between the best configuration of storage tank volume and the standard one

Since the best configuration considering the water production appears to be the one in use due to the fact that a reduced storage tank size increases temperatures, while the best configuration considering SF turns out to be the one with the biggest tank volume, this section will be devoted to the comparison between these two plant configurations.

As evident in Figure 3.36, the production of water decreases at almost every time during both summer and winter. This is a reflection of the storage temperature which, exactly as predicted, increases during night time and decreases during day time, because the temperature variation is reduced. The hypothesis of the storage acting as a pre-heater is confirmed by this plot: during winter the storage temperature barely reaches 50 °C (inlet MD temperature threshold), while it increases over it approximately at noon during summer. This is made more clear in Figure 3.37.

The collector is positively influenced by this configuration, in fact the maximum temperature is fixed by the control system, but the temperature during reduced irradiation hours is increased due to the storage tank inertia (see Figure 3.38).

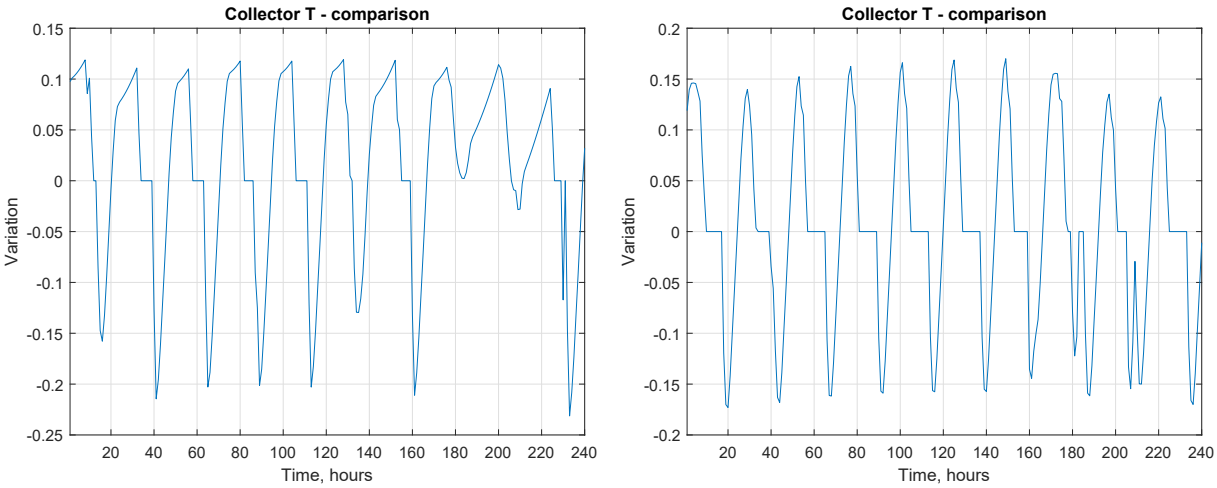

(a) First ten days of January (b) First ten days of July

Figure 3.34: Collector temperature variation with storage tank size over ten days

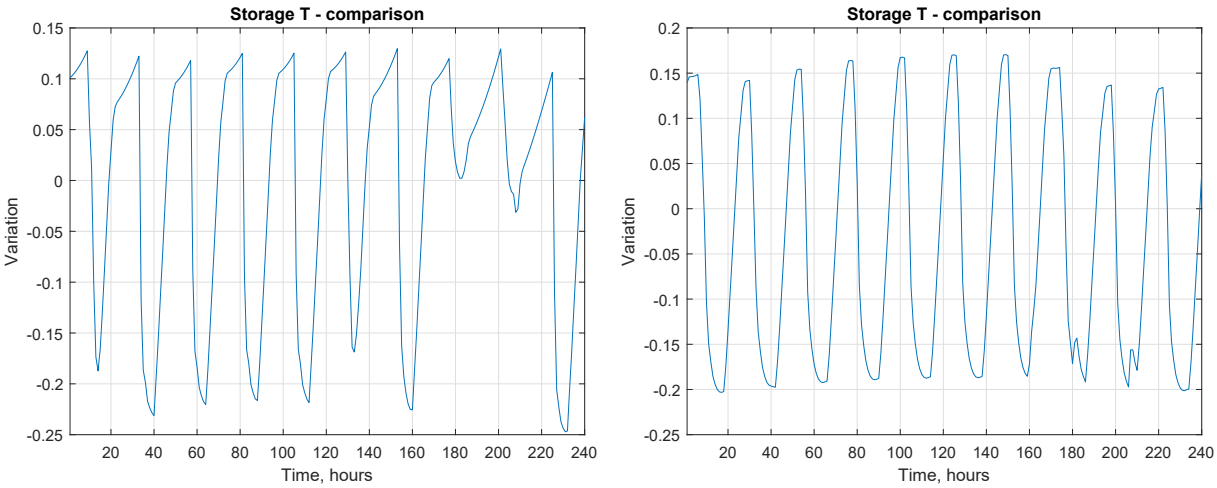

(a) First ten days of January (b) First ten days of July

Figure 3.35: Storage temperature variation with storage tank size over ten days

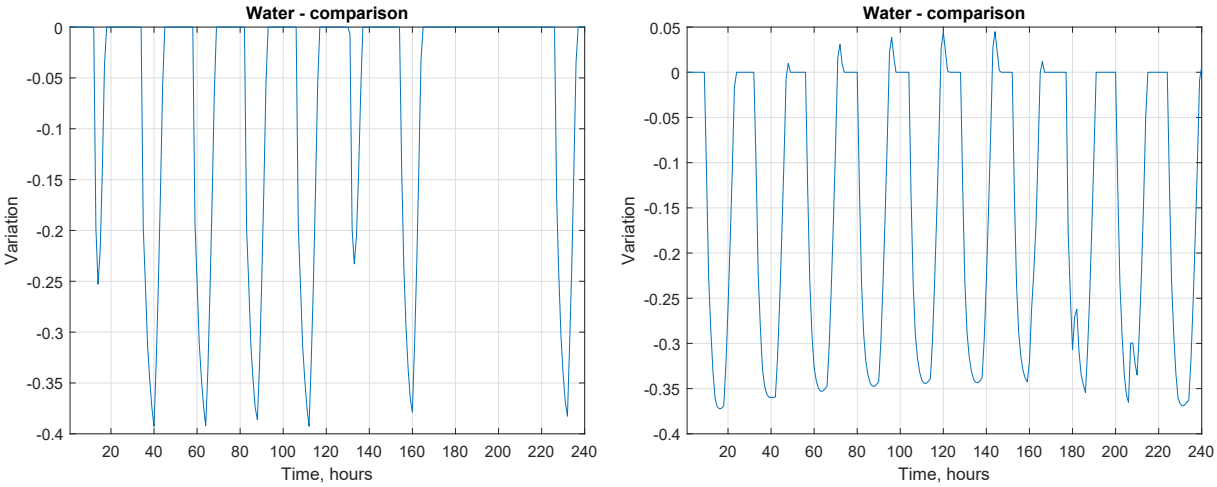

(a) First ten days of January (b) First ten days of July

Figure 3.36: Water production variation with storage tank size over ten days

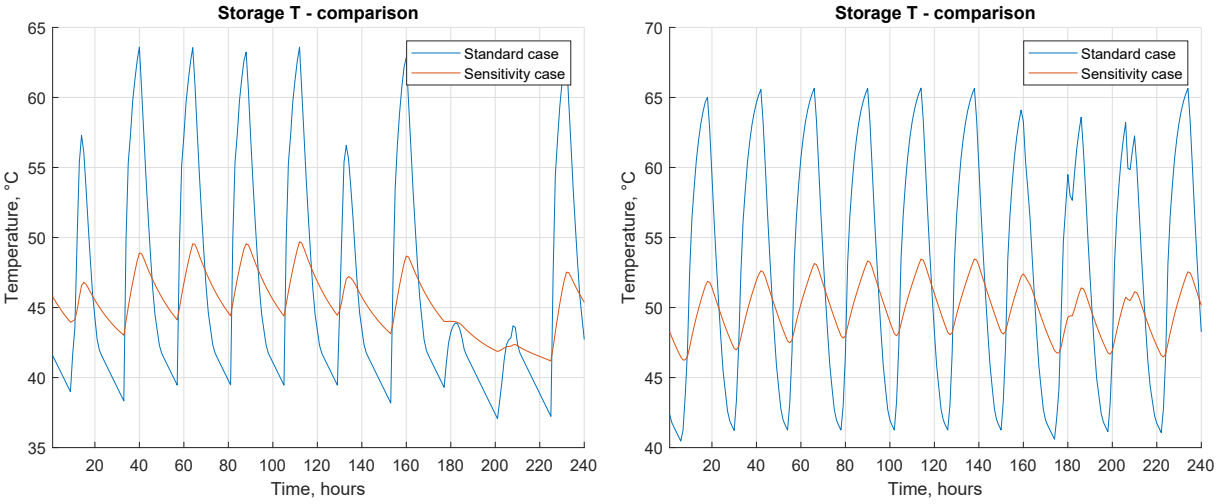

(a) First ten days of January (b) First ten days of July

Figure 3.37: Collector temperature comparison with storage tank size over ten days

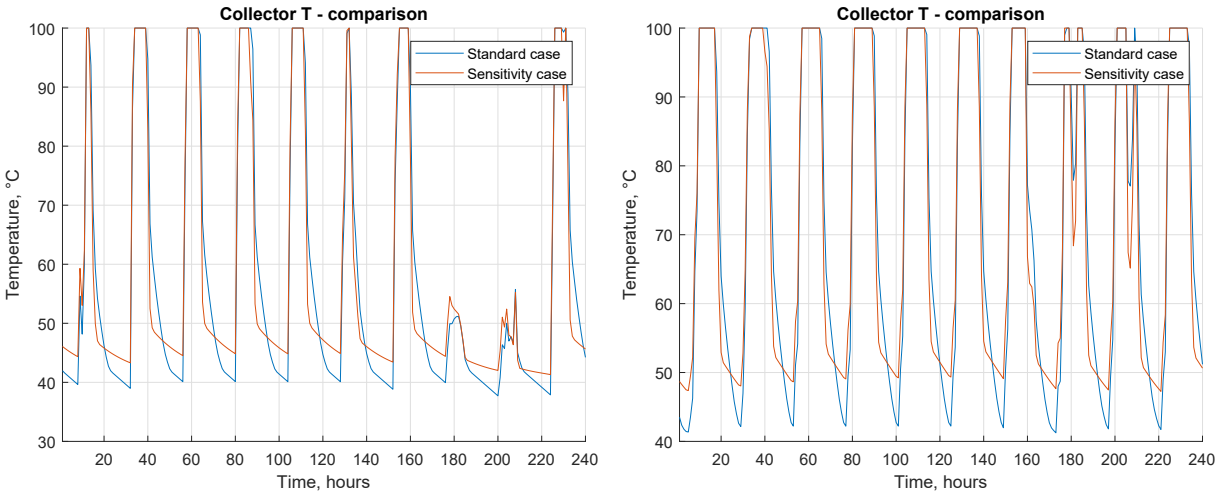

(a) First ten days of January

(b) First ten days of July

Figure 3.38: Collector temperature comparison with number of rows over ten days

3.6 Mass flow to MD

All the sensitivity analysis performed so far aim to increase water productivity (and SF, when convenient) through the temperature increase of saltwater flowing inside the MD unit. The search for the optimal collector position aims to provide the collector with the highest solar radiation possible, which is converted into a mass flow at higher temperature; the number of collectors balances this need with the request of a reduced cost increase; the parallel connection increases the temperature inside the storage tank, even though it decreases the collector outlet temperature; and the storage tank sizing is chosen to promote a temperature increase inside it (and consequently water production), rather than increase the size, and thus the solar fraction.

The analysis carried out in this section regards another aspect of the MD mechanism of water production: the mass flow to MD (which is set always equal to the mass flow circulating in the permeate side). Since the flow control system of the circulating MD pump works between 20 and 250 l/h, the range of this sensitivity anaysis is a 50 l/h interval between 50 l/h and 250 l/h. All the other parameteres were left unchanged.

3.6.1 Output data

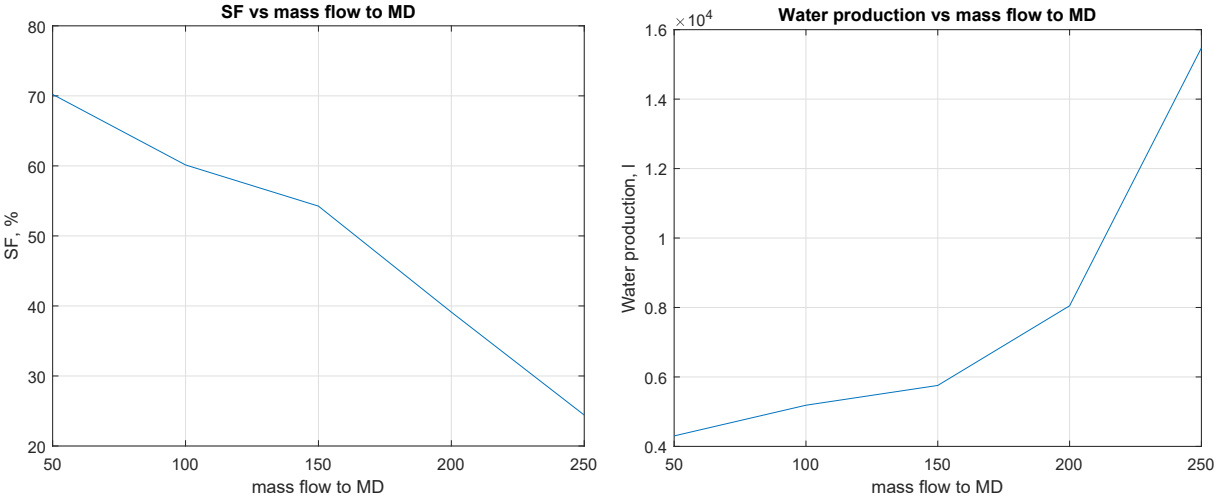

(a) SF variation

(b) Water produced variation

Figure 3.39: SF and water produced vs mass flow to MD

As expected, and shown in Figure 3.39, due to the enhanced heat transfer mechanism, the water productivity increases in a very relevat way (almost three times the standard value), but the SF decreases quickly to less than 25%.

3.6.2 Comparison between the best configuration of mass flow to MD and the standard one

To better understand the mechanism that drives this phenomenon, a comparison between the standard case and the 250 l/h case has been performed.

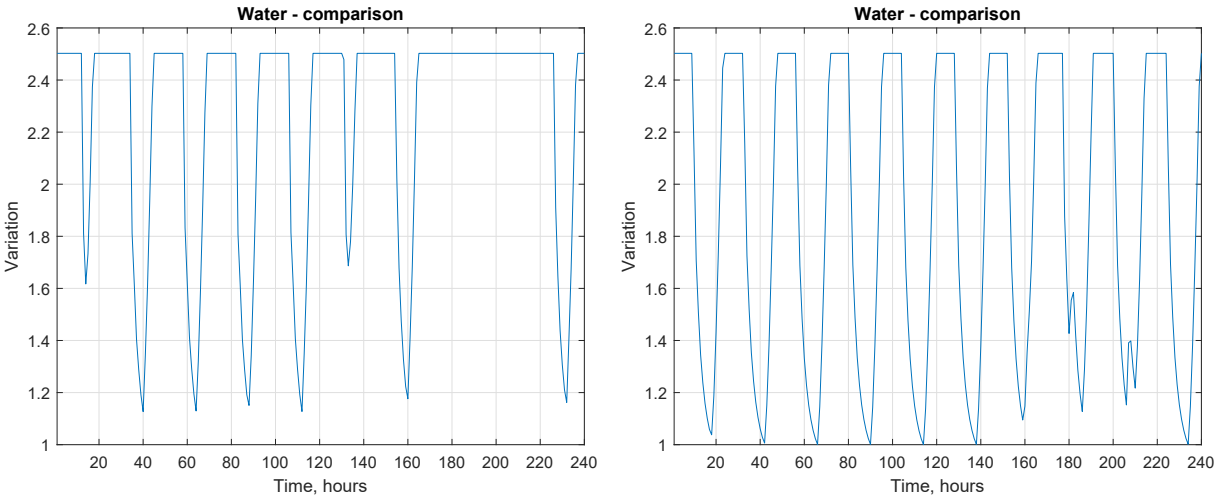

(a) First ten days of January

(b) First ten days of July

Figure 3.40: Water production variation with mass flow to MD over ten days

The increase of mass flow to MD and the thus enhanced heat transfer mechanism facilitate the water production, which experiences an increase in any time of the year (see Figure 3.40). But the analysis of hourly water production in absolute term (Figure 3.41) clearly shows the absence of the characteristic variations over the day, leading to the hypothesis that the temperature of the storage is constantly below the threshold of 50°C. Figure 3.42 and 3.43 demonstate this hypothesis: storage temperature is lower than the standard one at any time of the year. Figure 3.43 clearly shows wat was assumed: that in this configuration the storage acts as a pre-heater since its temperature is everywhere below 50°C, so the auxiliaries is constantly working to provide the necessary supplementary heat.

The increase in provided auxiliary heat is not matched with a corresponding increment of heat obtained through collectors: Figure 3.44 shows very little variation in this configuration, confirmed by Figure 3.45, which shows that the most relevant difference is the collector operation during night time, when the temperature is the one in the storage, lower than the standard configuration one according to what stated before.

Despite the increased water productivity, a bigger mass flow determines a poor behaviour of the solar part. So, since this is a regulation process, the standard mass flow is kept constant, with the awareness that, whether an increased production is needed, this parameter may be changed.

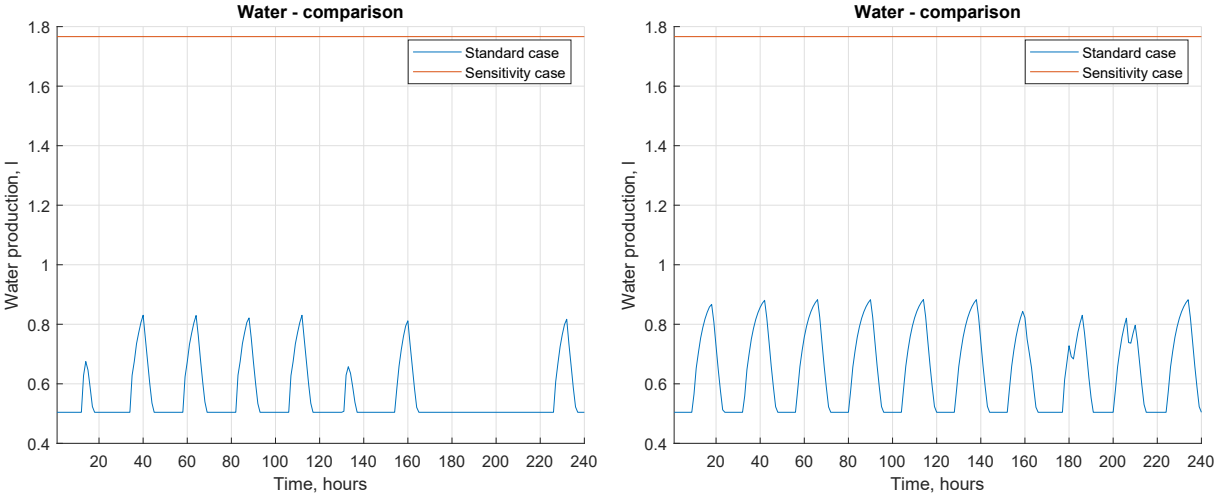

(a) First ten days of January (b) First ten days of July

Figure 3.41: Water production comparison with mass flow to MD over ten days

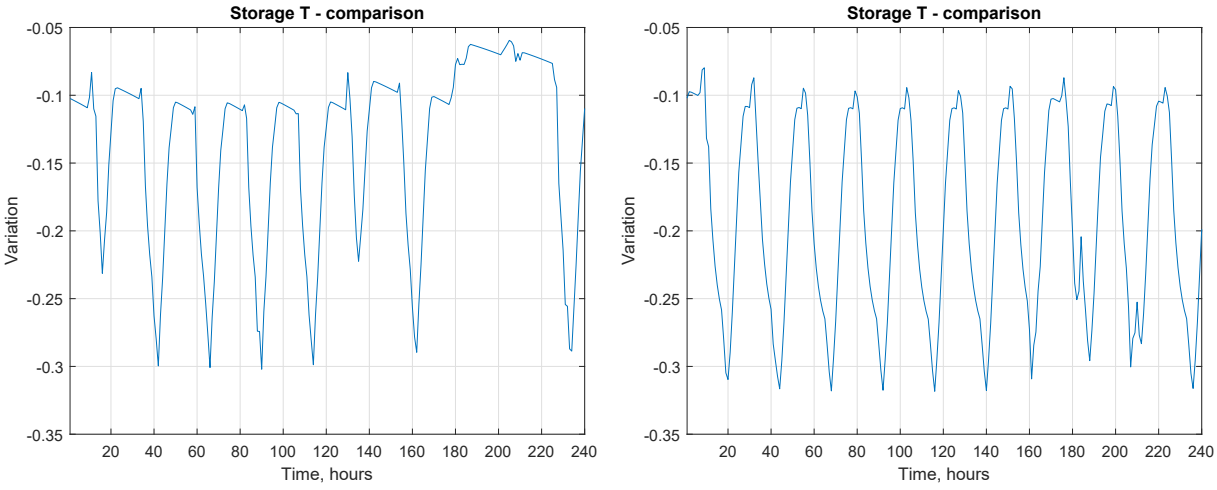

(a) First ten days of January (b) First ten days of July

Figure 3.42: Storage temperature variation with mass flow to MD over ten days

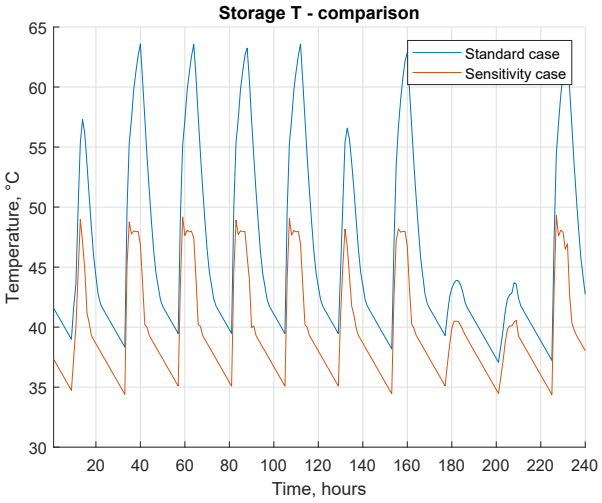

(a) First ten days of January

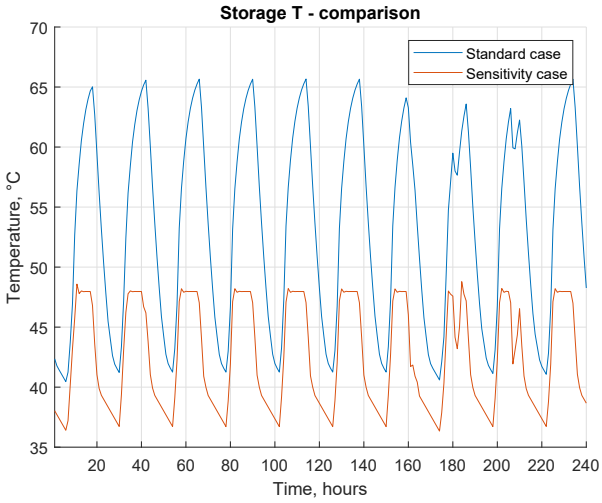

(b) First ten days of July

Figure 3.43: Collector temperature comparison with mass flow to MD over ten days

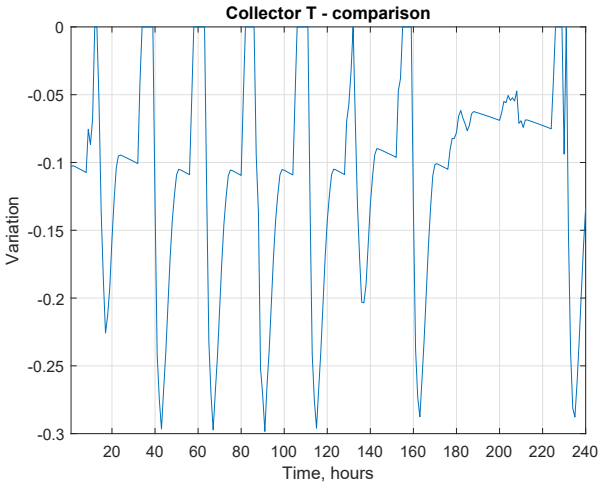

(a) First ten days of January

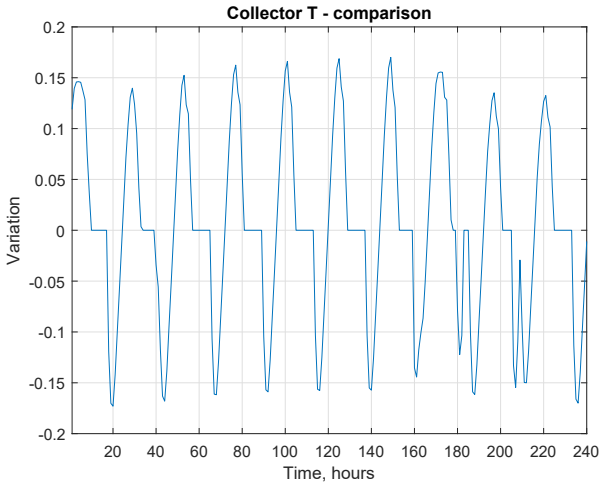

(b) First ten days of July

Figure 3.44: Collector temperature variation with mass flow to MD over ten days

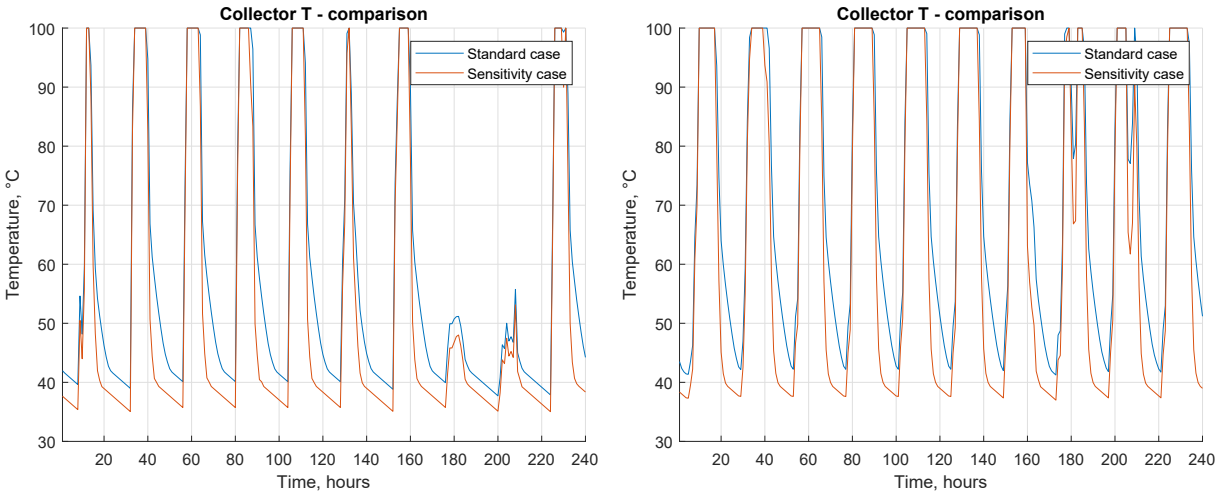

(a) First ten days of January

(b) First ten days of July

Figure 3.45: Collector temperature comparison with mass flow to MD over ten days

3.7 A further analysis: storage tank size and SF

A further analysis is conducted, that analyses the relationship between the tank size and the variation of the solar fraction, obtained through a finer variation (step of 20 l/h) of the mass flow to MD. The aim of this investigation is to better understand the connection between the size of the tank and the maximum temperature that saltwater inside it can reach when varying the withdrawal conditions. All other parameters were left unchanged.

3.7.1 Output data

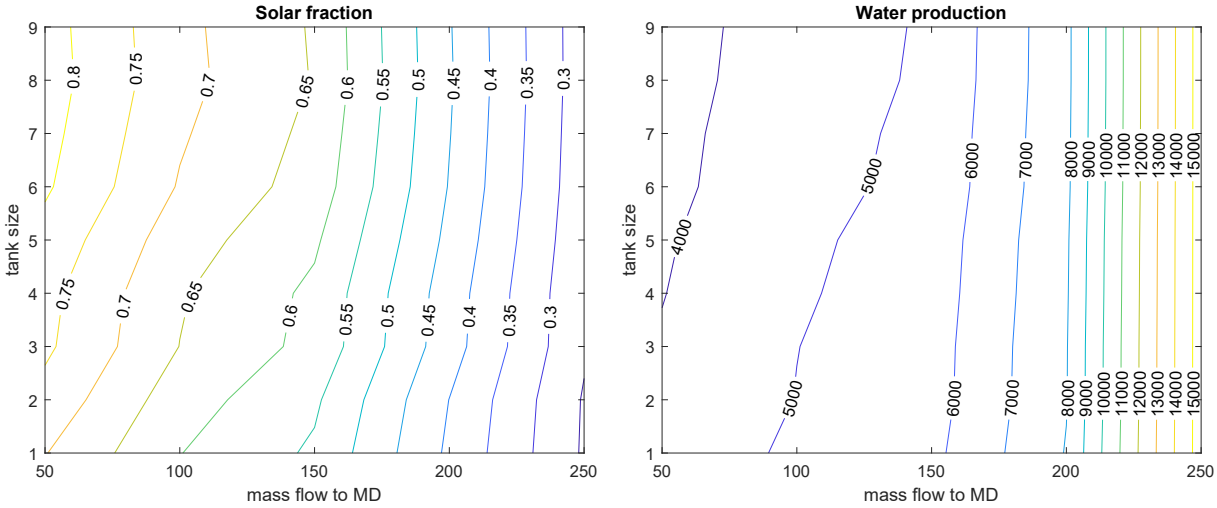

(a) SF variation

(b) Water produced variation

Figure 3.46: SF and water produced vs mass flow to MD

As it can be seen in Figure 3.46, SF and water production vary with the tank size when the mass flow to MD is reduced (approximately below 150 l/h). When this value increases, tank size turns out to be an almost irrelevant parameter in the evaluation of the system. Temperature variations in collector and storage components are much less significant, with values around 50 °C.

3.8 Optimized configuration

The parameters optimized during the previous analysis are listed in Table 3.5.

To sum up, the parameters which are not modified are:

- the number of collectors, due to the production-cost analysis;
- the storage volume, due to the conflicting need of maximizing water production and SF, where the water production was preferred;

Solar data		
β	25°	modified
Υ	-22.5°	modified
Collector data		
number of collectors	6	not modified
number of rows	6	modified
Storage data		
storage volume, l	150	not modified
MD unit data		
feed side flow rate, l/h	100	not modified

Table 3.5: Input data for the optimized model in Turin

- the feed side flow, since its variation leads to a dramatic decrease of SF, and it is a parameter that can be changed also during operation.

The global effect of these optimizations are investigated in the following section.

3.8.1 Output data

The following paragraphs will analyse the improvement caused by the optimization previously performed.

Sun subsystem

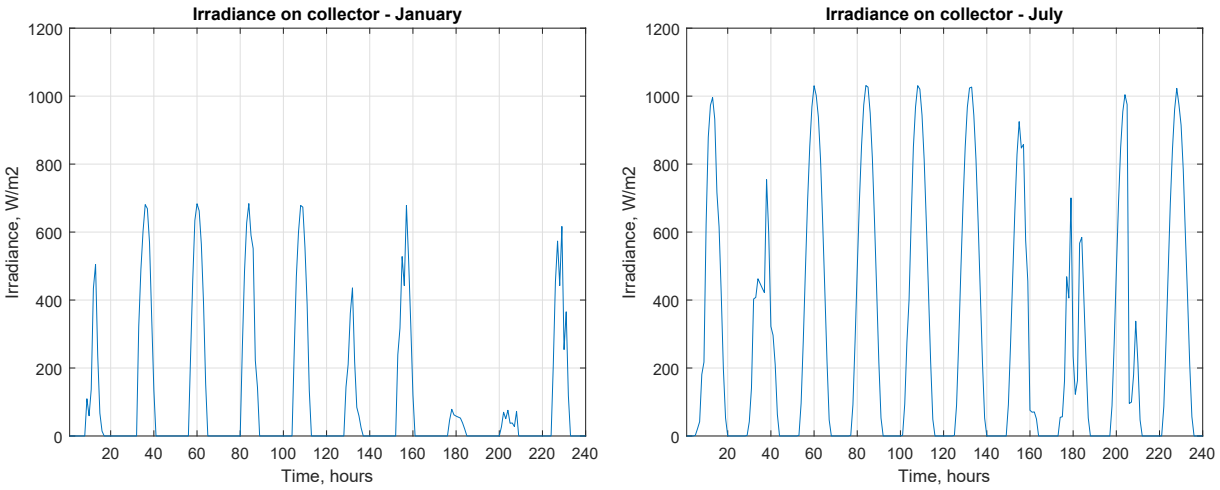

(a) First ten days of January

(b) First ten days of July

Figure 3.47: Irradiance per unit area of collector in the optimized configuration

Figure 3.47 is the practical demonstration of what stated in section 3.2: since the slope is set to optimize irradiation during summer, the irradiation in winter is decreased with respect to the standard configuration, with a maximum value of approximately 700 W/m^2, while irradiation in summer is increased as expected, reaching values higher than 1000 W/m^2.

Collector subsystem

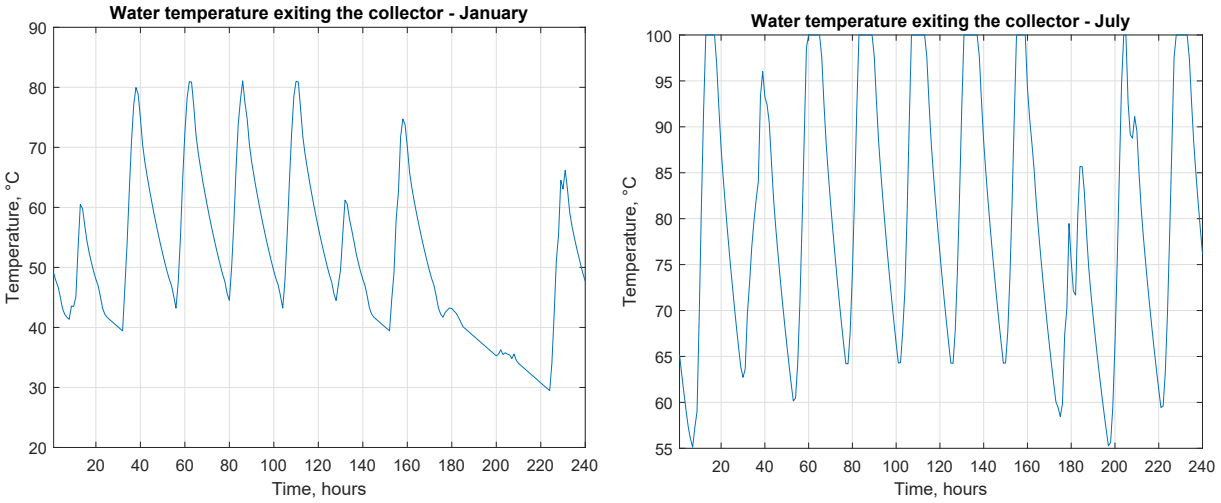

(a) First ten days of January

(b) First ten days of July

Figure 3.48: Collector temperature in the optimized configuration

Figure 3.48 explores the collector temperature variation. During winter, as a consequence of the low irradiance, temperatures are always lower, even though higher than the 50°C threshold but reaching only a 80 °C maximum during the first ten days of January; while during summer temperatures increase up to the upper limit of 100 °C almost every day.

Storage subsystem

The storage subsystem reflects the the collector temperature variations between summer and winter: as shown in Figure 3.49, the temperature in the storage is lower in winter than in summer. Furthermore, the temperature increase is relevantly higher all over the year due to the parallel connection configurations. During summer, temperatures increase up to a maximum value of 86 °C, while during winter the maximum temperature is significantly lower, with a minimum that can reach less than 30 °C, if more than one consecutive day without solar radiation occurs.

The variations in energy contributions to the storage are shown in Figure 3.50, demonstrating that the whole system works with higher energies in summer, as expected.

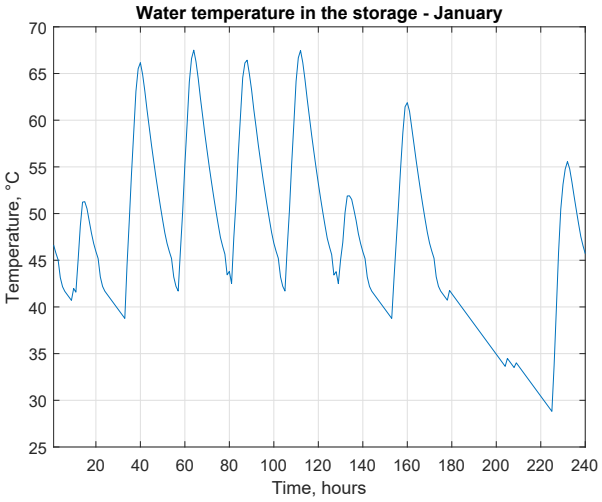

(a) First ten days of January

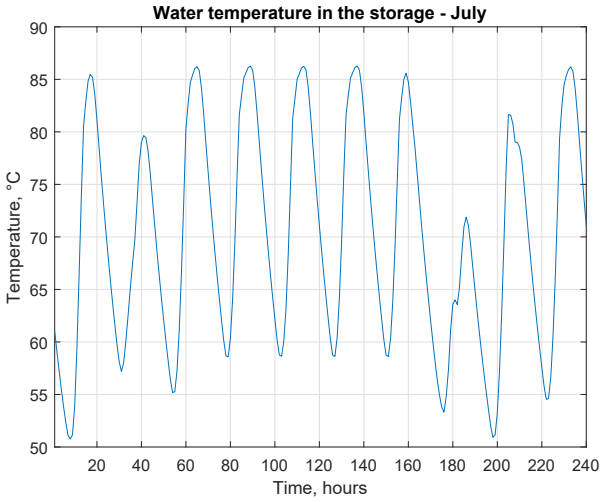

(b) First ten days of July

Figure 3.49: Storage temperature in the optimized configuration

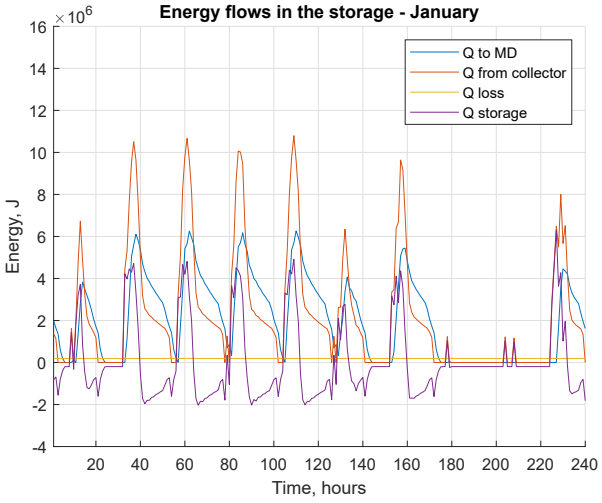

(a) First ten days of January

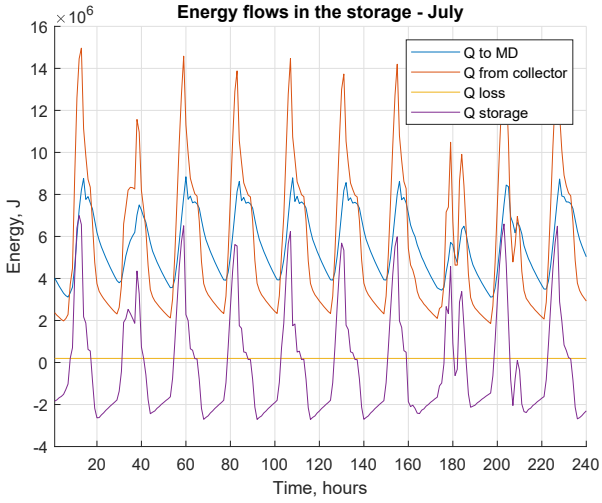

(b) First ten days of July

Figure 3.50: Storage energies in an hour in the optimized configuration

Auxiliaries subsystem

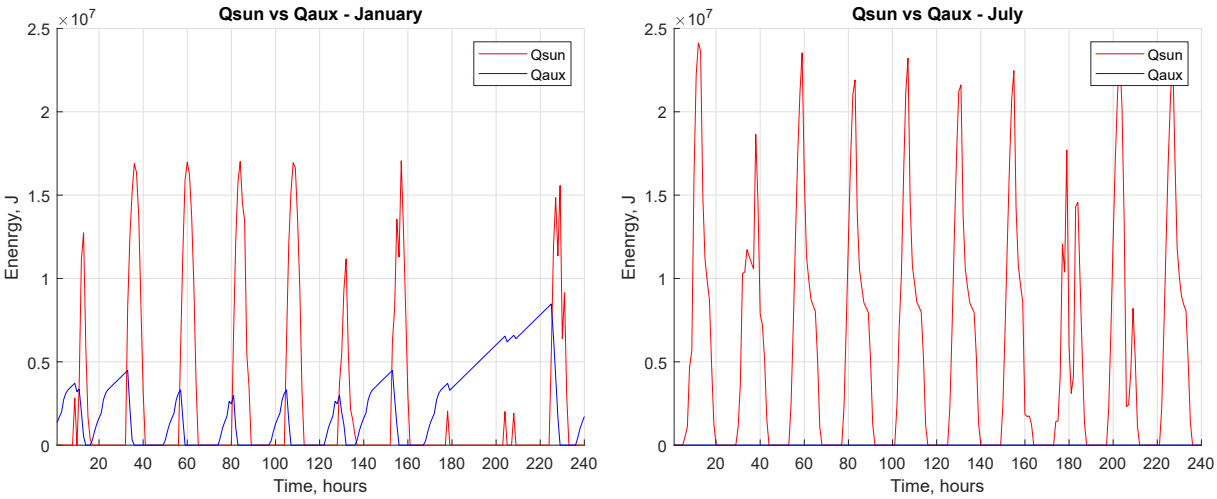

(a) First ten days of January

(b) First ten days of July

Figure 3.51: Solar and auxiliaries heat in the optimized configuration

The auxiliaries functioning is significantly reduced due to the adoption of a parallel configuration. While the auxiliaries work less in winter, it is completely turned off during summer, with a great advantage in terms of solar fraction. The advantages are shown in Figure 3.52

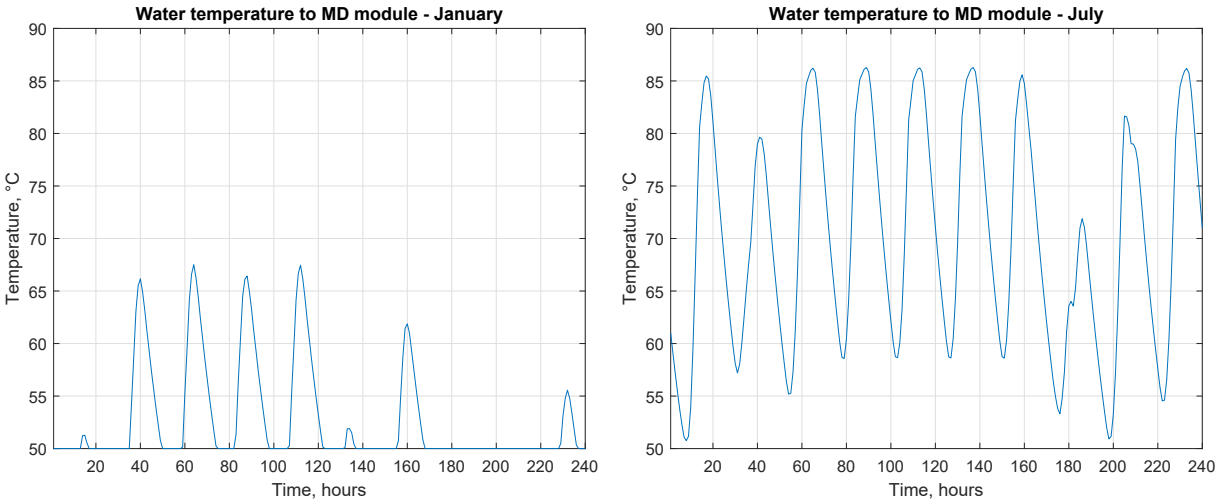

(a) First ten days of January

(b) First ten days of July

Figure 3.52: MD feed temperature in the optimized configuration

MD subsystem

Water production is increased at every time of the year, with a limited variation in winter, and a higher one in summer, with a peak of almost 1.5 l/h during summer noons. This will globally lead to a yearly water production of 6906 l/y. All the relevant parameters are listed in Table 3.6

SF, %	79.98
Yearly water production, l	6906
Daily average water production, l	18.9
Hourly average water production, l	0.788
Global energy consumption, kWh/m^3	1833

Table 3.6: Main output for the optimization model

The results of a further sensitivity analysis on the value of the mass flow to the MD module are shown in the following section.

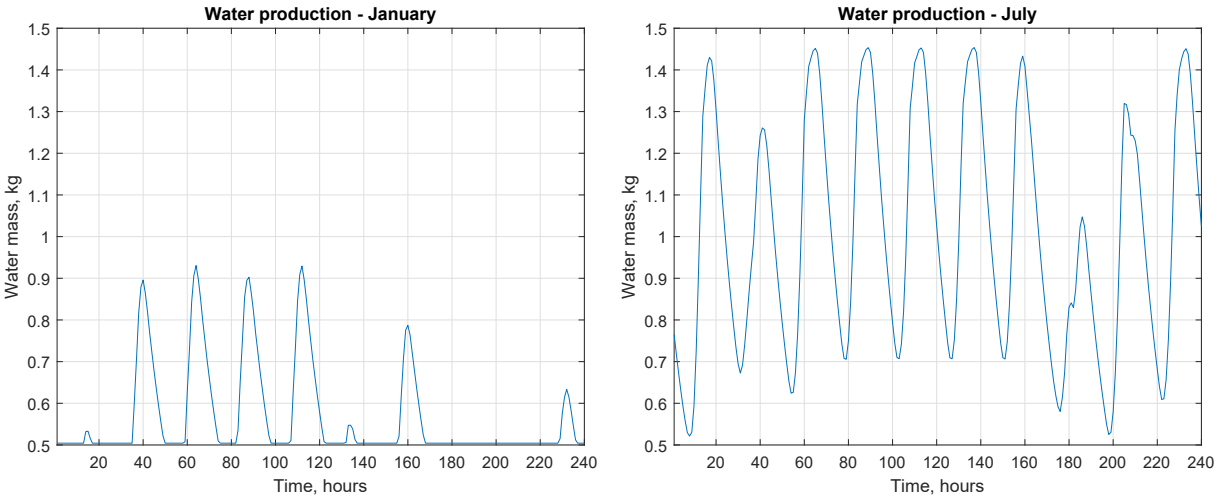

(a) First ten days of January

(b) First ten days of July

Figure 3.53: Hourly water production in the optimized configuration

3.8.2 Economical analysis

As far as the economical analysis is concerned, no modification on the CAPEX is introduced, since the number of collectors and the tank chosen in the standard case are the same. The relevant modified values are the water production and the heat produces by the auxiliaries, which is reflected in the part of the OPEX that analyses fuel consumption. As a consequence, the cost of the water is expected to decrease, since the water produced has increased: the cost retrieve with the procedure shown in subsection 3.1.3 is equal to 0.5183 €/l, with a decrease of 27.3% with respect of the standard value. The variation of MD unit cost explained before lead to a value of 0.1838 €/l when MD cost is reduced to 1/10, 0.1503 €/l when it is reduced to 1/100.

Since it is possible to change the mass flow to MD, an economical analysis of this scenario is performed: a change in water produced and auxiliaries energy are expected, and hence the variation in the water cost is evaluated. Results are shown in Table 3.7. According to the needs, plant can work with low mass flow and high SF, or with high mass flow and high water production and reduced water cost. Despite the increase in auxiliaries heat, the relevant amount of water produced is sufficient to counterbalance it and to decrease the water cost, even though it is still too high if compared to actual water prices.

Looking at data in Table 3.7, it is clear that it is more convenient to increase the mass flow to MD in order to produce more water and reduce its cost. This choice was not considered since it leads to a significant decrease of the SF, and the exploitation of the solar resource is one of the fundamental goals of this configuration. The advantages in terms of environmental footprint are difficult to be estimated based only on an economical analysis.

mass flow to MD, l/h	produced water, l	SF, %	water cost, €/l
50	6005	86.68	0.5808
100	6906	79.98	0.5183
150	7649	74.67	0.4797
200	10633	56.45	0.3873
250	16826	37.83	0.3004

Table 3.7: Variation in produced water, SF and water cost varying mass flow to MD

3.9 Lampedusa

It was previously stated that one of the most common applications of desalination is the water supply of remote areas or small islands. An example is the small Italian island of Lampedusa, which is currently water-fed by a desalination system [5]. Its more favourable position with respect to Turin (its latitude is 35°) should allow a solar plant placed on the island to achieve better results in terms of water production and SF.

Table 3.8 shows the results of the standard, sensitivity and best configuration analysis performed; Appendix C contains plots of the most relevant quantities. As can be seen, the foreseen result are confirmed by these data.

	best/ comparison value	produced water, l	SF, %	water cost, €/l
standard	-	5382	68.45	0.6746
sensitivity - slope and azimuth	β=15 ° γ=-45 °	5412	69.14	-
sensitivity - number of collectors	30	5706	76.84	-
sensitivity - number of rows	6	7806	96.03	-
sensitivity - storage tank volume	9	4506	82.60	-
sensitivity - mass flow to MD	250 l/h	15475	28.99	-
best configuration	β=15 ° γ=-45 ° number of rows=6	7646	94.08	0.4486

Table 3.8: Lampedusa - relevant results

Chapter 4

Conclusions

Water scarcity is a real and actual problem, as demonstrated by the cases of Cape Town and India, considered as representatives of the problems of an uncontrolled and not far-sighted management of water resources in both urban and agricultural context, especially when coupled with climate changes. Among the possible solutions, seawater desalination appears to be an interesting way to obtain the needed freshwater without depleting groundwater resources, whose extent is only roughly estimated. The interesting case of a solar thermal plant connected with an MD module is considered, since it has the great advantage of joining the possibility to exploit renewable energies, which can be useful on remote areas, with a novel technology which may allow a possible solution to one of the greatest desalination issues: brine disposal.

Simulink software has been used to develop a model that takes into account every component of the plant: the irradiation computation, the evaluation of the thermal energy gained thanks to the vacuum tube solar collectors, the brine storage tank dynamics, the presence and intervention of the auxiliaries, and the MD module itself, which converts hot saltwater into freshwater. This model was coupled with an economical analysis, with the aim to assess plant costs and to estimate water cost considering the whole life of the plant.

The standard configuration has a yearly water production of 5186 l, with a solar fraction of approximately 60%, a global energy consumption of 1915 kWh/m^3 and a water cost estimated in 0.71 €/l, more than 1000 times higher that current water prices. A sensitivity analysis has been carried out, considering all the most relevant parameters of the plant. Slope and azimuth adjustments provide only a small increment in both solar fraction (+1.6%) and water production (+0.5%). The number of collectors increases both the SF and the water producton, but the water cost increases exceeding 1 €/l. A Pareto curve has been drawn, comparing the total cost during the plant life and the total water production during the same period, and the initial configuration results to be the best trade-off between high production and low cost. As far as series or parallel connection are concerned, the parallel configuration is the best one, since it guarantees a remarkable increase in both SF (+34.2%) and water production (+33.1%) due to a better exploitation of the solar resources. The increase in storage tank size allows a better solar exploitation (SF increases), but the temperature decreases, and thus also the water production decreases: the choice of a bigger tank results unconvenient. The variation of the flow to the MD component has a very relevant impact on both SF and water production: the enhanced heat

transfer mechanism inside MD may increase water production of more than twice the standard configuration value, but the SF decreases in a dramatic way, reaching 25%. So, it is suggested to adopt the best slope and azimuth angles retrieved along with a parallel configuration, while MD flow can be varied according to the necessities, to enhance solar resource use or to increase water production. The final configuration allows to obtain almost 7000 l (6906 l) with a solar fraction of approximately 80% at a cost of 0.52€/l; this value can be increased to a maximum water production of 16826 l, a SF of 37.83% and a water cost of 0.30 €/l. A comparison with another Italian location, Lampedusa island, has been performed: this change allows a slight improvement in terms of water production, SF and cost.

The low water production may be justified with the following reasons:

- MD technology is still a R&D technology;
- DCMD module is the less performing of the MD category, since it is the basic concept of the technology, and has no enhancing mechanism;
- no heat recovery is performed in this plant due to the presence of a chiller;
- the module used is a laboratory one: its dimensions, in particular as far as the membrane is concerned, are very reduced: while small lants for water production have membrane of several m^2 [58], this module has only 0.05 m^2 of membrane; the water production is directly proportional to the membrane area, so the production is heavily influenced. This is the most relavant reason of the poor performance of the plant.

So, the use of production modules and of more performing MD technologies are expected to increase the performance of the plant. Moreover, it can be considered the use of a stratified tank, evaluating the influence that saltwater use as a storage fluid can have on stratification, and, if appropriate, substitute it with water. Also, a coupling with another desalination technology, such as RO, can be evaluated.

Appendices

Appendix A

Seawater properties

A.1 Seawater dynamic viscosity

This physical property is calculated according to empirical correlations from [51], as cited in [94]. The ranges of temperature T and salinity S in which this correlation is valid are, respectively, from 10 to 180 °C and from 0 to 130 g/kg; these are also the unit or measure to be considered in the equation.

Dynamic viscosity η is calculated in cP (10^3 Pa s), with a maximal error of 2%.

$$\eta = \eta_w \, \eta_R \tag{A.1}$$

where:

$$\log \eta_w = -3.79418 + \frac{604.129}{139.18 + T}$$

$$\eta_R = 1 + a_1 \, S + a_2 \, S^2$$

$$a_1 = 1.474 \cdot 10^{-3} + 1.5 \cdot 10^5 \, T - 3.927 \cdot 10^{-8} \, T^2$$
$$a_2 = 1.0734 \cdot 10^{-5} - 8.5 \cdot 10^{-8} \, T + 2.23 \cdot 10^{-10} \, T^2$$

A.2 Seawater density

This physical property is calculated according to empirical correlations from [51], as cited in [94]. The ranges of temperature T and salinity S in which this correlation is valid are, respectively, from 10 to 180 °C and from 0 to 160 g/kg; these are also the unit or measure to be considered in the equation.

Density ρ is calculated in kg/dm^3.

$$\rho = 0.5 \, a_0 + a_1 \, Y + a_2 \, (2 \, Y^2 - 1) + a_3 \, (4 \, Y^3 - 3 \, Y) \tag{A.2}$$

where:

$$a_0 = 2.01611 + 0.115313\,\sigma + 0.000326\,(2\sigma^2 - 1)$$
$$a_1 = -0.0541 + 0.001571\,\sigma - 0.000423\,(2\sigma^2 - 1)$$
$$a_2 = -0.006124 + 0.00174\,\sigma - 0.000009\,(2\sigma^2 - 1)$$
$$a_3 = 0.000346 + 0.000087\,\sigma - 0.000053\,(2\sigma^2 - 1)$$

$$Y = \frac{2\,T - 200}{160}$$

$$\sigma = \frac{2\,S - 150}{150}$$

A.3 Seawater thermal capacity

This physical property is calculated according to empirical correlations from [51], as cited in [94]. The ranges of temperature T and salinity S in which this correlation is valid are, respectively, from 10 to 160 °C and from 0 to 160 g/kg; these are also the unit or measure to be considered in the equation.

Thermal capacity c_p is calculated in J/(kg K), with a maximal error of 1%.

$$c_p = A + B\,T + C\,T^2 + D\,T^3 \tag{A.3}$$

where:

$$A = 4206.8 - 6.6197\,S + 1.2288 \cdot 10^{-2} S^2$$
$$B = -1.1262 + 5.4178 \cdot 10^{-2}\,S - 2.2719 \cdot 10^{-4}\,S^2$$
$$C = 1.2026 \cdot 10^{-2} - 5.3566 \cdot 10^{-4}\,S + 1.8906 \cdot 10^{-6}\,S^2$$
$$D = 6.8774 \cdot 10^{-7} + 1.5170 \cdot 10^{-6}\,S - 4.4268 \cdot 10^{9}\,S^2$$

A.4 Seawater thermal conductivity

This physical property is calculated according to empirical correlations from [51], as cited in [94]. The ranges of temperature T and salinity S in which this correlation is valid are, respectively, from 10 to 150 °C and from 0 to 100 g/kg; these are also the unit or measure to be considered in the equation. As suggested in [94] and [79], salinity is always set to zero.

Thermal conductivity λ is calculated in W/(m K).

$$\lambda = (A + B\,T + C\,T^2) \cdot 10^{-3} \tag{A.4}$$

where:

$$A = 576.6 - 34.64\,CA + 7.286\,CA^2$$
$$B = (1526 + 466.2\,CA - 226.8\,CA^2 + 28.67\,CA^3) \cdot 10^{-3}$$
$$C = -(581 + 2055\,CA - 991.6\,CA^2 + 146.4\,CA^3) \cdot 10^{-5}$$

$$CA = \frac{28.17\,S}{1000 - S}$$

Considering tht salinity is set to zero, the final equation will be:

$$\lambda = (576.6 + 1526 \cdot 10^{-3}\,T - 581 \cdot 10^{-5}\,T^2) \cdot 10^{-3} \tag{A.5}$$

A.5 Seawater vapour pressure

The relation between water vapour pressure and seawater vapour pressure is known from [79]:

$$p_{v,w}/p_{v,sw} = 1 + 0.57357 \cdot fracS1000 - S \tag{A.6}$$

Water vapour pressure is thus computed using Antoine law, whose coefficient are expressed in a form that requires temperature T in K and is valid between 255.9 and 373 K [68]. Output is in bar.

$$\log_{10} p = A - \frac{B}{T + C} \tag{A.7}$$

where:

$$A = 4.6543$$
$$B = 1435.264$$
$$C = -64.848$$

Appendix B

Heat exchanger analysis

B.1 Heat exchanger properties

Source [10] provides the information listed in Table B.1 for heat exchanger ETW-B3-23x40, under the assumptions of the coupling betwen solar panels and a buffer:

It is known that:

$$Q = (UA)LMTD \tag{B.1}$$

where U is the global heat transfer coefficient and $LMTD$ is the logarithmic mean temperature difference, defined as:

$$LMTD = \frac{\Delta T_{out} - \Delta T_{in}}{\log \frac{\Delta T_{out}}{\Delta T_{in}}} \tag{B.2}$$

where:

- ΔT_{out} is the difference between the exiting temperatures;
- ΔT_{in} is the difference between the entering temperatures.

So, UA is equal to:

$$UA = \frac{Q}{LMTD} \simeq 323.5 \frac{W}{K} \tag{B.3}$$

Power transferred, kW	7
Inlet T, glycol-water side, °C	60
Outlet T, glycol-water side, °C	35
Inlet T, water side, °C	30
Outlet T, water side, °C	50

Table B.1: Data from the HE manifacturer[10]

B.2 ε-NTU method

$\varepsilon - NTU$ method is one of the ways in which a HE can be analysed. Its key parameters are:

- NTU, or Number of Transfer Units, defined as:

$$NTU = \frac{UA}{\dot{C}_{min}} \tag{B.4}$$

  where $\dot{C}$ is the heat capacity rate, equal to:

$$\dot{C} = \dot{m}c \tag{B.5}$$

  for every flux involved.

- ε, defined as the thermal efficiency:

$$\epsilon = \frac{Q}{Q_{max}} \tag{B.6}$$

  where Q_{max} is the maximum heat flux, defined as the one that raises the temperature of the flux characterized by the smallest heat capacity rate until it reaches the inlet temperature of the other fluid [9]:

$$Q_{max} = \dot{C}_{min}(T_{in,max} - T_{in_min}) \tag{B.7}$$

- r, defined as the ratio between the minimum and the maximum heat capacity rate:

$$r = \frac{\dot{C}_{min}}{\dot{C}_{max}} \tag{B.8}$$

Under the assumption that $r = 1$, both heat capacity rates are equal to $m_{coll}c$. If a case of perfect counter-current is considered, the thermal efficiency is equal to [9]:

$$\varepsilon = \frac{NTU}{NTU + 1} \tag{B.9}$$

In the considered case, the thermal efficiency is 0.85.

Appendix C

Relevant plots - Lampedusa

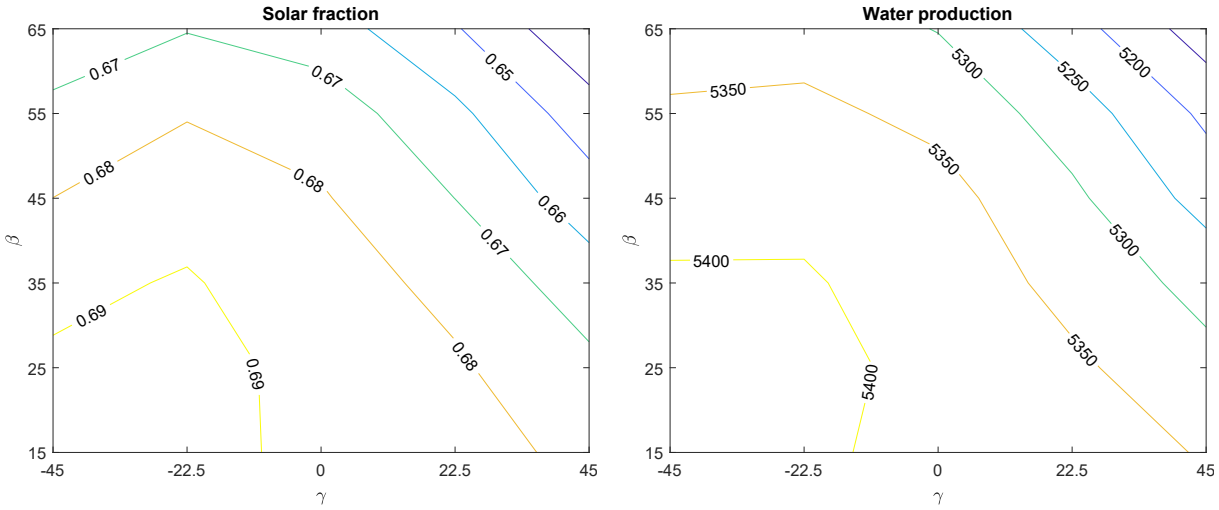

(a) SF variation

(b) Water produced variation

Figure C.1: SF and water produced vs β and γ

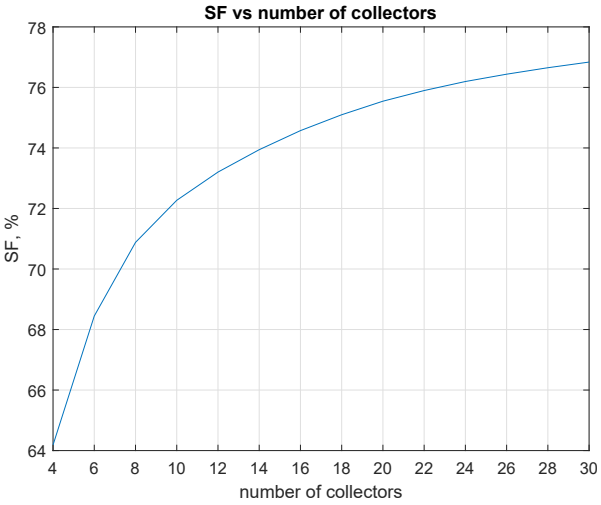

(a) SF variation

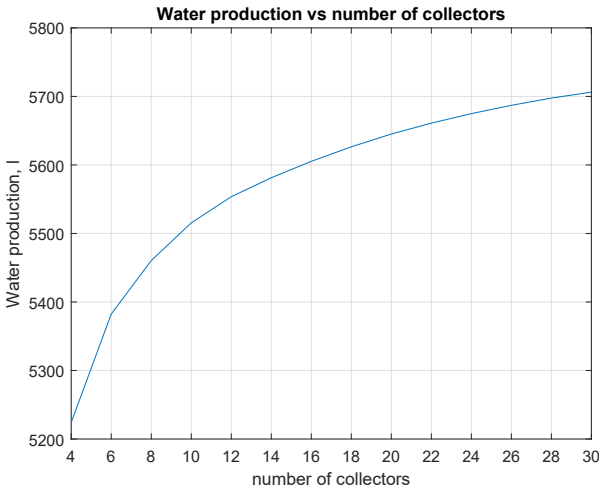

(b) Water produced variation

Figure C.2: SF and water produced vs number of collectors

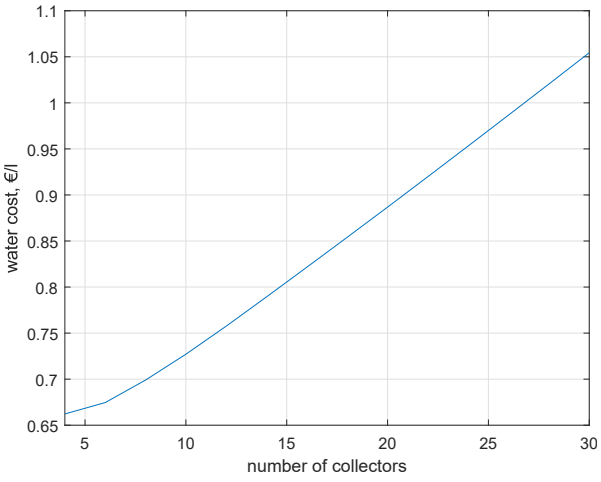

(a) Cost of water

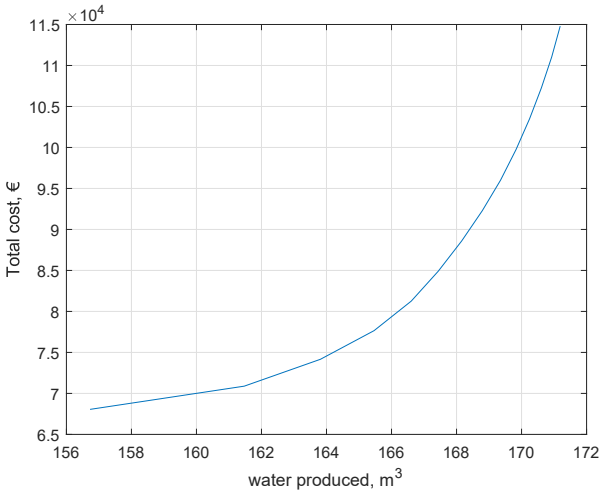

(b) Pareto curve

Figure C.3: Cost of water and Pareto curve vs number of collectors

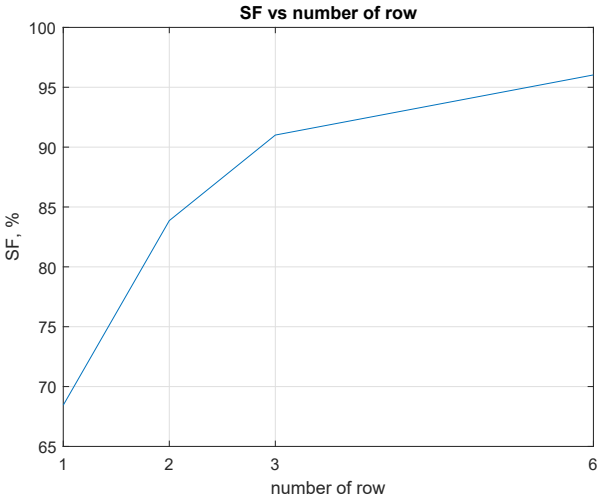

(a) SF variation

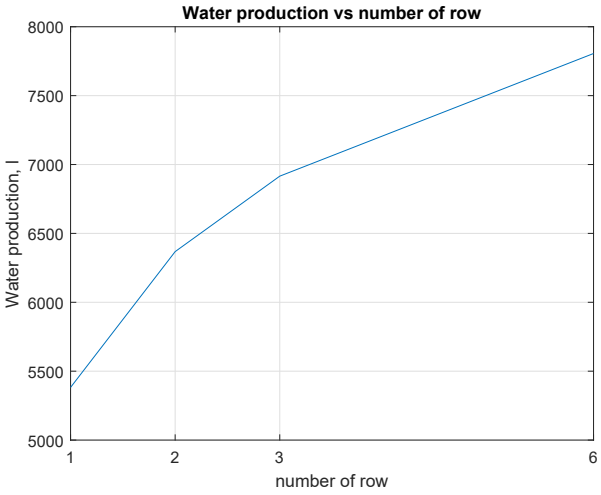

(b) Water produced variation

Figure C.4: SF and water produced vs number of rows

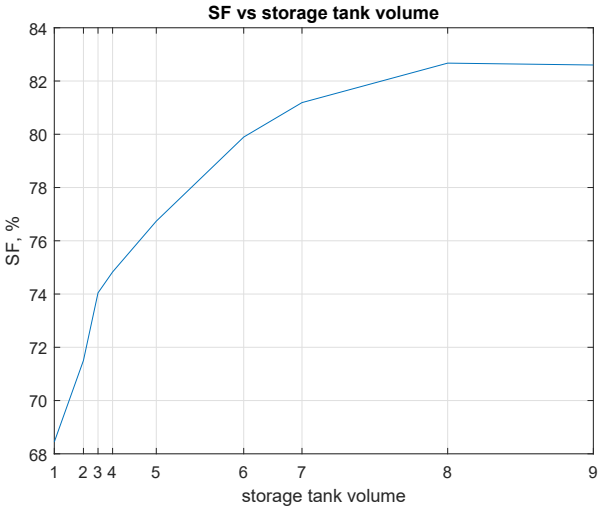

(a) SF variation

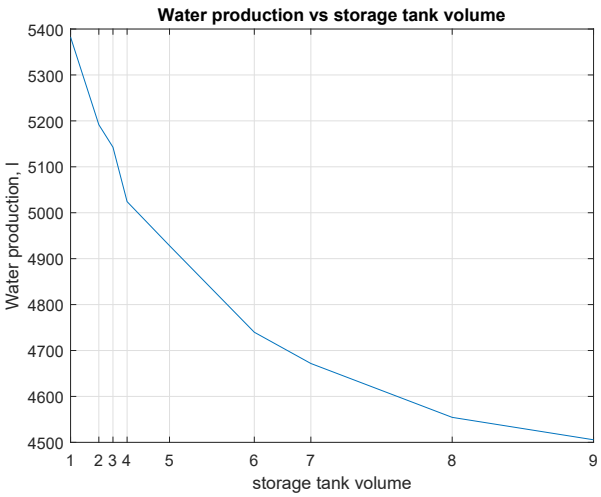

(b) Water produced variation

Figure C.5: SF and water produced vs storage tank size

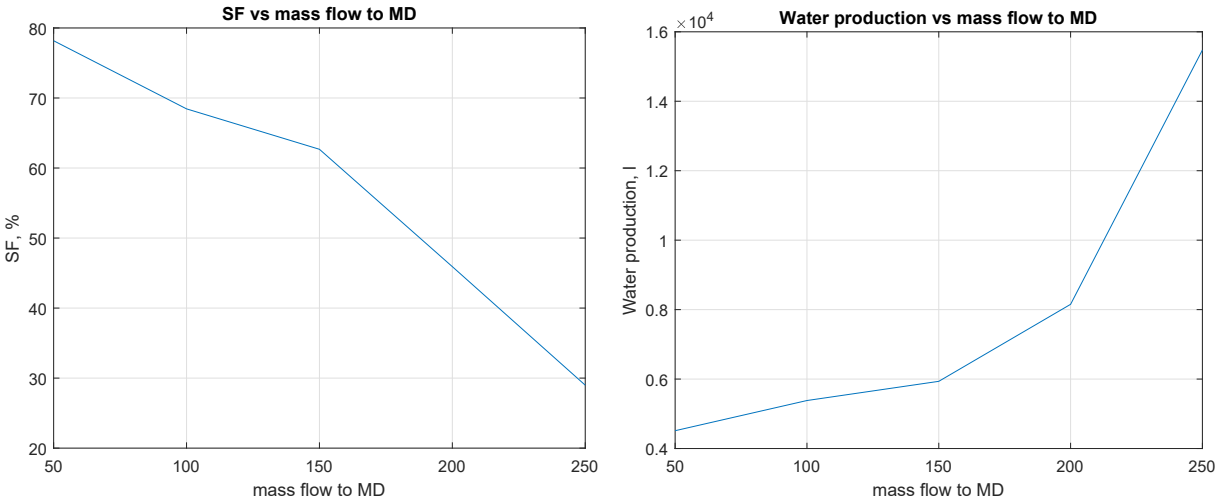

(a) SF variation (b) Water produced variation

Figure C.6: SF and water produced vs mass flow to MD

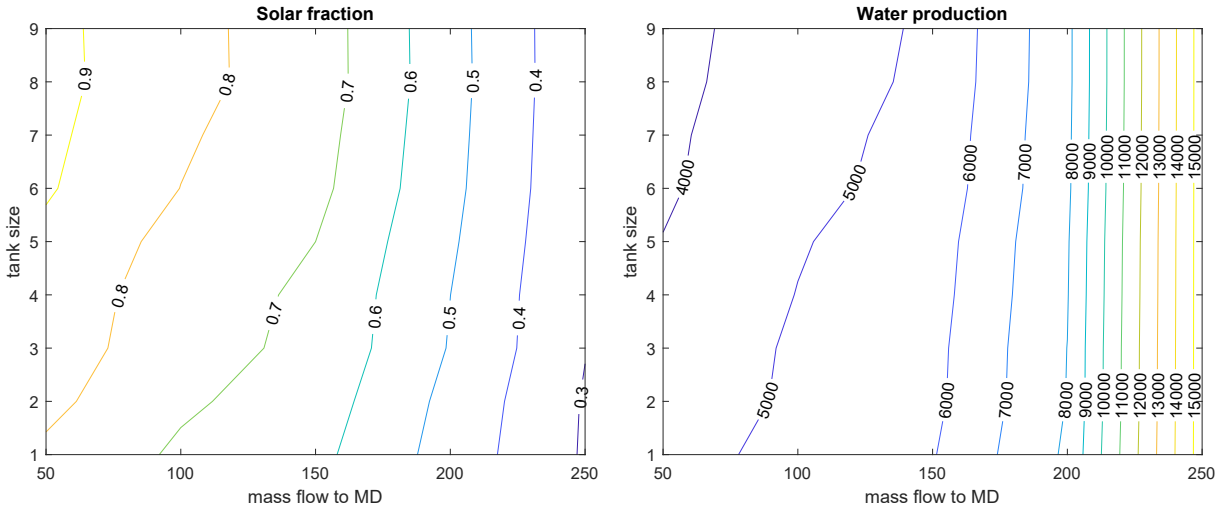

(a) SF variation (b) Water produced variation

Figure C.7: SF and water produced vs storage tank volume and mass flow to MD

Nomenclature

Abbreviations

AGMD Air Gap Membrane Distillation

APFMGS Andhra Pradesh Farmer-Managed Groundwater Systems

DCMD Direct Contact Membrane Distillation

DHW Domestic Hot Water

ENSO El Niño Southern Oscillation

ETC Evacuated tube collectors

EU European Union

FAO Food and Agriculture Organization

FPC Flat-plate collectors

GDP Gross Domestic Product

GNI Gross National Income

GRACE Gravity Recovery And Climate Experiment

HDI Human Development Index

HE Heat Exchanger

HTF Heat Transfer Fluid

IPCC Intergovernamental Panel for Climate Change

Istat Istituto nazionale di Statistica

LEP Liquid Entry Pressure

MD Membrane Distillation

MED Multiple-Effect Distillation

MSF Multi Stage Flash

MVC Mechanical Vapour Compression

NASA National Aeronautics and Space Administration

NF Nano Filtration

NGO Non-Governmental Organization

NITI National Institution for Transforming India

PV photovoltaic

PVGIS Photovoltaic Geographical Information System

RO Reverse Osmosis

SGMD Sweeping Gas Membrane Distillation

TMY Typical Meteorological Year

TVC Thermal Vapour Compression

UN United Nations

US United States

VMD Vacuum Membrane Distillation

VTC Vacuum tube collectors

Subscripts

$_0$ reference conditions

$_{amb}$ ambient

$_{coll}$ collector

$_{disp}$ dispersed

$_D$ diffusion

$_e$ external

$_{feed}$ feed side of MD module

$_f$ feed side of MD module

$_{ins}$ insulation

$_{in}$	inlet
$_{i}$	internal
$_{Kn}$	Knudsen
$_{loss}$	losses
$_{max}$	maximum
$_{MD}$	Membrane Distillation module
$_{min}$	minimum
$_{m}$	membrane
$_{out}$	outlet
$_{p}$	permeate
$_{stor}$	storage
$_{sw}$	seawater
$_{u}$	useful
$_{w}$	water

Symbols

β	slope
δ	declination
δ_m	membrane thickness, m
$\dot{m}$	mass flow rate
$\dot{Q}$	thermal power
$\dot{C}$	heat capacity rate
η	collector efficiency
η_0,c_1,c_2	efficiency coefficients
γ	surface azimuth angle
NTU	Number of Transfer Unit

μ	dynamic viscosity	
ω	hour angle	
ϕ	latitude	
ρ	albedo	
ρ	density	
θ	angle of incidence of BNI on the surface	
ε	thermal efficiency in a HE	
A	area	
BNI	Beam Normal Irradiance	
C	membrane coefficient, kg/(s m^2 Pa)	
c	specific heat	
d	tube diameter	
DHI	Diffuse Horizontal Irradiance	
F_{c-g}	collector-ground view factor	
F_{c-s}	collector-sky view factor	
G	total irradiance	
G_k	irradiation constant	$800\,W/m^2$
GHI	Global Horizontal Irradiance	
h	convection heat transfer coefficient	
I_T	irradiation on collector	
K	global transfer coefficient	
k	heat conductivity	
k	thermal conductivity	
$LMTD$	logarithmic mean temperature difference	
m	mass	
N	mass transferred per unit area of the membrane, kg/(s m^2)	
Nu	Nusselt number	

p_v	vapour tension, Pa
Pr	Prandtl number
Q	energy
r	radius
Re	Reynolds number
SF	solar fraction, -
T	temperature
t	time
T_m	mean temperature of the collector
T_{pm}	mean (absorber) plate temperature
U	global heat transfer coefficient
U_L	overall loss coefficient
v	fluid mean velocity
x	efficiency variable

Bibliography

[1] Autorità d'ambito n. 3 "Torinese". *ARTICOLAZIONE TARIFFARIA PER IL SERVIZIO IDRICO INTEGRATO ANNO 2018)*. URL: http://www.ato3torinese.it/site2015/utenti/tariffe/004_tariffe-TICSI-2018_del-704.pdf. (accessed: 25.02.2019).

[2] NITI Aayog. *Composite water management index*. A tool for water management - June 2018. URL: http://www.niti.gov.in/writereaddata/files/document_publication/2018-05-18-Water-index-Report_vS6B.pdf. (accessed: 05.03.2019).

[3] Mohamed Abduljawad and Usama Ezzeghni. "Optimization of Tajoura MSF desalination plant". In: *Desalination* 254.1-3 (2010), pp. 23–28. DOI: https://doi.org/10.1016/j.desal.2009.12.019.

[4] A. Alkhudhiri, Darwish N., and N. Hilal. "Membrane distillation: A comprehensive review". In: *Desalination* 287 (2012), pp. 2–18. DOI: https://doi.org/10.1016/j.desal.2011.08.027.

[5] Nino Amadore. "Lampedusa, il pasticcio dell'acqua". In: *Sole24Ore* (Aug. 3, 2016). URL: https://www.ilsole24ore.com/art/impresa-e-territori/2016-08-02/lampedusa-pasticcio-dell-acqua-115728.shtml?refresh_ce=1.

[6] Aquastill. *MD Lab scale unit*.

[7] ARERA. *Andamento del prezzo del gas naturale per un consumatore domestico tipo in regime di tutela*. URL: https://www.arera.it/it/dati/gp27new.htm. (accessed: 25.02.2019).

[8] Francesco Artuso. *Solar Concentration and Membrane Distillation coupling: System Model and Case Studies*. 2018.

[9] Cesare Bonacina, Alberto Cavallini, and Lino Mattarolo. *Trasmissione del Calore*. Cleup, 1989.

[10] *Brazed plate heat exchangers - Examples of application*. URL: http://www.brazed-plate-heat-exchanger.com/anwendungen.htm. (accessed: 15.02.2019).

[11] Alan Buis and Janet - NASA Global Climate Change Wilson. *Study: A third of big groundwater basins in distress*. URL: https://climate.nasa.gov/news/2297/study-a-third-of-big-groundwater-basins-in-distress/. (accessed: 05.03.2019).

[12] U. Caldera, D. Bogdanov, and C. Breyer. "Local cost of seawater RO desalination based on solar PV and wind energy: A global estimate". In: *Desalination* 385 (2016), pp. 207–216. DOI: https://doi.org/10.1016/j.desal.2016.02.004.

[13] City of Cape Town. *City of Cape Town*. URL: https://www.capetown.gov.za/. (accessed: 05.03.2019).

[14] City of Cape Town. *Statement by the City's Executive Deputy Mayor - 29 January 2018*. URL: http://www.capetown.gov.za/Media-and-news/50%5C%20litres%5C%20per%5C%20day%5C%20will%5C%20help%5C%20us%5C%20to%5C%20avoid%5C%20Day%5C%20Zero. (accessed: 05.03.2019).

[15] City of Cape Town. *Statement by the City's Executive Mayor - 31 May 2017*. URL: http://www.capetown.gov.za/media-and-news/Water%5C%20resilience%5C%20a%5C%20heightened%5C%20approach%5C%20to%5C%20avoiding%5C%20water%5C%20shortages%5C%20and%5C%20achieving%5C%20long-term%5C%20water%5C%20security. (accessed: 05.03.2019).

[16] City of Cape Town. *Think water*. URL: www.capetown.gov.za/thinkwater. (accessed: 05.03.2019).

[17] M.T. Chaibi and Ali M. El-Nashar. "Solar Thermal Processes". A Review of Solar Thermal Energy Technologies for Water Desalination. In: Andrea Cipollina, Giorgio Micale, and Lucio Rizzuti. *Seawater Desalination*. Springer, 2009. DOI: https://doi.org/10.1007/978-3-642-01150-4_6.

[18] Andrea Cipollina, Giorgio Micale, and Lucio Rizzuti. "Seawater Desalination for Freshwater Production". In: *Seawater Desalination*. Springer, 2009. DOI: https://doi.org/DOI10.1007/978-3-642-01150-4_1.

[19] IPCC - Intergovernamental Panel for Climate Change. *Climate Change 2014: Impacts, Adaptation, and Vulnerability - Part B: Regional Aspects*. WG II - Working Group II contribution to the Fifth Assessment Report of the Intergovernamental Panel for Climate Change. URL: https://www.ipcc.ch/site/assets/uploads/2018/02/WGIIAR5-PartB_FINAL.pdf. (accessed: 05.03.2019).

[20] OIC - Organismo Italiano di Contabilità. *Principi contabili - Immobilizzazioni materiali*. Testo del principio contabile emanato nel dicembre 2016 ed aggiornato con gli emendamenti pubblicati il 29 dicembre 2017. URL: http://www.fondazioneoic.eu/wp-content/uploads/2011/02/2017-12-OIC-16-Immobilizzazioni-materiali.pdf. (accessed: 25.02.2019).

[21] Efrem Curcio and Enrico Drioli. "Membranes for Desalination". In: Andrea Cipollina, Giorgio Micale, and Lucio Rizzuti. *Seawater Desalination*. Springer, 2009. DOI: https://doi.org/DOI10.1007/978-3-642-01150-4_3.

[22] M.O. Cuthbert et al. "Global patterns and dynamics of climate-groundwater interactions". In: *Nature climate change* 9 (2019), pp. 137–141. DOI: https://doi.org/10.1038/s41558-018-0386-4.

[23] Derek van Dam. "Cape Town contends with worst drought in over a century". In: *CNN* (June 1, 2018). URL: https://edition.cnn.com/2017/05/31/africa/cape-town-drought/index.html.

[24] PubChem database. *Propylene Glycol*. URL: https://pubchem.ncbi.nlm.nih.gov/compound/1_2-propanediol#section=Heat-of-Vaporization. (accessed: 08.02.2019).

[25] K.F. Davis et al. "Alternative cereals can improve water use and nutrient supply in India". In: *Science Advances* 4.7 (2018). DOI: https://doi.org/10.1126/sciadv.aao1108.

[26] Deloitte. *Corporate Tax Rates 2018*. URL: https://www2.deloitte.com/content/dam/Deloitte/global/Documents/Tax/dttl-tax-corporate-tax-rates.pdf. (accessed: 25.02.2019).

[27] Population Division of the Department of Economic and Social Affairs of the United Nations Secretariat. *2017 Revision of World Population Prospects*. URL: https://population.un.org/wpp/. (accessed: 05.03.2019).

[28] Z. Ding, R. Ma, and A.G. Fane. "A new model for mass transfer in direct contact membrane distillation". In: *Desalination* 151.3 (2003), pp. 217–227. DOI: https://doi.org/10.1016/S0011-9164(02)01014-7.

[29] UN - Statistics Division. *Population, latest available census and estimates*. Last updated 7 February 2019. URL: https://unstats.un.org/unsd/demographic-social/products/vitstats/seratab2.pdf. (accessed: 05.03.2019).

[30] John A. Duffie and William A. Beckman. *Solar Engineering of Thermal Processes*. Wiley, 2013.

[31] A. Ertug Ercin and Arjen Y. Hoekstra. "Water footprint scenarios for 2050: A global analysis". In: *Environment International* 64 (2014), pp. 71–82. DOI: https://doi.org/10.1016/j.envint.2013.11.019.

[32] Mohamed Essalhi and Mohamed Khayet. "Membrane Distillation (MD)". In: Steve Tartleton. *Progress in Filtration and Separation*. Springer, 2015. DOI: https://doi.org/10.1016/B978-0-12-384746-1.00003-3.

[33] Hisham Ettouney. "Conventional Thermal Processes". In: Andrea Cipollina, Giorgio Micale, and Lucio Rizzuti. *Seawater Desalination*. Springer, 2009. DOI: https://doi.org/DOI10.1007/978-3-642-01150-4_2.

[34] Hisham Ettouney and Mark Wilf. "Commercial Desalination Technologies". An Overview of the Current Status of Applications of Commercial Seawater Desalination Processes. In: Andrea Cipollina, Giorgio Micale, and Lucio Rizzuti. *Seawater Desalination*. Springer, 2009. DOI: https://doi.org/DOI10.1007/978-3-642-01150-4_4.

[35] L. Eykens et al. "Characterization and performance evaluation of commercially available hydrophobic membranes for direct contact membrane distillation". In: *Desalination* 392 (2016), pp. 63–73. DOI: https://doi.org/10.1016/j.desal.2016.04.006.

[36] A.G. Fane, R.W. Schofield, and C.J.D. Fell. "The efficient use of energy in membrane distillation". In: *Desalination* 64 (1987), pp. 231–243. DOI: https://doi.org/10.1016/0011-9164(87)90099-3.

[37] FAO - Food and Agriculture Organization. *Andhra Pradesh Farmer-Managed Groundwater Systems*. URL: http://www.fao.org/land-water/overview/projects/previous-projects/andhra-pradesh-farmer-managed-groundwater-systems/en/. (accessed: 05.03.2019).

[38] FAO - Food and Agriculture Organization of the United Nations: How to feed the world 2050. *Global agriculture towards 2050*. URL: http://www.fao.org/fileadmin/templates/wsfs/docs/numbers_papers/HLEF2050_Global_Agriculture.pdf. (accessed: 05.03.2019).

[39] FAO - Food and Agriculture Organization of the United Nations. *Acqua per usi agricoli*. URL: http://www.fao.org/3/Y3918I/y3918i03.htm. (accessed: 05.03.2019).

[40] FAO - Food and Agriculture Organization of the United Nations. *Crop water needs*. URL: http://www.fao.org/3/S2022E/s2022e02.htm. (accessed: 05.03.2019).

[41] FAO - Food and Agriculture Organization of the United Nations. *Did you know..? Fact and figures about irrigation areas, irrigated crops, environment*. URL: http://www.fao.org/nr/water/aquastat/didyouknow/index3.stm. (accessed: 05.03.2019).

[42] FAO - Food and Agriculture Organization of the United Nations. *Global and regional food consumption patterns and trends*. URL: http://www.fao.org/3/AC911E/ac911e05.htm. (accessed: 05.03.2019).

[43] FAO - Food and Agriculture Organization of the United Nations. *World Agriculture: Towards 2015/2030*. URL: http://www.fao.org/docrep/pdf/004/y3557e/y3557e.pdf. (accessed: 05.03.2019).

[44] World Economic Forum. *The Global Risks Report 2018*. URL: http://www3.weforum.org/docs/WEF_GRR18_Report.pdf.

[45] J. Fulton, H. Cooley, and P.H. Gleick. "Water footprint". In: P.H. Gleick. *The World's Water*. Springer, 2014.

[46] T. Gleeson et al. "The global volume and distribution of modern groundwater". In: *Nature geoscience* 9 (2016), pp. 161–167. DOI: https://doi.org/10.1038/ngeo2590.

[47] Murat Gökçek. "Integration of hybrid power (wind-photovoltaic-diesel-battery) and seawater reverse osmosis systems for small-scale desalination applications". In: *Desalination* 435 (2018), pp. 210–220. DOI: https://doi.org/10.1016/j.desal.2017.07.006.

[48] Western Cape Government. *City of Cape Town - Socio-Economic Profile 2016*. URL: https://www.westerncape.gov.za/assets/departments/treasury/Documents/Socio-economic-profiles/2016/City-of-Cape-Town/city_of_cape_town_2016_socio-economic_profile_sep-lg.pdf. (accessed: 05.03.2019).

[49] A.M. Helal and S.A. Al-Malck. "Design of a solar-assisted mechanical vapor compression (MVC) desalination unit for remote areas in the UAE". In: *Desalination* 197.1-3 (2006), pp. 273–300. DOI: https://doi.org/10.1016/j.desal.2006.01.021.

[50] A.Y. Hoekstra et al. *The Water Footprint Assessment Manual: Setting the Global Standard*. Earthscan, 2011.

[51] H. Hömig. *Seawater and Seawater Distillation*. Vulkan-Verlag, 1978.

[52] Thomas Huld, Richard Müller, and Attilio Gambardella. "A new solar radiation database for estimating PV performance in Europe and Africa". In: *Solar Energy* 86.6 (2012), pp. 1803–1815. DOI: https://doi.org/10.1016/j.solener.2012.03.006.

[53] Frank P. Incropera et al. *Introduction to Heat Transfer, sixth edition*. Wiley, 2011.

[54] WRI - World Research Institute. *Aqueduct Water Risk Atlas*. URL: https://www.wri.org/our-work/project/aqueduct/.

[55] Soudeh Iranmanesh et al. "Thermal performance enhancement of an evacuated tube solar collector using graphene nanoplatelets nanofluid". In: *Journal of Cleaner Production* 162 (2017), pp. 121–129. DOI: https://doi.org/10.1016/j.jclepro.2017.05.175.

[56] Edward Jones et al. "The state of desalination and brine production: A global outlook". In: *Science of the Total Environment* 657 (2019), pp. 1343–1356. DOI: https://doi.org/10.1016/j.scitotenv.2018.12.076.

[57] M. Khayet, A. Velásquez, and J.I. Mengual. "Modelling mass transport through a porous partition: effect of pore size distribution". In: *Journal of Non-Equilibrium Thermodynamics* 29.3 (2004), pp. 279–299. DOI: https://doi.org/10.1515/JNETDY.2004.055.

[58] J. Koschikowski, M. Wieghaus, and Rommel M. "Membrane Distillation for Solar Desalination". In: Andrea Cipollina, Giorgio Micale, and Lucio Rizzuti. *Seawater Desalination*. Springer, 2009. DOI: https://doi.org/DOI10.1007/978-3-642-01150-4_7.

[59] Chr. Lamnatou et al. "Building-integrated solar thermal systems based on vacuum-tube technology: Critical factors focusing on life-cycle environmental profile". In: *Renewable and Sustainable Energy Reviews* 65 (2016), pp. 1199–1215. DOI: https://doi.org/10.1016/j.rser.2016.07.030.

[60] Sabine Lattemann. "Protecting the Marine Environment". In: Andrea Cipollina, Giorgio Micale, and Lucio Rizzuti. *Seawater Desalination*. Springer, 2009. DOI: https://doi.org/DOI10.1007/978-3-642-01150-4_11.

[61] C.L Martin and D.Y. Goswami. *Solar Energy Pocket Reference*. Ises, 2005.

[62] R.I. McDonald et al. "Urban growth, climate change, and freshwater availability". In: *PNAS - Proceedings of the National Academy of Sciences of the United States of America* 108.15 (2011), pp. 6312–6317. DOI: https://doi.org/10.1073/pnas.1011615108.

[63] David McKenzie and Brent Swails. "Day Zero deferred, but Cape Town's water crisis is far from over". In: *CNN* (Mar. 9, 2018). URL: https://edition.cnn.com/2018/03/09/africa/cape-town-day-zero-crisis-intl/index.html.

[64] Mesfin M. Mekonnen and Arjen Y. Hoekstra. "Four billion people facing severe water scarcity". In: *Science Advances* 2.2 (2016). DOI: https://doi.org/10.1126/sciadv.1500323.

[65] H. Moghadam, F.F. Tabrizi, and A.Z. Sharak. "Optimization of solar flat collector inclination". In: *Desalination* 265.1-3 (2011), pp. 107–111. DOI: https://doi.org/10.1016/j.desal.2010.07.039.

[66] Paul P. Murphy. "In less than 3 months, a major international city will likely run out of water". In: *CNN* (Jan. 31, 2018). URL: https://edition.cnn.com/2018/01/24/africa/cape-town-water-crisis-trnd/index.html.

[67] NETL. *Cost Estimation Methodology for NETL Assessments of Power Plant Perfomance.*

[68] NIST. *NIST Chemistry WebBook - Water*. URL: https://webbook.nist.gov/cgi/cbook.cgi?ID=C7732185%5C&Mask=4. (accessed: 25.02.2019).

[69] Michael Papapetrou et al. "Operating RE/Desalination Units". In: Andrea Cipollina, Giorgio Micale, and Lucio Rizzuti. *Seawater Desalination*. Springer, 2009. DOI: https://doi.org/DOI10.1007/978-3-642-01150-4_10.

[70] N. Philippon et al. "The influence of ENSO on winter rainfall in South Africa". In: *International Journal of Climatology* 32.15 (2011), pp. 2333–2347. DOI: https://doi.org/10.1002/joc.3403.

[71] *Photovoltaic Geographical Information System (PVGIS)*. URL: http://re.jrc.ec.europa.eu/pvgis.html. (accessed: 06.02.2019).

[72] United Nations Development Programme. *Human Development Data (1990-2017)*. URL: http://hdr.undp.org/en/data. (accessed: 05.03.2019).

[73] United Nations Development Programme. *Human Development Index (HDI)*. URL: http://hdr.undp.org/en/content/human-development-index-hdi. (accessed: 05.03.2019).

[74] *PVGIS: Typical Meteorological Year*. URL: http://re.jrc.ec.europa.eu/pvg_tools/en/tools.html#TMY. (accessed: 06.02.2019).

[75] A.S. Richey et al. "Quantifying renewable groundwater stress with GRACE". In: *Water Resources Research* 51.7 (2015), pp. 5217–5238. DOI: https://doi.org/10.1002/2015WR017349.

[76] A.S. Richey et al. "Uncertainty in global groundwater storage estimates in a Total Groundwater Stress framework". In: *Water Resources Research* 51.7 (2015), pp. 5198–5216. DOI: https://doi.org/10.1002/2015WR017351.

[77] The USGS Water Science School. *The World's Water*. URL: https://water.usgs.gov/edu/earthwherewater.html.

[78] The USGS Water Science School. *Water Questions & Answers: How much water does the average person use at home per day?* URL: https://water.usgs.gov/edu/qa-home-percapita.html. (accessed: 05.03.2019).

[79] M.H. Sharqawi, John H. Lienhard, and S.M. Zubair. "Thermophysical properties of seawater: A review of existing correlations and data". In: *Desalination and water treatment* 16.1-3 (2010), pp. 354–380. DOI: https://doi.org/10.5004/dwt.2010.1079.

[80] SMAT. *XIV Bilancio Consolidato - XVIII Bilancio Sociale - Anno 2017 (Situazione patrimoniale-finanziaria consolidata - Patrimonio netto e passività)*. URL: https://www.smatorino.it/wp-content/uploads/2018/09/BILANCIO-SMAT-31-12-2017.pdf. (accessed: 25.02.2019).

[81] S. Srisurichan, R. Jiraratananon, and A.G. Fane. "Mass transfer mechanisms and transport resistances in direct contact membrane distillation process". In: *Journal of Membrane Science* 277.1-3 (2006), pp. 186–194. DOI: https://doi.org/10.1016/j.memsci.2005.10.028.

[82] I.Stat - Istituto Nazionale di Statistica. *Acqua - Consumo per uso domestico*. URL: http://dati.istat.it/Index.aspx?QueryId=20136#. (accessed: 05.03.2019).

[83] *Tavolla*. URL: https://www.tavolla.com/. (accessed: 08.02.2019).

[84] P. van Thienen et al. "Water, Life, and Planetary Geodynamical Evolution". In: *Space Science Reviews* 129.1-3 (2007), pp. 167–203. DOI: https://doi.org/10.1007/s11214-007-9149-7.

[85] Marco F. Torchio. *Tabelle di termodinamica Applicata e Trasmissione del Calore*. CLUT, 2012.

[86] Eftihia Tzen. "Wind and Wave Energy for Reverse Osmosis". In: Andrea Cipollina, Giorgio Micale, and Lucio Rizzuti. *Seawater Desalination*. Springer, 2009. DOI: https://doi.org/DOI10.1007/978-3-642-01150-4_9.

[87] Vaillant. *aguaFLOW*. URL: https://www.vaillant.it/home/prodotti/aguaflow-11072.html. (accessed: 08.02.2019).

[88] Vaillant. *auroTHERM exclusive*. URL: https://www.vaillant.it/home/prodotti/aurotherm-exclusive-1986.html. (accessed: 08.02.2019).

[89] Vaillant. *auroTHERM plus*. URL: https://www.vaillant.it/home/prodotti/aurotherm-plus-1987.html. (accessed: 08.02.2019).

[90] Vaillant. *VTK 1140/2 data sheet*.

[91] H.A.J. Van Lanen et al. "Hydrological drought across the world:impact of climate and physical catchment structure". In: *Hydrology and Earth System Sciences* 17.5 (2013), pp. 1715–1732. DOI: https://doi.org/10.5194/hess-17-1715-2013.

[92] Y. Wada, L.P.H. van Beek, and M.F.P. Bierkens. "Nonsustainable groundwater sustaining irrigation: A global assessment". In: *Water Resources Research* 48.6 (2012). DOI: https://doi.org/10.1029/2011WR010562.

[93] Y. Wada, D. Wisser, and M.F.P. Bierkens. "Global modeling of withdrawal, allocation and consumptive use of surface water and groundwater resources". In: *Earth System Dynamics* 5 (2014), pp. 15–40. DOI: https://doi.org/10.5194/esd-5-15-2014.

[94] Daniel Winter. "Membrane Distillation". A Thermodynamic, Technological and Economic Analysis. PhD thesis. University of Kaiserslautern, 2014.

[95] L.T. Wong and W.K. Chow. "Solar radiation model". In: *Applied Energy* 69.3 (2001), pp. 191–224. DOI: https://doi.org/10.1016/S0306-2619(01)00012-5.

[96] G. Zakrzewska-Trznadel, M. Harasimowicz, and A.G. Chmielewski. "Concentration of radioactive components in liquid low-level radioactive waste by membrane distillation". In: *Journal of Membrane Science* 163.2 (1999), pp. 257–264. DOI: https://doi.org/10.1016/S0376-7388(99)00171-4.

[97] P.P. Zolotarev et al. “Treatment of waste water for removing heavy metals by membrane distillation”. In: *Journal of Hazardous Materials* 37.1 (1994), pp. 77–82. DOI: https://doi.org/10.1016/0304-3894(94)85035-6.